DA-1T061102A33B
AMCMS Code: 501B.11.71200
HDL Proj: 3FL31

HDL-TR-1555

VISCOUS VORTEX RATE SENSOR

by

Arthur J. Ostdiek

November 1971

U.S. ARMY MATERIEL COMMAND
HARRY DIAMOND LABORATORIES
WASHINGTON, D.C. 20438

UNCLASSIFIED
Security Classification

DOCUMENT CONTROL DATA - R & D

(Security classification of title, body of abstract and indexing annotation must be entered when the overall report is classified)

1. ORIGINATING ACTIVITY (Corporate author) Harry Diamond Laboratories Washington, D. C. 20438	2a. REPORT SECURITY CLASSIFICATION Unclassified 2b. GROUP

3. REPORT TITLE

VISCOUS VORTEX RATE SENSOR

4. DESCRIPTIVE NOTES (Type of report and inclusive dates)

5. AUTHOR(S) (First name, middle initial, last name)

Arthur J. Ostdiek

6. REPORT DATE	7a. TOTAL NO. OF PAGES	7b. NO. OF REFS
November 1971	148	19

8a. CONTRACT OR GRANT NO.	9a. ORIGINATOR'S REPORT NUMBER(S)
b. PROJECT NO. DA-1T061102A33B	HDL-TR-1555
c. AMCMS Code: 501B.11.71200	9b. OTHER REPORT NO(S) (Any other numbers that may be assigned this report)
d. HDL Proj: 3FL31	

10. DISTRIBUTION STATEMENT

Approved for public release; distribution unlimited.

11. SUPPLEMENTARY NOTES	12. SPONSORING MILITARY ACTIVITY
	U. S. Army Materiel Command

13. ABSTRACT

The operation of a flueric vortex rate sensor is discussed for flows in the fully developed range, the range in which the entrance conditions at the periphery of the chamber do not appreciably influence the radial velocity profile throughout most of the chamber. Operation in this range is far different from that in the small boundary layer range usually considered in previous investigations. An intuitive examination shows that the frequency response and rate threshold of the sensor are inferior in the small-boundary-layer range, chosen originally for its desirable gain features.

The Navier-Stokes equations as they apply to flow in the chamber for the fully developed range are simplified through very slight approximations, and a method of solving the resulting equations is outlined. A good approximation of this lengthy method is used to obtain closed form expressions that predict the gain and frequency response of the sensor. These predictions show close qualitative agreement with data obtained from a model of the present design. The only important source of error originates from the viscous losses in the sink region, which are not fully analyzed. However, it is shown that this error does correlate with the governing parameters, so that the performance can be predicted to within about 10 percent once a single experiment to measure the losses in the sink is

(Cont'd)

DD FORM 1 NOV 68 1473 REPLACES DD FORM 1473, 1 JAN 64, WHICH IS OBSOLETE FOR ARMY USE.

UNCLASSIFIED
Security Classification

14. KEY WORDS	LINK A		LINK B		LINK C	
	ROLE	WT	ROLE	WT	ROLE	WT
Vortex rate sensor	8	3				
Fluidics	8	3				
Fluerics	8	3				
Rate gyro	8	3				

conducted on a given pickoff-drain design. This is verified with several experiments.

The results predict that the frequency response of the sensor can be increased by about an order of magnitude over that of the present designs without reducing sensitivity. Although the flow field in the fully developed range could be less noisy than in the boundary-layer range, the noise level of the present test model is not reduced in the fully developed range because of its design.

Final discussion covers design changes that should significantly reduce the noise level and make the sensor more rugged. It also mentions planned future analytical work aimed at developing a sensor that compensates for environmental changes.

ABSTRACT

The operation of a flueric vortex rate sensor is discussed for flows in the fully developed range, the range in which the entrance conditions at the periphery of the chamber do not appreciably influence the radial velocity profile throughout most of the chamber. Operation in this range is far different from that in the small-boundary-layer range usually considered in previous investigations. An intuitive examination shows that the frequency response and rate threshold of the sensor are inferior in the small-boundary-layer range, chosen originally to obtain maximum gain.

The Navier-Stokes equations as they apply to flow in the chamber for the fully developed range are simplified through very slight approximations, and a method of solving the resulting equations is outlined. A good approximation of this lengthy method is used to obtain closed form expressions that predict the gain and frequency response of the sensor. These predictions show close quantitative agreement with data obtained from a model of the present design. The only important source of error originates from the viscous losses in the sink region, which are not fully analyzed. However, it is shown that this error does correlate with the governing parameters, so that the performance can be predicted to within about 10 percent once a single experiment to measure the losses in the sink is conducted on a given pickoff-drain design. This is verified with several experiments.

The results predict that the frequency response of the sensor can be increased by about an order of magnitude over that of the present designs without reducing sensitivity. Although the flow field in the fully developed range could be less noisy than in the small boundary layer range, the noise level of the present test model is not reduced in the fully developed range because of its design.

Final discussion covers design changes that should significantly reduce the noise level and make the sensor more rugged. It also mentions planned future analytical work aimed at developing a sensor that compensates for environmental changes.

PREFACE

This paper presents some of the rate sensor work done at HDL since 1968. At that time the basic solution for flow in the chamber of a particular rate sensor concept, which was first tested in 1965, was completed.

Although this paper, as HDL's rate sensor program, is mostly theoretical, it may have wide practical impact. New concepts directly suggested by the analysis are (1) a rate sensor with effectively no time delay and a corner frequency in excess of 1 kHz, (2) a rate sensor with much less signal drift than the present model, (3) a sensor whose rate sensitivity is immune to environmental factors, and (4) a single sensor that measures both angular rate and angular acceleration.

These would seem to have both commercial and military applications; however, corroborating experimental data is largely absent.

This early disclosure is being made should some other laboratory be in a better and more urgent position to take advantage of these findings and pursue the necessary exploratory and develcpmental efforts.

CONTENTS

FIGURES

1. INTRODUCTION

1.1 Background

There has been much interest in the flueric device known as the vortex rate sensor since its invention about a decade ago. In this device, fluid is forced radially into a short cylindrical chamber through the porous outer wall (the coupler) and exhausts through a drain in one or both end walls at the chamber axis (fig. 1). This sensor produces a signal that is a function of the rate at which it turns in inertial space about its longitudinal axis. In most designs the signal is obtained in the drain from an air foil pickoff whose output is a function of the streamline angle generated by the rotation.

There are three quantities of principal interest in a rate sensor output: (1) sensitivity, or signal gain; (2) rate threshold, i.e., minimum angular rate that can be resolved above noise; and (3) the frequency response. Signal gain has been of primary interest in the previous literature (ref 1-5)*; noise (ref 6) and sensor dynamics (ref 7) have undergone less extensive investigation. None of these studies has examined thoroughly the analytical relationships among these quantities.

For many applications in vehicle guidance or stabilization, the present vortex rate sensor has two shortcomings, a high noise level and an unsatisfactory frequency response. An effort is made here to determine whether these limitations on noise level and frequency response are inescapable.

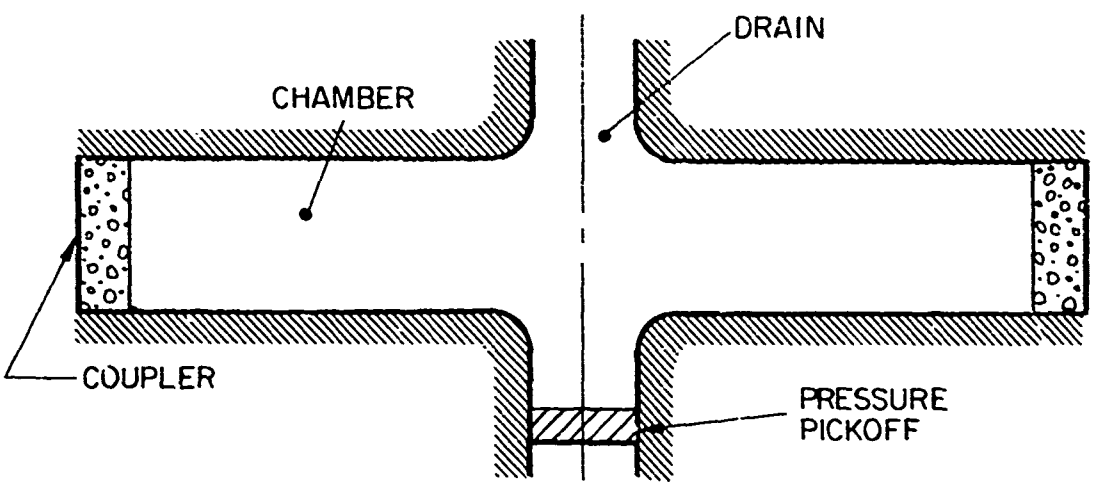

Figure 1. Vortex rate sensor.

* See pp. 72-73 for references.

Nearly all previous analytical studies of the rate sensor have been concerned with its operation when viscous effects can be treated from boundary layer concepts. These presentations imply that viscous dissipation in the chamber should be small since it reduces the vortex strength and thus reduces signal gain. However, the effect of relative boundary layer size and viscous dissipation on the frequency response and the noise level should be considered before such a restriction is placed on rate sensor design. The following examination of the rate sensor operation when the boundary layers are small compared with the chamber height indicates that both the sensor dynamics and signal-to-noise (S/N) ratio should be relatively poor.

1.2 Dynamic Characteristics when the Boundary Layers are Small

The sensor dynamics can be characterized by a simple time delay between a rate input and the sensor output if the flow in the chamber is essentially inviscid (that is, if the boundary layers are small compared with the chamber height), if the radial velocity profile at the coupler is uniform and axisymmetric, and if the transport times along the various streamlines in the vicinity of the drain entrance are small compared with those in the outer portion of the chamber. Since the flow can be considered incompressible except possibly near the drain, the delay time T is given approximately by a quotient of the chamber volume and Q_o, the volumetric flow rate in the outer portion of the chamber:

$$T = \frac{\pi R_o^2 h}{Q_o} \tag{1}$$

where R_o = chamber radius, and h = chamber height.

If no dissipation occurs in the chamber, the velocity components in the drain are independent of h if the flow rate is fixed. This implies that the signal gain of a pickoff in the drain is independent of h.

If h is made small, T decreases and gain does not change if the boundary layers are small. However, for fixed Q_o, ν and R_o, the boundary layer size will become significant if h is less than some as yet unspecified value. In that case, (1) will no longer hold, and the gain will depend on h.

This simple approach indicates that the height should be made so small that the relative size of the boundary layers becomes significant, because this results in greater frequency

response at no sacrifice in gain if Q_o is fixed. A further decrease in height should cause a further improvement in frequency response (but result in a sacrifice of gain) since the flow would become strongly coupled to the top and bottom plates and would therefore receive angular rate information that is an update of the information it received at the coupler.

1.3 Resolution of the Present Sensor

1.3.1 Streamline Angle Resolution

The problems concerning the S/N ratio of present sensors can best be seen by using an inviscid analysis to obtain an approximate value for the angle between a fluid streamline in the chamber and a radial line. Empirical values can then be used in this relationship to indicate the order of magnitude of the disturbance that limits the resolution of this angle in the present sensor.

When the sensor is turning at a constant rate Ω_o, the angle α that a streamline makes with a radial line is given by

$$\alpha = \arctan \frac{V_\theta}{|V_r|} \tag{2}$$

where V_θ = tangential velocity at a radial distance r from the longitudinal axis of the chamber, and V_r = radial velocity at r. If V_θ is small, then

$$\alpha \cong \frac{V_\theta}{|V_r|} \tag{3}$$

If the sensor is turning at a constant rate Ω_o and if the flow is incompressible and inviscid, then

$$V_\theta = \frac{\Omega_o R_o^2}{r} \tag{4}$$

and

$$V_r = -\frac{U_o R_o}{r} = -\frac{Q_o}{2\pi h}\frac{1}{r} \tag{5}$$

where U_o = average radial velocity at R_o.

Therefore,

$$|a| \cong \frac{|\Omega_o| R_o}{U_o} = 2 |\Omega_c| T \qquad (6)$$

A value for the minimum change in angle of the vortex streamlines in the chamber that can be resolved by the pressure pickoff can be obtained by substituting in (6) the empirical values claimed for the rate threshold and response time of typical vortex rate sensors. Values obtained in this manner are in the range from 0.01 to 0.001 deg.

1.3.2 Fluid Phenomena Which Cause Output Noise

There are three factors that inhibit resolution of the streamline angle in present rate sensors: high frequency noise, drift (low frequency noise), and null shift (a dc shift of the entire curve of output signal versus angle rate during operation, or a lack of repeatability of the curve when the power supply is shut off and then turned on again). Although the exact origin of these disturbances is not fully understood, an intuitive examination can shed some light on the nature of the problem.

Most of the high frequency noise probably results from turbulence in the drain region. If the gain of the device is to be high, the mass flow rate must be large and the drain radius small. Since the Reynolds number in the drain is directly proportional to the mass flow rate and inversely proportional to the drain radius, it is invariably true that in a high-gain rate sensor of the present design the Reynolds number in the drain is higher than the critical value for the onset of turbulence.

A portion of the high frequency noise is probably due to turbulence generated when the probe is inserted into the flow. Even if the undisturbed flow were laminar, separation would occur at some point downstream of the sensing ports on the surface of a typical pickoff at a typical operational condition. The propagation of this noise in the upstream direction would then lead to noise at the sensing ports.

The signal drift probably is due in part to a change in the distribution of the fluid at the outer portion of the chamber. A change of environmental conditions, power supply level, or downstream load could cause a change in the degree of distortion of the field caused by the manifolding system

or the coupler, a ready source of anomalies. Because the pickoff in the present design extends across the origin in the drain, the output of the sensor is very sensitive to the degree of nonaxisymmetry in the field.

The signal drift probably is also related in another fashion to variations in power supply level. The pickoff in the typical sensor is of the push-pull variety, one that has sensing ports on either side of the stagnation point. A change in angle of attack thus generates pressure changes of opposite signs at the two ports, and a differential signal is then a measure of the angle, or a function of the angular rate.

It is not possible to orient the pickoff so that the differential output is perfectly zero when the sensor is stationary. As a result the differential signal at zero angular rate is not zero and in particular is dependent upon the flowrate. Thus, variations in flowrate inhibit the measurement of small changes of angular rate about zero rate.

The null shift probably results from flexing or shifting in the pickoff drain assembly. Present rate sensors typically have a very small pickoff mechanically mounted inside a small drain, an assembly which can easily be susceptible to mechanical or thermal disturbances. Since the pickoff is situated at a position where the magnitude of the tangential velocity varies sharply with radial location, even a very small movement can result in a significant output shift.

It may also be true that a nonaxisymmetric flow distribution at the coupler that varies with supply pressure can lead to a null shift, for under those circumstances the features of the flow field at zero rate could depend upon the manner in which the power supply is brought up to working level. However, this possible noise source then becomes closely linked with one of the speculated sources of low frequency noise, and thus would be attacked in any program planned to eliminate the latter.

1.3.3 Output Noise

The problem of noise in the output signal can now be put into perspective. It is probably surprising to most observers that an angle of 0.001 deg can be resolved in a turbulent field by a pickoff that may be sensitive even to the thermal stresses induced by a change in temperature of the working fluid. But the purported causes of low frequency noise are just as disquieting when referenced to this small angle.

Suppose, for instance, that the pickoff were mechanically oriented in the field at an angle of 0.1 deg from the angle for perfect null. Then (3) indicates that a one percent

change in flowrate would be sufficient to cause an output shift equivalent to an angular change of 0.001 deg. Since both of these requirements are realistic if not optimistic estimates of the accuracies of present techniques, it would seem that this effect alone could be sufficient to limit the performance of the rate sensor. However, the requirements on axisymmetry of the field appear at first glance to be even more stringent.

The continuity equation can be used to show that a nonaxisymmetric upstream disturbance generates perturbations with respect to θ of approximately the same order in V_r and V_θ. This implies that the present noise level is equivalent to a time-varying perturbation with respect to θ in V_r at the pickoff that is about four orders of magnitude smaller than the mean value, because

$$10^{-4} \cong |\alpha|_{min.} \cong \left| \frac{V_{\theta_{perturb}}}{V_{r_{mean}} + V_{r_{perturb}}} \right| \cong \left| \frac{V_{r_{perturb}}}{V_{r_{mean}}} \right| \qquad (7)$$

This is an amazingly low disturbance if one observes that little attention has been given to the designing of a manifolding system that is capable of supplying the outer portion of the chamber with a flow whose time-varying distortion with respect to θ is less than even one percent of the mean when the sensor is powered by a typical power supply. This implies that the noise at the pickoff due to entrance effects is probably at least two orders of magnitude less than that at the coupler.

The sensor resolution has been enhanced somewhat by the design of the push-pull pickoff discussed previously, since noise at the ports that has positive correlation tends to cancel. However, the only fluid mechanism used effectively to condition the field properly for precision measurement is the fields' natural acceleration as it flows toward the sink, which serves to decrease upstream nonaxisymmetry.

It should not be surprising that the present vortex rate sensor does not have the desired resolution for applications that are within the capabilities of other gyro technologies since the specifications for those applications would require extremely high integrity in a vortex field. In an absolute sense, the present sensor is quite effective at measuring very small streamline angles, due at least as much to a fortunate choice of initial sensor concept as to any

later design effort. The sink field, chosen because it provides a mechanism for amplifying small signals at the coupler, has a side benefit in its effect on noise. The only reason that the present vortex rate sensor works as even a moderately effective sensor seems to be that the acceleration of the sink field leads to a drastic reduction of the noise due to entrance conditions.

It seems clear that a limit has been reached in sensor performance, and that it would be unreasonable to expect any improvement unless a great deal of care is taken to eliminate noise. Of the three types of noise discussed, signal drift seems to be the most troublesome. Null shift can be eliminated for some applications by using a high-pass filter, and high frequency noise by using a low-pass filter. However, the low frequency noise appears in any bandwidth chosen for the sensor response. If this latter noise is related in part, as suggested, to entrance conditions, then special care should be taken to properly condition the flow field for precision measurement.

1.4 Proposed Changes

It was suggested in Section 1.2 that h should at least be made so small that the boundary layer size is not negligible when compared to h. This change would seem to be compatible with the discussion in Section 1.3 concerning the low frequency noise, because the most logical methods of conditioning the flow would lead to significant viscous effects in the chamber.

The most obvious way to condition the flow would be to make the chamber radius so large that the entrance conditions do not noticeably influence the flow near the pickoff. This requires at the same time that the coupler have no effect on the signal output. The signal would then be introduced by means of wall shear, a much less noisy means than the use of a coupler, which has been shown (ref 8) to introduce very high distortion in the flow field. If the chamber is sufficiently large. the only output noise seen by a rugged pickoff would be that due to changes in the power level and that which propagates upstream from the drain. But since the signal propagates in a direction normal to the wall or in a direction normal to the direction of propagation of these noises, it may be possible by proper signal processing to significantly decrease the effect on the output of even that fluid noise which careful design does not eliminate.

No mention has been made of the effect that increasing the chamber radius would have on frequency response and gain of the sensor. It might help at this point to try to establish intuitively what this effect would be. However, it is doubtful that such a discussion would encourage the reader to endure the

lengthy analysis of the problem to follow later since it would be necessary for an adequate discussion to redefine old concepts for use in a new area with definitions that anticipate later mathematical difficulties, and thus possibly only generate confusion.

Perhaps some reader concern can be allayed if it is pointed out that a theory is developed here which adequately predicts, among other things, the gain of the device for all values of h for which the boundary layers merge. If the pickoff is located in the drain, then the gain decreases monotonically to zero as the height is decreased. For sufficiently large h, it is found that the curve of gain versus height is nearly flat, that is, that gain is relatively independent of h. At small h, it is a linear function of it. In this later region, the theory indicates that the coupler ha no influence on the output signal. The gain is reduced by a factor of about two in reducing h from a value in the "flat" range to one in the upper portion of this linear range, but the frequency response is increased by a factor of about twenty.

It can be then shown that if one were to increase R_o and decrease h in such a fashion that some characteristic frequency (such as that at which the phase lag is 90 deg) remains constant, the gain would increase. It would increase by about an order of magnitude while the configuration is changed from one in which the flow in the chamber is nearly inviscid to one in which the entrance conditions do not appreciably affect the signal.

If the gain and frequency response are independent of R_o, as they would be under this latter condition, the coupler could then be made large enough to properly condition the flow. The limit on size would be fixed by physical restrictions. If these do not allow a sufficiently large R_o for the desired noise reduction, then several schemes other than a single cylindrical cavity could be tried. One would be a stack of thin annular chambers mounted coaxially above the rate sensor chamber. By proper interconnections, the fluid could alternately flow inward and outward through successive chambers as it progressed through the stack before it enters the working chamber and flows out the sink. If the deceleration the fluid experiences in each alternate outward stage does not permit stable flow, either the chamber height could be changed with radius to ensure stability or other schemes should be tried. It is not important to discuss various schemes at this time, particularly since it appears that their number is limited only by the imagination of the designer for a particular set of physical restrictions.

In summary, it seems evident that the operation of a rate sensor should be considered for the general regime in which the viscous effects are not negligible, since the changes required to increase frequency response and reduce noise lead either directly or indirectly to the consideration of significant viscous effects.

1.5 Boundary Layer Effects

1.5.1 Condition for Fully Developed Flow

In order to discuss the effect of viscous losses on the sensor characteristics, it is necessary first to establish which dimensionless viscous parameter specifies the relative size of the boundary layers. Approximate values can then be sought for this parameter that divide its range into regions of negligible, partial, and complete viscous interaction of the top and bottom plates.

The boundary layer problem for sink flow over a single flat disc has been attacked by Sarpkaya, Goto, and Kirshner (ref 9) through the use of an integral-momentum method. The results obtained with their method are shown in figure 2. The boundary layer is thickest at $r = 0.55\ R_o$ with

$$\delta_{max} = 2.6 \sqrt{\frac{R_o \nu}{U_o}} \tag{8}$$

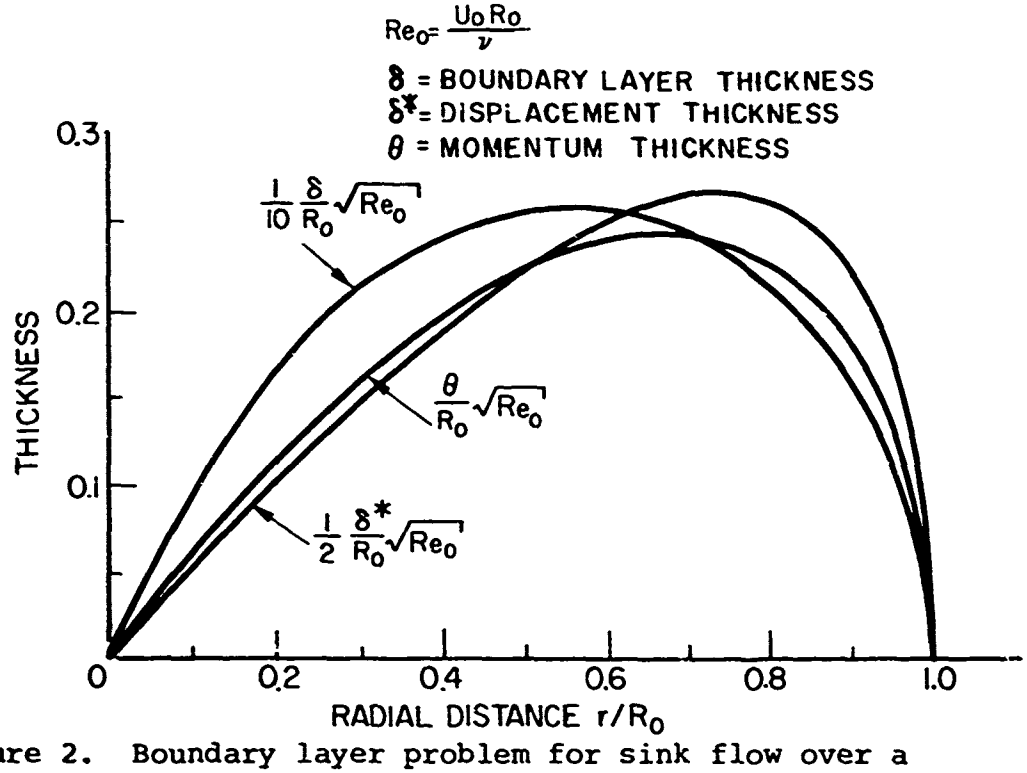

Figure 2. Boundary layer problem for sink flow over a single flat disc (method of Sarpkaya, Goto and Kirshner).

There has been no known published work that examines in detail the problem of profile development for sink flow between two flat discs. However, an approximate value for the pertinent viscous parameter at which the radial velocity profile first becomes fully developed can be obtained by using (8) together with some physical arguments based on the profile development for plane flow between two flat plates. The phrase "fully developed" is used here to describe a profile at a radius where the influence of the entrance conditions is no longer significant, even though the velocity profile might change with decreasing radius due to acceleration effects.

The laminar boundary layer thickness for plane flow over a flat plate at zero angle of incidence to a uniform external field is given (ref 10) by

$$\delta = 4.93\sqrt{\frac{x_1 \nu}{U_\infty}} \tag{9}$$

where x_1 is the distance from the leading edge and U_∞ is the free stream velocity. The entrance length ℓ_e, for fully developed plane flow between parallel flat plates separated by a distance h is given (ref 11) by

$$\ell_e = 0.04 \frac{U_\infty h^2}{\nu} \tag{10}$$

Equations (9) and (10) can be used to establish an approximate criterion in terms of the boundary layer thickness over a single plate at $x_1 = \ell_e$ and the plate separation distance h. This approximate criterion is that the boundary layer on a single plate (in the absence of the other plate) has a thickness at ℓ_e of

$$\delta_{\ell_e} = 1.0\, h \tag{11}$$

Now consider sink flow between two flat discs as h is decreased from a large value while Q_o, ν and R_o are fixed. At some critical value of h, the flow will become fully developed at some radius in the chamber. If this radius is just that at which the boundary layer over a single disc is at its thickest and if a relationship similar to (11) holds, then an approximate value for the modified Reynolds number, Re'_o, for this case can be found from (8) given by

$$Re'_{O_{crit}} \cong 7 \tag{12}$$

where

$$Re'_O = \frac{U_O R_O}{\nu} \frac{h^2}{R_O^2}$$

It should be noted that (9) refers to a boundary layer in the absence of an external pressure gradient and that an accelerating radial pressure gradient is present in sink flow. Since the boundary layer profile in an accelerating pressure gradient is blunter in the region near the free stream, it could be argued that the boundary layer thickness from criterion (11) is not sufficiently large to ensure profile development between parallel discs. However, the velocity profile that the fluid attempts to attain is made blunter by the acceleration effects than the profile that would exist in the absence of an accelerating pressure gradient, so the degree by which the viscous forces must alter a uniform entrance profile is not so severe for flow in the presence of an accelerating pressure gradient. The sign of the error in the approximation used in obtaining (11) must remain unspecified at this time; however, the magnitude of the error should not be large.

1.5.2 Features of Flow Field for $Re'_O < Re'_{O_{crit}}$

If the free stream thickness is small, the additional acceleration effects caused by the displacement of the streamlines toward the centerplane should cause the boundary layers to become relatively flat midway in the chamber. Consequently, if the point in the chamber at which the flow may be considered fully developed is much different from R_O at $Re'_{O_{crit}}$, the point rapidly moves toward the coupler (R_O) as Re'_O is decreased below the critical value. Then the flow can be considered fully developed throughout most of the chamber for values of Re'_O less than the critical value.

1.5.3 Features of Flow Field for $Re'_O > Re'_{O_{crit}}$

Now consider the flow when Re'_O is large. The shape of the velocity profile in the boundary layers is specified by the parameter Λ where

$$\Lambda = \frac{\delta^2}{\nu} \frac{d(V_{r\,\text{free stream}})}{dr} \tag{13}$$

If the boundary layer effects on the free stream are small and the flow is incompressible, (5) can be used for the free stream velocity in (13) to show that

$$\Lambda = \frac{R_o^2}{r^2}\left(\frac{\delta^2}{h^2} Re_c'\right) \tag{14}$$

At a given r/R_o, the quantity $\left(\frac{\delta^2}{h^2} Re_o'\right)$ is a constant to the approximation of small boundary layers, since figure 2 indicates that $\left(\frac{\delta^2}{R_o^2} Re_o\right)$ is a function of $\frac{r}{R_c}$ only. Then Λ is a function of $\frac{r}{R_o}$ only, and, in particular, is independent of the relative size of the boundary layer. Thus, the boundary layer features can be treated simultaneously for all Re_o' when the relative size is small. Such a discussion could be extended to a good approximation into the range of Re_o' in which the boundary layers interact simply by observing what effect the associated change in Λ would have.

From figure 2,

$$\Lambda\Big|_{r=R_{max}} \cong 22 \tag{15}$$

where R_{max} is the radius at which the boundary layer thickness is a maximum ($0.55R_o$). The value of Λ at R_{max} increases as the thickness of the boundary layers approaches the chamber height, due to the added acceleration of the free stream.

When the boundary layers first touch, the interactions near the center plane are extremely small due to the bluntness of the velocity profile in this region. The most severe interactions will occur near R_{max}. For the value of Λ in (15), the velocity profile for a single boundary layer is so blunt (ref 12) that the boundary layers on the top and bottom plates could overlap by as much as 30 percent without causing more than a few percent variation in the velocity throughout the overlapping region. When the overlap is greater, the profile obtained near

the centerplane by a simple superposition of the boundary layer profiles does not differ significantly from a good estimate of the actual solution in that region. Since the greatest signal contribution of the pickoff comes from the fluid passing through the region near the centerplane of the chamber, the output of the sensor can be described fairly well from boundary layer analysis even if the overlapping of the boundary layers is significant.

The increase in Λ that occurs as the relative size of the boundary layers grows causes the viscous effects near the centerplane to be weaker than the previous discussion anticipates. Since it is more valid to approximate viscous effects by a superposition of boundary layers if these effects are weaker, the previous discussion still holds.

It would seem, then, that the interactions of the boundary layers are not significant in the case of slight overlapping. Furthermore, even in the case of severe overlapping, the sensor output can be described adequately through boundary layer analysis.

1.5.4 General Features of the Flow Field

In summary, the range of Re_D' for rate sensors having a cylindrical chamber can be divided rather sharply into two regions, one in which boundary layer analysis applies and one in which the radial velocity profile can be considered fully developed throughout the entire chamber. The value of Re_D' which divides these two regions is about 7.

1.6 Purpose of Investigation

It was indicated in Section 1.4 that the operation of the sensor should be considered when the relative size of the boundary layers is not negligible. Section 1.5.4 then indicates that the characteristics of the sensor should be examined in the fully developed range. It cannot be established a priori whether some gain needs to be sacrificed to both increase the frequency response and improve the rate threshold to the desired level; however, that is not of great consequence at the present, since the shortcomings of the present vortex rate sensors are its poor rate threshold and poor frequency response, not its gain characteristics. Since the sensor feature for which the rest of the control system usually can most easily compensate is a modest deficiency of gain, a limited sacrifice in gain is not an obstacle.

An investigation of the characteristics of a vortex rate sensor for that range in which the entrance conditions do not appreciably influence the radial velocity is then of paramount interest.

2. ANALYSIS

2.1 Formulation of Problem

2.1.1 Analytical Model

In what follows an approximate solution will be found for the governing equations for inward flow in a thin cylindrical chamber when the angular rate has been a sinusoidal function of time for an infinite length of time. The no-slip condition will be imposed on both the radial and tangential velocities at the top and bottom plates and on the tangential velocity at the coupler wall. The entrance effects on the radial profile will be neglected, in keeping with the purpose of this study as stated in Section 1.6. The influence of the drain on the flow in the chamber will be ignored; the reasons for this restriction will be discussed briefly.

In attempting to attack the problem analytically, it is best to divide the physical problem into three regions; the chamber, the drain and the corner region between the two. The chamber is that region in which the velocity normal to the top and bottom plates is very small. The drain is that region in which the streamlines are nearly parallel to the drain walls. Since a different set of terms in the governing equations can be ignored in each region, it is logical to obtain the general solutions for each region separately and then to match the solutions at the dividing surfaces.

Only the chamber problem is discussed in detail in this paper, although the qualitative effect of the corner and the drain on the rate sensor characteristics is attacked analytically. There are two reasons for considering only the chamber in detail. First, since the corner problem does not lend itself readily to analytical methods, the importance of the corner effects should be established before one undertakes the prodigious task of solving the differential equations that apply in that region by computer techniques. This importance can be established if the corner is the only significant source of error that is ignored in attempting to describe the output characteristics of the sensor, as will be done here. Second, if the corner region represents a noise source or if the viscous losses are significant in that region, the rate sensor probably should be designed with a pickoff just upstream of the corner. Intuition indicates that the corner does have just such features, so that the sensor

which finally results from this effort can probably be designed on the basis of the chamber solution alone.

In keeping with this restriction on the scope of the problem to be attacked, it is assumed (1) that the drain is a small tubular sink concentric with the chamber axis, (2) that the pickoff extends the length of the chamber near the sink, (3) that the pickoff responds as an angle of attack sensor, and (4) that the pickoff's pressure output is an average over the entire length of the pressure at the angular location of the sensing port. Figure 3 is an illustration of this model.

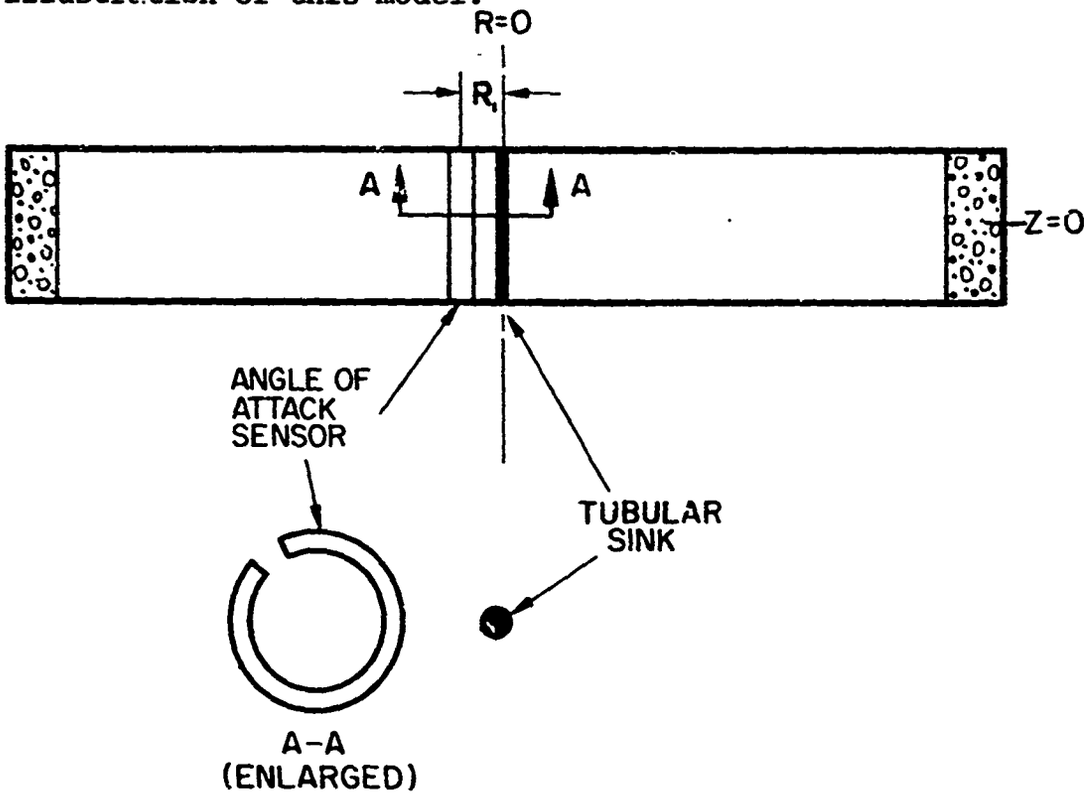

Figure 3. Vortex rate sensor analytical model.

The radial location of the pickoff in the mathematical model is set equal to the drain radius R_1 of the experimental model. The output of the pickoff located in the drain of the real sensor is assumed to be a linear function of the output of this hypothetical pickoff in the mathematical model of the chamber. The implications of this assumption will be explored as the analysis progresses.

The radius of the sink tube should be small enough that the shear generated on its surface does not affect the flow near the pickoff because the corner-drain effects are to be ignored. It will be shown later that, for the values of

flow paramaters in this experiment, the sink tube radius need only be very slightly smaller than R_1. This requires that in the mathematical model the pressure at the sink tube wall must be slightly lower than that in the larger drain of the real model so that the flowrate through both models will be the same for the same supply pressures.

The statement that the drain tube need only be slightly smaller than R_1 may be surprising if one expects the center of the field to behave in rigid body fashion, which is a feature of three-dimensional sink flow. It can be shown (App A) that no such rigid-body core exists for steady, inward flow between two concentric, porous, rotating cylinders that are very long in the axial direction. If the cylindrical cavity is short, the viscous effects from the top and bottom plates complicate the mathematics and the physical understanding of the problem, but the essential features of the flow fields are quite similar.

The drain tube cannot be made arbitrarily small for a given pressure and flow rate in the exterior part of the chamber since the pressure at the drain wall would have to be zero at some finite radius in order that such a field exist. This is the so-called "limit circle" effect. But in reality, the exterior field cannot be established unless the pressure at the drain tube is set at some meaningful value, nor does a conscientious designer ever specify the flow rate and supply pressure at which a model is to work without checking the pressure drop across the model to see if the exit pressure is physically realizable. To restrict the range of r because of the artificial concept of a "limit circle" for some situations that cannot be achieved in reality is to needlessly complicate the resulting design equations. With this understanding of the problem the radius of the drain tube is allowed to be a small value, ϵ_1.

Figure 4 shows a schematic of the drain region of the rate sensor that was tested in this study. The drain dimensions are so small that the size of the pickoff output port must be of the same order as that of the drain to make the power output of the pickoff readily compatible with present flueric amplifiers. In addition, since the Reynolds number based on pickoff tube diameter and velocity in the drain tube is of the order of 10^4 in this experiment, the local disturbance due to the pickoff probably causes any variation in signal level across the stream to be reduced, if not washed out. Because of this, one of the basic assumptions of this analysis is that the pickoff integrates across the entire flow stream, as indicated previously in this section.

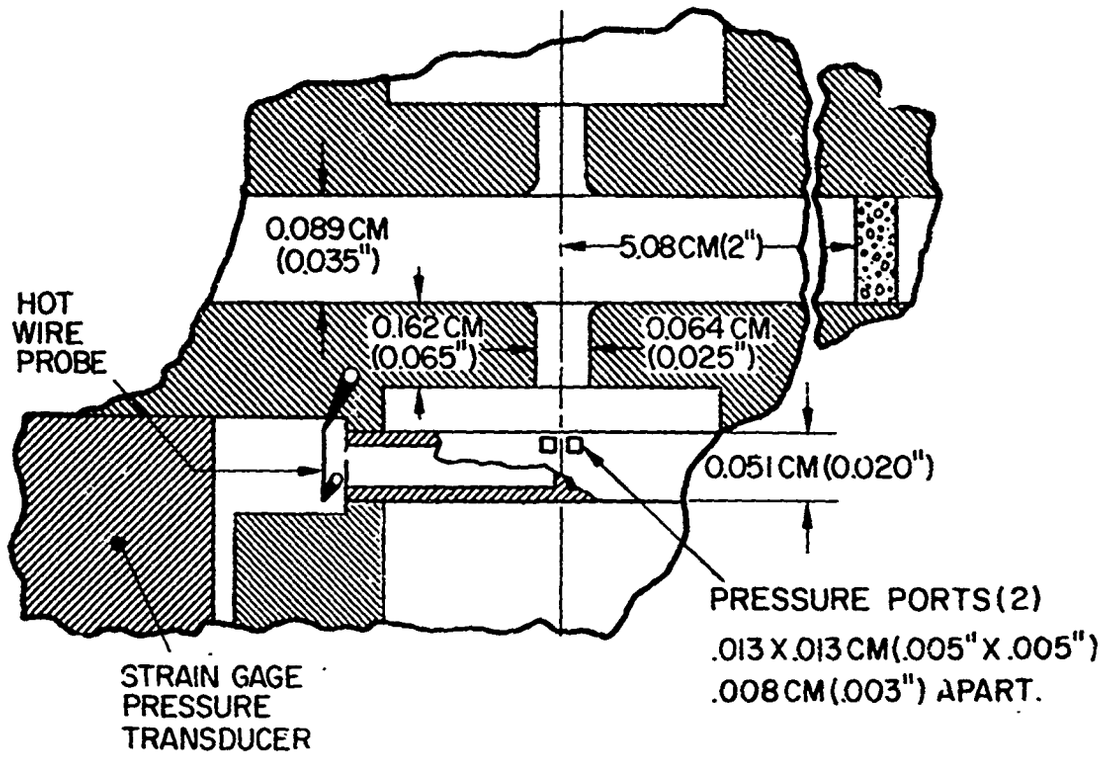

Figure 4. Rate sensor drain region.

2.1.2 Assumptions

The following assumptions are made about the flow in the chamber:

(a) The flow is laminar and incompressible.

(b) The flow is axisymmetric with respect to the longitudinal axis of the chamber.

(c) The vortex is weak, (that is $|V_\theta| \ll |V_r|$).

(d) The displacement of a fluid particle in a direction normal to the end walls as it flows toward the sink is small compared with the chamber height.

(e) The body forces are small.

Assumption (d.) and the conditions that the chamber is thin can be used to show that

$$\left|\frac{V_z}{V_r}\right| \ll \frac{h}{Ro} \ll 1 \qquad (16)$$

2.1.3 Governing Equations

The governing equations in cylindrical coordinates for laminar, incompressible flow are

$$\rho\left(\frac{\partial v_r}{\partial t} + v_r\frac{\partial v_r}{\partial r} + \frac{v_\theta}{r}\frac{\partial v_r}{\partial \theta} - \frac{v_\theta^2}{r} + v_z\frac{\partial v_r}{\partial z}\right) =$$

$$F_r - \frac{\partial p}{\partial r} + \mu\left(\frac{\partial^2 v_r}{\partial r^2} + \frac{1}{r}\frac{\partial v_r}{\partial r} - \frac{v_r}{r^2} + \frac{1}{r^2}\frac{\partial^2 v_r}{\partial \theta^2} - \frac{2}{r^2}\frac{\partial v_\theta}{\partial \theta} + \frac{\partial^2 v_r}{\partial z^2}\right) \tag{17}$$

$$\rho\left(\frac{\partial v_\theta}{\partial t} + v_r\frac{\partial v_\theta}{\partial r} + \frac{v_\theta}{r}\frac{\partial v_\theta}{\partial \theta} + \frac{v_r v_\theta}{r} + v_z\frac{\partial v_\theta}{\partial z}\right) =$$

$$F_\theta - \frac{1}{r}\frac{\partial p}{\partial \theta} + \mu\left(\frac{\partial^2 v_\theta}{\partial r^2} + \frac{1}{r}\frac{\partial v_\theta}{\partial r} - \frac{v_\theta}{r^2} + \frac{1}{r^2}\frac{\partial^2 v_\theta}{\partial \theta^2} + \frac{2}{r^2}\frac{\partial v_r}{\partial \theta} + \frac{\partial^2 v_\theta}{\partial z^2}\right) \tag{18}$$

$$\rho\left(\frac{\partial v_z}{\partial t} + v_r\frac{\partial v_z}{\partial r} + \frac{v_\theta}{r}\frac{\partial v_z}{\partial \theta} + v_z\frac{\partial v_z}{\partial z}\right) = F_z - \frac{\partial p}{\partial z} + \mu\left(\frac{\partial^2 v_z}{\partial r^2} + \frac{1}{r}\frac{\partial v_z}{\partial r} + \frac{1}{r^2}\frac{\partial v_z}{\partial \theta^2} + \frac{\partial^2 v_z}{\partial z^2}\right) \tag{19}$$

$$\frac{\partial v_r}{\partial r} + \frac{v_r}{r} + \frac{1}{r}\frac{\partial v_\theta}{\partial \theta} + \frac{\partial v_z}{\partial z} = 0 \tag{20}$$

If the assumptions (b), (c), and (e), and (16) are used, these equations become

$$\rho\left(\frac{\partial V_r}{\partial t} + V_r \frac{\partial V_r}{\partial r}\right) = -\frac{\partial p}{\partial r} + \mu\left(\frac{\partial^2 V_r}{\partial r^2} + \frac{1}{r}\frac{\partial V_r}{\partial r} - \frac{V_r}{r^2} + \frac{\partial^2 V_r}{\partial z^2}\right) \tag{21}$$

$$\rho\left(\frac{\partial V_\theta}{\partial t} + V_r \frac{\partial V_\theta}{\partial r} + V_r \frac{V_\theta}{r}\right) = \mu\left(\frac{\partial^2 V_\theta}{\partial r^2} + \frac{1}{r}\frac{\partial V_\theta}{\partial r} - \frac{V_\theta}{r^2} + \frac{\partial^2 V_\theta}{\partial z^2}\right) \tag{22}$$

$$\frac{\partial p}{\partial z} = 0 \tag{23}$$

$$\frac{\partial V_r}{\partial r} + \frac{V_r}{r} + \frac{\partial V_z}{\partial z} = 0 \tag{24}$$

2.1.3.1 Simplified Radial Momentum Equation

Notice that V_θ does not appear in (21). Since the time-dependent boundary conditions apply only to V_θ, under the above assumptions and boundary conditions V_r is independent of time. Thus, the time derivative in equation (21) can be dropped. Before the rest of the equation can be reduced, it is necessary first to examine the relationship between V_r/r and $\partial V_r/\partial_r$.

If the radial velocity profile at R_o has only one maximum, then at all r it will have only one maximum. This implies that V_z can have only three zeroes, one at each wall, and one at the point where V_r is a maximum. In addition, if the radial profile at R_o is not sharp, V_z must be a rather smooth function of z for all r. These facts, together with the observation that the magnitude of V_r increases smoothly as r decreases, can be used with inequality (16) to show that

$$\left|\frac{\partial V_r}{\partial r}\right| >> \left|\frac{\partial V_z}{\partial z}\right| \tag{25}$$

This has the same consequence in the continuity equation as saying that the mass flux through an elemental surface lying in the z-plane can be ignored in comparison to that through

an elemental cylindrical surface perpendicular to r.

Equation (24) and inequality (25) can then be used to show the approximate relationship

$$\frac{V_r}{r} = -\frac{\partial V_r}{\partial r} - \frac{\partial V_z}{\partial z} \cong \frac{\partial V_r}{\partial r} \tag{26}$$

This expression implies that (21) can be closely approximated by

$$-\rho \frac{V_r^2}{r} = \frac{\partial p}{\partial r} + \mu \frac{\partial^2 V_r}{\partial z^2} \tag{27}$$

If one lets

$$V_r = \frac{-A(r)\,k(r,z)}{r} \tag{28}$$

and integrates (24) with respect to z from, -h/2 to h/2, it can be shown that

$$A(r) = \frac{Q_o}{4\pi \int_0^{h/2} k(r,z)\,dz} \tag{29}$$

where $k(r,o) = 1$, $k(r, \pm h/2) = 0$.

The condition that $k(r,o) = 1$ has been artificially imposed in an effort to clarify the problem. The function k represents a normalized velocity profile, and the function A defines the magnitude of the velocity in the centerplane.

If (23) and (28) are used, (27) becomes

$$\mu \frac{A}{r} \frac{\partial^2 k}{\partial z^2} = \frac{A^2 \rho k^2}{r^3} - \frac{dp}{dr} \tag{30}$$

Under assumption (d), A is a weak function of r, because A would be constant if the displacement were zero. (If it is zero, then the profile is fixed and $k(r,z) = k(z)$ in (29) so that A(r) would be independent of r). Since k is monotonic from $z = 0$ to $z = h/2$, the ratio of the two terms involving k

in (30) can then be approximated by

$$\overline{\left|\mu \frac{A}{r} \frac{\partial^2 k}{\partial z^2}\right|} \Big/ \overline{\left|\frac{A^2 \rho k^2}{r^3}\right|} \cong \frac{R(r)}{Re_0'} \tag{31}$$

where R(r) has a dependence on r of the order of r^2 and the bar refers to an average over z. Thus, at sufficiently large r (assuming that r were not restricted to values less than R_0), the numerator of the left side of (31) is much larger than the denominator, and (30) becomes

$$-\mu A_\infty \frac{\partial^2 k_\infty}{z^2} = \frac{r dp}{dr} \tag{32}$$

Equation (32) implies that $\partial^2 k_\infty / \partial z^2$ is independent of z. If this result is integrated twice and the boundary conditions are imposed, one has

$$k_\infty = \left(1 - \frac{4z^2}{h^2}\right) \tag{33}$$

Furthermore, from (29)

$$A_\infty = \frac{3Q_0}{4\pi h} \tag{34}$$

At small r (except near the points r = 0, z = ± h/2), the k^2 term predominates, and (30) becomes

$$A_0^2 \rho k_0^2 = \frac{r^3 dp}{dr} \tag{35}$$

This implies that k_0 is independent of z for a point away from the wall. Therefore,

$$k_0 = 1 \quad \text{for} \quad |z| < \frac{h}{2} \tag{36}$$

and

$$A_0 = \frac{Q_0}{2\pi h} \tag{37}$$

As the fluid flows toward the origin from a large radius, the radial velocity profile changes smoothly from parabolic to uniform, and A decreases to two-thirds of its value at a large radius. Therefore, the r dependence of $A(r) \cdot k(r,z)$ is much weaker than that of the 1/r term except possibly near the points $(0, \pm h/2)$. Thus, the radial velocity in the vicinity of some finite radius r_1 can be approximated closely by

$$V_r = \frac{-A_1 k_1(z)}{r} \tag{38}$$

where $A_1 = A(r_1)$ and $k_1(z) = k(r_1, z)$.

2.1.3.2 Simplified Tangential Momentum Equation

The simplified tangential momentum equation is

$$\frac{\partial V_\theta}{\partial t} + V_r\left(\frac{\partial V_\theta}{\partial r} + \frac{V_\theta}{r}\right) = \nu\left[\frac{\partial}{\partial r}\left(\frac{\partial V_\theta}{\partial r} + \frac{V_\theta}{r}\right) + \frac{\partial^2 V_\theta}{\partial z^2}\right] \tag{39}$$

The boundary conditions for V_θ at the solid boundaries are given by

$$V_\theta(Ro, z) = R_o \Omega_o e^{i\omega t} \tag{40}$$

$$V_\theta\left(r, \pm \frac{h}{2}\right) = r \Omega_o e^{i\omega t} \tag{41}$$

$$V_\theta(\epsilon_1, z) = \epsilon_1 \Omega_o e^{i\omega t} \tag{42}$$

where ϵ_1 = sink tube radius.

Although the effect of the entrance conditions on the radial velocity profile has been ignored, their effect on the tangential profile is considered, as defined by (40). Since the type of equation and the boundary conditions satisfied by each of the two components of velocity are different, the "entrance

lengths" in general will not be the same. Therefore, the effect of the entrance conditions on the tangential profile is retained to discover a posteriori whether they significantly influence the flow field after entrance effects on the radial profile have been assumed to disappear.

Since (39) is linear, it may lend itself readily to analysis if V_r is found first. In this paper, a method is shown for finding V_θ if V_r is given by a set of functions A_1 and k_1 that apply in appropriately thin annular regions that together fill the chamber. A less complicated method is used to obtain bounding expressions for the gain and frequency response of the rate sensor.

2.2 Solution of Tangential Momentum Equation

2.2.1 Solution in a Given Annulus

Assume that the solution for V_θ in the region about r_1 in which A_1 and k_1 apply is of the form

$$V_\theta = \left[u_1(r,z) + u_2(r,z)\right] \Omega_0 e^{i\omega t} \tag{43}$$

The function u_1 is chosen such that it satisfies the boundary conditions on the top and bottom plate for all r, assuming that k_1 applies over all r, that R_0 is infinite, and that the drain effects are ignored. The function u_2 is then used to satisfy the upstream and downstream boundary conditions on the annulus in which k_1 applies.

The boundary conditions at the top and bottom plates are therefore given by

$$u_1\left(r, \pm \frac{h}{2}\right) = r \tag{44}$$

and

$$u_2\left(r, \pm \frac{h}{2}\right) = 0 \tag{45}$$

Assume that

$$u_1 = \left[\frac{g_1(z)}{r} + r\right] g_2(z) \tag{46}$$

where

$$g_1\left(\pm\frac{h}{2}\right)=0 \tag{47}$$

and

$$g_2\left(\pm\frac{h}{2}\right)=1 \tag{48}$$

From (38), (43), and (46), it can be shown that (39) will be satisfied if

$$\frac{d^2g_2}{dz^2}=\frac{i\omega g_2}{\nu} \tag{49}$$

$$-2A_1k_1g_2=\nu\left(g_2\frac{d^2g_1}{dz^2}+2\frac{dg_2}{dz}\frac{dg_1}{dz}\right) \tag{50}$$

and

$$i\omega u_2-\frac{A_1k_1}{r}\left(\frac{\partial u_2}{\partial r}+\frac{u_2}{r}\right)=\nu\left[\frac{\partial}{\partial r}\left(\frac{\partial u_2}{\partial r}+\frac{u_2}{r}\right)+\frac{\partial^2u_2}{\partial z^2}\right] \tag{51}$$

Equations (49) and (50) can be integrated directly and the boundary conditions in (47) and (48) can be imposed to obtain

$$g_2(z)=\frac{\cosh(az)}{\cosh\left(a\frac{h}{2}\right)} \tag{52}$$

and

$$g_1(z)=\frac{2A_1}{\nu}\int_z^{h/2}\frac{1}{\cosh^2(a\eta)}\int_0^{\eta}k_1(\xi)\cosh^2(a\xi)\,d\xi\,d\eta \tag{53}$$

where $a\equiv\sqrt{\frac{i\omega}{\nu}}$

Now consider (51) for the case in which $k_1\equiv k_o=1$. Because this is a linear partial differential equation which has coefficients constant with respect to z and which has only one term that involves differentiation with respect to z, it can be separated into two ordinary differential equations if $u_2(r,z)$ is chosen to be a product of a function f(r) and a function $\Psi(z)$, or more generally, a summation of such products.

Since boundary conditions that are symmetric with respect to the centerplane will be imposed at a given radius, the proper form of u_2 is

$$u_2 = \sum_n C_n (f_1)_n \psi_n + \sum_n D_n (f_2)_n \psi_n \qquad (54)$$

where $(f_1)_n$ and $(f_2)_n$ are the two independent solutions of the equation governing f_n and ψ_n is the solution of the Ψ_n equation that is symmetric with respect to the centerplane. The function $(f_1)_n$ is chosen as the solution that specifies the manner in which information propagates in the downstream direction, while $(f_2)_n$ specifies the upstream propagation.

Equation (54) does not apply exactly in the region near the drain, because the drain radius is finite (implying that the radial velocity profile is not exactly uniform). However, this solution for $(f_2)_n$ should accurately describe how information propagates upstream in this region. It can be used to show approximately how small the drain tube should be to eliminate its effect on the pickoff, but will otherwise be ignored in keeping with the initial description of the problem.

Consider then only the effect of information that propagates in the downstream direction from the upstream solid boundary, the coupler. If only the effect of the coupler (as well as the top and bottom plates) on the flow in the chamber is considered, then the term $\frac{\partial}{\partial r}\left(\frac{\partial u_2}{\partial r} + \frac{u_2}{r}\right)$ in equation (51) can be ignored. This will be verified later for the case in which $k_1 \equiv k_o$ (that is, when the radial profile is uniform) by showing that the solution for $(f_1)_n$ obtained by ignoring this term is very nearly equal to the solution obtained when it is included. In addition, since it can also be shown that the ratio

$$\left| \frac{\partial}{\partial r}\left(\frac{\partial u_2}{\partial r} + \frac{u_2}{r}\right)\right|_{z=0} \Bigg/ \left|\frac{\partial^2 u_2}{\partial z^2}\right|_{z=0}$$

is a maximum for the case in which $k_1 = k_o$, this term can be neglected in the general case. If this term is neglected, then (54), with $D_n = 0$, represents the general form of the solution of (51) for all k_1. The governing equations are

$$\frac{-A_1}{\nu r}\left[\frac{d(f_1)_n}{dr} + \frac{(f_1)_n}{r}\right] = \beta_n (f_1)_n \qquad (55)$$

and

$$\frac{d^2\psi_n}{dz^2} = \left(a^2 + \beta_1 k_1\right)\psi_n \tag{56}$$

where β_n is a separation constant. The boundary conditions on ψ_n are

$$\psi_n\left(\pm\frac{h}{2}\right) = 0 \tag{57}$$

It should be noted that the ordinary differential equations (49), (50), (55) and (56) have been obtained just by assuming the form of the solution of (39), that is, by using (43), (46) and (54). However, the partial differential equation (39) is linear and the boundary conditions specified by (40), (41) and (42) are such that the problem is well-posed. Then the complete solution thus obtained is unique if it satisfies the appropriate boundary conditions, because existence is a necessary and sufficient condition for uniqueness in this class of problems.

Equation (55) has the solution

$$(f_1)_n = \frac{1}{r} e^{-\frac{v\beta_n r^2}{2A_1}} \tag{58}$$

where an arbitrary multiplicative constant of this solution has been absorbed into ψ_n.

It is clear that in a region near r_1, u_2 has a solution

$$u_2 = \sum_n C_n \frac{1}{r} e^{-\frac{v\beta_n r^2}{2A_1}} \psi_n \tag{59}$$

and that this is an eigenvalue problem. The eigenfunctions ψ_n depend on k_1 in that region. The eigenvalues can be found by imposing the boundary conditions given by (57). The coefficients c_n can be found by requiring the solution to

satisfy a boundary condition at the upstream limit of the region in which k_1 holds.

It should be pointed out that this eigenvalue problem is not Sturm-Liouville. The eigenvalues are complex and the differential operator is not self-adjoint since a^2 in (56) is imaginary. Nevertheless, it is still possible (App B) to use typical orthogonal expansion techniques in finding C_n. However, before the integration is performed to find C_n, both sides of the boundary value equation (obtained from (43), (59) and the upstream boundary condition) must be multiplied by $k_1 \psi_m$ instead of the complex conjugate of this quantity, which is the usual procedure with a Sturm-Liouville problem.

2.2.2 Solution for the Entire Chamber

An approximate solution for V_θ at the pickoff can be found through a stepwise procedure. The procedure is started by specifying the functions A_1 and k_1 near the coupler and the range over which these functions will be applied. The boundary condition at R_o given by (40) is used to find the coefficients of the series solution for u_2 valid in that region. The solution is then found for the lower limit of r at which these expressions for A_1 and k_1 apply. This function is taken as the upstream boundary condition for the next annulus in which a new pair of expressions for A_1 and k_1 apply, and the process continues until a solution is obtained in the vicinity of the hypothetical pickoff location. When this solution is found, the characteristics of the rate sensor can be described.

It should be pointed out that the tangential shear is not continuous across the boundaries of the annuli. Since $(f_2)_n$ has been ignored, the shear is not continuous if the velocities are matched. However, the error can be made appropriately small by choosing annuli that are sufficiently thin in the r direction.

According to assumptions (3) and (4) made in Section 2.1, the output, Φ, of the hypothetical pickoff is given by

$$\Phi = \frac{\partial}{\partial \Omega} \left\{ \left\{ \frac{\rho K_1}{h} \int_0^{h/2} \left[\left(V_{\theta_{rel}}^2 + V_r^2 \right) \sin \left\{ \arctan \frac{V_{\theta_{rel}}}{V_r} \right\} \right]_{r=R_1} dz \right\} \right\} \tag{60}$$

where $V_{\theta rel}$ is the tangential velocity relative to the wall and K_1 is some constant. Since $|V_\theta| \ll |V_r|$ and V_θ is a linear function of Ω_o,

$$\Phi \cong \frac{\rho K_1}{\Omega_o h e^{i\omega t}} \int_0^{h/2} \left[V_{\theta_{rel}} V_r \right]_{r=R_1} dz \tag{61}$$

It has also been assumed that the output of the pickoff in the actual sensor is a linear function of that in the mathematical model; that is,

$$\int_0^{h/2} \left[V_{\theta_{rel}} V_r\right]_{r=R_1} dz = K_2 \int_0^{R_1} \left[V_{\theta_{rel}} V_z\right]_{z=z_1} r dr \tag{62}$$

where z_1 is the pickoff location in the drain.

If experimental data obtained from a sensor with a pickoff in the drain is compared to expressions for the output of the hypothetical pickoff in the mathematical model, then changes in K_2 during an experiment can lead to an error that is not related to the accuracy of the analysis in predicting the features of the flow in the chamber, the domain in which this solution applies.

In the real sensor, K_2 will be influenced by changes in the fluid losses in the corner-drain region brought on by changes in the fluid parameters, and by any dependence that the streamline pattern may have on the Mach number. It should be remembered that one purpose of this approach is to establish the significance of these effects by ignoring them in the analysis. Thus, in the theoretical results it is necessary to assume that K_1 is some appropriate constant without any attempt at justification. Because of the assumption used to obtain (62), this is equivalent to assuming that K_2 is constant.

By comparing the output at $\omega = 0$ to that which would exist if the flow in the chamber were inviscid (and $\omega=0$), K_1 can be eliminated from the expression for d-c gain. From (4), (5), and (60), the expression, G_0, for d-c gain would be given by

$$G_0 = \frac{\int_0^{h/2} \left[V_{\theta_{rel}} V_r\right]_{\substack{r=R_1 \\ \omega=0}} dz}{-\frac{Q_0}{4\pi} \frac{R_0^2}{R_1^2} \Omega_0} \tag{63}$$

Even though this expression is 1 for large Re_D' (assuming that a solution over the entire range of Re_D' were known), this does

not imply that the efficiency of the sensor is 100 percent in that range of Re_o', for the losses in the drain region could be significant. The value of (63) is independent of such losses.

If K_1 is chosen so that Φ is 1 at $\omega = 0$, another function, $G_{i\omega}$, is obtained that describes the frequency response of the sensor.

2.3 Bounding Expressions for the Stepwise Solution

The method described here will involve a great deal of effort, principally because of the stepwise procedure outlined. Before this task is undertaken, the importance of the changes in k_1 with respect to r should be established. This can be done by solving two hypothetical problems, one in which the radial velocity profile is assumbed parabolic throughout the chamber, and one in which it is assumed uniform.

It can be shown (App C) that these two solutions will provide upper and lower bounds for the results obtained by the lengthy stepwise procedure for at least a portion of the ranges of the governing parameters. The parabolic solution can be shown to provide an upper bound for G_o, and the uniform one, a lower bound. To discuss the nature of the bounds these solutions provided for $G_{i\omega}$, the contributions of u_1 and u_2 to the output signal must be discussed separately.

For all ω' (where $\omega'=\omega h^2/\nu$), the parabolic solution provides a maximum expression (and the uniform a minimum) for phase lag in the signal due to u_1. At small ω', the amplitude of $G_{i\omega}$ due to u_1 depends only weakly on the shape of the radial profile, although it does appear that the parabolic solution provides a maximum expression for amplitude, and the uniform, a minimum. As ω' increases, the effect on the amplitude caused by the variation of the radial profile eventually becomes significant. For large ω', the uniform solution provides a maximum, and the parabolic, a minimum for the amplitude of $G_{i\omega}$ due to u_1.

For the portion of $G_{i\omega}$ due to u_2, the uniform solution provides a maximum expression for phase shift, and a minimum for amplitude. The parabolic provides a minimum for phase shift and a maximum for amplitude.

Several interesting features of $G_{i\omega}$ should be pointed out. The amplitude of the contribution of u_1 to $G_{i\omega}$ diminishes to zero, and the phase lag approaches some constant as the frequency increases. The amplitude of the contribution of u_2 to $G_{i\omega}$ approaches a constant roughly $4/Re_o'$ times that at dc, and the phase lag increases without limit.

If Re_0' is sufficiently small, the dc signal due to u_2 is attenuated so much as it is transported from the coupler to the pickoff that its contribution is below the noise level for all ω'. Then only the contribution due to u_1 need be considered and the hypothetical solutions provide bounds as specified above.

At small ω', if Re_0' is not sufficiently small to wipe out the contribution due to u_2 but small enough to ensure that the contribution due to u_1 predominates, then either expression for the amplitude may be used because of their slight difference, while a maximum value for phase shift can be found from the parabolic solution and a minimum from the uniform.

At sufficiently large Re_0', the u_2 contribution predominates and specifies the nature of the bounds these expressions provide. At intermediate values of Re_0' when ω' is small, both contributions are of nearly equal magnitude, and the behavior is mixed.

As ω' increases, the value of Re_0' at which the behavior becomes mixed decreases, as does the value at which the contribution due to u_2 predominates. At sufficiently large ω', u_2 predominates for all values of Re_0' sufficiently large to insure that its amplitude is not attenuated below the noise level.

This information has been summarized in the representation in figure 5, with some added information based on a number of comparisons of the solutions to be obtained in 2.3.1 and 2.3.2.

Zone 1 represents the region in which u_1 predominates. Either solution can be used to express the amplitude of $G_{i\omega}$ at small ω'. At larger ω', the difference between these two expressions for amplitude is not small. In that range of ω', the parabolic solution expresses a lower bound for amplitude, and the uniform, an upper bound. The parabolic solution expresses a maximum for phase shift, and the uniform, a minimum for all ω'.

Zone 2 is the region in which the contribution due to u_1 and u_2 must both be considered, but in which the phase lag of either is small. If the difference in amplitude or phase of the two solutions is significant, they may be regarded as bounding expressions. Otherwise, either expression may be used.

Zone 3 represents the only region in which these two solutions cannot be used directly to bound the amplitude and phase of $G_{i\omega}$. In this region, the contributions due to u_1 and

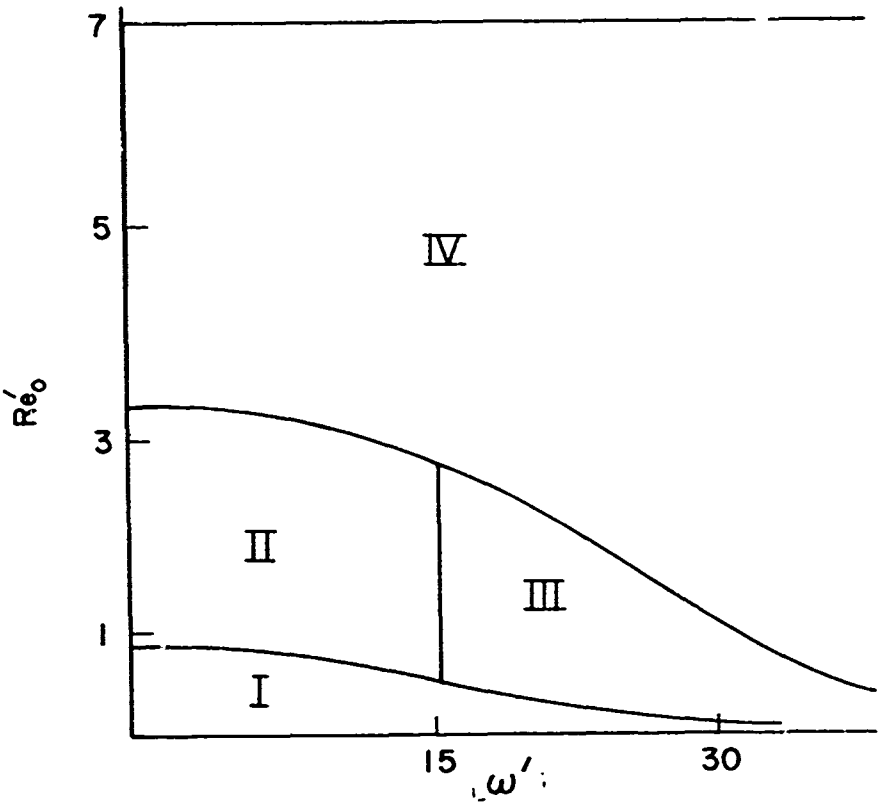

Figure 5. Boundary zones of hypothetical solutions.

u_2 can interfere destructively, since they are nearly of equal amplitude but out of phase by large margins. The amplitude and phase can change radically with ω' in this zone. This behavior is reflected in both solutions, but the values of ω' and Re_o' at which similar phenomena occur are different in the two solutions. This implies that the two solutions can be used to isolate the range of Re_o' at which a specific frequency response feature occurs (such as sudden reduction and subsequent recovery of amplitude of $G_{i\omega}$ as ω' increases), as well as the range of ω' in which this behavior occurs. However, the two solutions at a specific Re_o' and ω' cannot be used in a direct manner to estimate the actual behavior. The solution at neighboring values of Re_o' and ω' is required for this.

The exact range of zone 3 has not been accurately specified at this time, but it appears to extend from approximately .5 to 3 on the Re_o' axis when $\omega' = 15$.

Zone 4 represents the region in which u_2 predominates. In this region, the parabolic solution provides an estimate for the maximum amplitude of $G_{i\omega}$ and the minimum phase lag. The uniform solution has the complimentary features.

2.3.1 Solution for a Parabolic Profile

If (33) and (34) are assumed to apply throughout the chamber, it can be shown (App D) that

$$G_0 = Re_0' \left[\frac{17}{70} - \frac{9}{4} \sum_{n=0}^{\infty} \left\{ \left(e^{\frac{-o\lambda_n}{3Re_0'}} \right) \frac{o I_n' \, o I_n''}{o I_n'''} \right\} \right] \tag{64}$$

and

$$G_{i\omega} = \frac{9Re_0'}{G_0} \left[\phi_1(\omega') - \frac{1}{4} \sum_{n=0}^{\infty} \left\{ \left(e^{\frac{-\lambda_n}{3Re_0'}} \right) \frac{I_n' I_n''}{I_n'''} \right\} \right] \tag{65}$$

where

$$\phi_1(\omega') = \frac{-4}{3(\omega')^2} \left(1 + i \frac{165}{\omega'} \right) - \frac{32}{(\omega')^2} \left(1 - i \frac{55}{4\omega'} \right) \frac{\tanh\left(\frac{\sqrt{i\omega'}}{2} \right)}{\sqrt{i\omega'}} + \frac{4}{3(\omega')^2} \left(1 + i \frac{3}{\omega'} \right) \tanh^2 \left(\frac{\sqrt{i\omega'}}{2} \right) \tag{66}$$

$$I_n' = \int_0^1 \left\{ \frac{\cosh\left(\frac{w}{2} \sqrt{i\omega'} \right)}{\cosh\left(\frac{1}{2} \sqrt{i\omega'} \right)} \left[\phi_2(w, \omega') + \frac{2}{3Re_0'} \right] - \frac{2}{3Re_0'} \right\} (1 - w^2) \psi_n \, dw \tag{67}$$

$$I_n'' = \int_0^1 (1 - w^2) \psi_n \, dw \tag{68}$$

$$I_n''' = \int_0^1 (1 - w^2) \psi_n^2 \, dw \tag{69}$$

$$\phi_2(w, \omega') = \left[-\left(\frac{1}{2} + \frac{i}{\omega'} \right) w + \frac{w^3}{6} \right] \frac{\tanh\left(\frac{w}{2} \sqrt{i\omega'} \right)}{\sqrt{i\omega'}} - \frac{i}{2\omega'} \left(1 - w^2 \right) + \left(\frac{1}{3} + \frac{i}{\omega'} \right) \tanh \frac{\left(\frac{1}{2} \sqrt{i\omega'} \right)}{\sqrt{i\omega'}} \tag{70}$$

$$\psi_n = e^{\frac{\gamma_n'}{4}(w^2)} M\left[-p_n, \frac{1}{2}, -\frac{\gamma_n'}{2}(w^2)\right] \tag{71}$$

$$\gamma_n' = -\left(1+\sqrt{1+i\omega'+S_n}\right) \tag{72}$$

$$P_n = \frac{S_n}{8\left(1+\sqrt{1+i\omega'+S_n}\right)} \tag{73}$$

$$\lambda_n = i\omega' + S_n + 2\left(1+\sqrt{1+i\omega'+S_n}\right). \tag{74}$$

$$\omega' = \frac{\omega h^2}{\nu} \tag{75}$$

$$M\left[a_1, a_2, x\right] = \sum_{n=0}^{\infty} \frac{\Gamma(a_1+n)\Gamma(a_2)x^n}{\Gamma(a_2+n)\Gamma(a_1)\,n!}. \tag{76}$$

$M\left[a_1, a_2, x\right]$ is the confluent hypergeometric function, and S_n is a member of the ordered set of values which satisfy the equation

$$M\left[-\frac{S}{8\left(1+\sqrt{1+i\omega'+S}\right)}, \frac{1}{2}, \frac{1}{2}\left(1+\sqrt{1+i\omega'+S}\right)\right] = 0, \tag{77}$$

The prescript "o" used in (64) is used to denote the values of I_n', I_n'', I_n''', and λ_n when ω' is zero.

The computer program used to numerically evaluate (64) and (65) is presented in Appendix E. The series in both (64) and (65) have been truncated after the first term in the evaluation presented. The reason for this can be discussed more clearly when the solution for a uniform radial profile has been shown.

2.3.2 Solution for a Uniform Profile

If (36) and (37) are used, it can be shown (app F) that the functions that describe the gain and frequency response are given by

$$G_0 = Re_0' \left[\frac{1}{6} - \sum_{n=0}^{\infty} \frac{16}{(2n+1)^4 \pi^4} e^{\frac{-(2n+1)^2 \pi^2}{Re_0'}} \right] \tag{78}$$

and

$$G_{i\omega} = \frac{Re_0'}{G_0} \left\{ \frac{1}{i\omega'} \left[\tanh^2 \left(\frac{\sqrt{i\omega'}}{2} \right) + \frac{2}{\sqrt{i\omega'}} \tanh \left(\frac{\sqrt{i\omega'}}{2} \right) - 1 \right] \right.$$
$$\left. - \sum_{n=0}^{\infty} \frac{16}{(2n+1)^2 \pi^2} \frac{\left[\frac{(2n+1)^2 \pi^2}{i\omega' + (2n+1)^2 \pi^2} - \frac{i\omega'}{2Re_0'} \right]}{i\omega' + (2n+1)^2 \pi^2} e^{\frac{-\left[i\omega' + (2n+1)^2 \pi^2 \right]}{2Re_0'}} \right\} \tag{79}$$

In these equations both of the infinite series expressions, which have been generated by u_2, can be truncated after the first term. The reasons for this deserve elaboration.

When Re_0' is of the order of 1, the magnitude of the exponential term diminishes rapidly as n increases. This results from the fact that the higher harmonics of ψ_n are attenuated more than the fundamental as the signal propagates from the coupler to the pickoff due to the higher viscous shear they generate.

In addition, the contribution of each mode due to the boundary condition at the coupler varies with the order of the mode. Since the function that the series must satisfy at the coupler when ω' is small has a single maximum and no inflection points, the fundamental mode contributes most strongly to the series representation at small ω'. In (78), the coefficient of the exponential for n=0 is 81 times that for n=1. This is nearly the same as in the series in (64). Thus, for small ω', even for that range of Re_0' in which the higher order modes are not greatly attenuated between the coupler and the pickoff, their contributions are not significant.

As ω' increases, the significance of the higher order modes increase, but never predominates. For very large ω', the coefficient in (79) for n=0 is 9 times that for n=1. Again, the behavior is nearly the same in (65). It might be argued that this significance is not sufficiently weak to warrant truncation. However, in that range of ω', the amplitude $G_{i\omega}$ is so much less than the d-c value that the exact features are not of great interest to a control system designer. Therefore, the series can be truncated after the first term for all Re_0' and ω' within the intent of this investigation.

No program is presented for the solution of (78) and (79) because of their rather simple nature. It should be noted however, that double precision is required in evaluating the bracket containing the hyperbolic tangent terms when ω' is very small.

2.4 Sources of Errors

2.4.1 Error due to Neglecting $\frac{\partial}{\partial r}(\frac{\partial u_2}{\partial r} + \frac{u_2}{r})$ when the Radial Profile is Uniform

Suppose that V_θ were found near the pickoff by using (59), by applying the boundary condition at R_o given by (40), and assuming that the radial profile were uniform throughout the chamber. Suppose further that this same procedure were repeated except that the term $\frac{\partial}{\partial r}(\frac{\partial u_2}{\partial r} + \frac{u_2}{r})$ were retained in finding an equation analogous to (59). Now let the ratio of the first term in the series of the former result to the first term in the latter result be defined as the quantity B. It can be shown (app G) that B is given by

$$B = e^{-\left(i\omega' + \pi^2\right)\frac{\upsilon R_o'}{2A_o h^2}} \sum_{m=o}^{\infty} \frac{\left[\frac{1}{4}\left(i\omega' + \pi^2\right)\frac{R_o^2}{h^2}\right]^m \Gamma\left(\frac{A_o}{2\upsilon}\right)}{m!\,\Gamma\left(\frac{A_o}{2\upsilon} + m\right)} \tag{80}$$

If $h \ll R_o$, and if Re_o' is of the order of one, the dominant term in the series above is the term for which m is equal to the positive integer nearest the value $(\frac{\pi^2}{2Re_o'})-1$. The number of terms that must be considered in this series is then of the order of 10. However, since

$$\frac{A_o}{2\upsilon} = \frac{Re_o'}{2}\frac{R_o^2}{h^2} >> \frac{R_o}{h} >> 1, \tag{81}$$

it is seen that

$$\sum_{m=o}^{\infty} \frac{\left[\frac{1}{4}\left(i\omega' + \pi^2\right)\frac{R_o^2}{h^2}\right]\Gamma\left(\frac{A_o}{2\upsilon}\right)}{m!\,\Gamma\left(\frac{A_o}{2\upsilon} + m\right)} \cong \sum_{m=o}^{\infty} \frac{\left[\frac{1}{4}\left(i\omega' + \pi^2\right)\frac{R_o^2}{h^2}\right]^m}{m!}\left(\frac{A_o}{2\upsilon}\right)^{-m} \tag{82}$$

$$= e^{\left(i\omega' + \pi^2\right)\frac{\upsilon R_o^2}{2A_o h^2}}$$

Thus, from (80) and (82), B is extremely close to 1 when Re_o' is of order 1 or larger and $h \ll R_o$.

The error in the solution for u_2 caused by neglecting this viscous term will be larger if Re_o' is very small, because more terms of the series in (80) must then be considered, making the approximation for the ratio of the gamma functions less accurate. However, when Re_o' is very small, the contribution of u_2 to the solution for V_θ near the pickoff is negligible. Thus the error generated in G_o and $G_{i\omega}$ by neglecting the term $\partial/\partial r(\partial u_2/\partial r + u_2/r)$ is small for all Re_o' in the fully developed range when the radial profile is uniform. As indicated in Section 2.2.1, this implies that the error is small in general.

2.4.2 Error Due to Neglecting Entrance Effects on the Radial Velocity Profile

It was assumed that the entrance effects did not influence the radial profile throughout the chamber. In the actual sensor the radial profile should be significantly influenced by the upstream boundary conditions in the outer portion of the chamber for the values of Re_o' near 7. When Re_o' is decreased by changing h in the upper portion of the fully developed range, the decrease in V_θ in the actual sensor will not be as large as that predicted by this analysis, since the viscous losses in the actual model are not as large. When Re_o' is decreased in the lower portion of the fully developed range, however, the proportionate decrease of V_θ should be predicted accurately, since the range of r in which the profile is not fully developed is quite small. Consequently, if the theoretical curve and the data are normalized so that they intersect when Re_o' is 7, the slope of the theoretical curve of G_o as a function of Re_o' in the upper portion of the fully developed range should not be as flat as that of the empirical curve.

2.4.3 Effects of the Corner and Drain on Sensor Characteristics

It is shown in Appendix C that if $k_1 = k_o$, the function $(f_2)_n$ which describes the propagation of the information in the upstream direction is given by

$$(f_2)_n = r^{\frac{-Re_o}{2}} K_{\frac{Re_o}{2}-1}\left(\sqrt{i\omega' + (2n+1)^2\pi^2}\,\frac{r}{h}\right) \qquad (83)$$

where $Re_o = U_o R_o/\nu = Q/2\pi h\nu$, and $K_{(Re_o/2)-1}$ is the modified Bessel function of the second kind of order $(Re_o/2)-1$.

Just upstream of the drain, $(f_2)_n$ behaves nearly as r^{1-Re_o}. Since Re_o is on the order of 10^4 in this experiment, drain effects are extremely localized. The corner in the real sensor can then be defined as the region extending from a radius just upstream of the drain to a plane sufficiently far downstream in the drain to ensure that the streamlines lie in a cylindrical surface concentric with the drain wall.

Consider what would happen if $(f_2)_n$ were retained in the chamber solution, and the corner region of a two drain sensor were instead described simply as a curve F(r,z) as shown in figure 6. The curve F(r,z) is chosen so that continuity is satisfied locally when the two transport velocity profiles are matched.

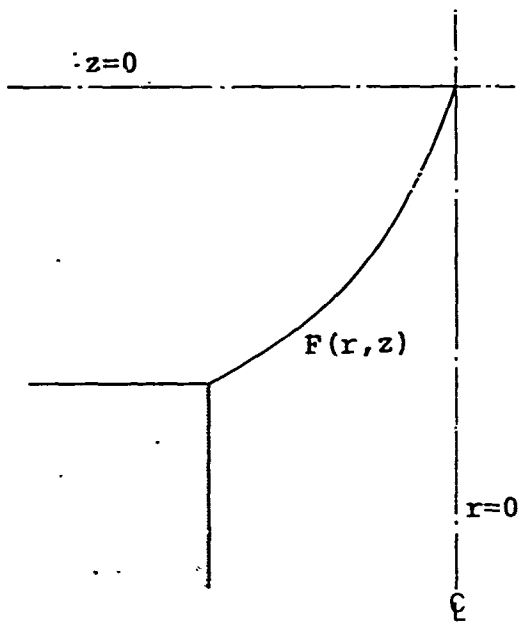

Figure 6. Corner Region Model

Since the fluid particles approach F(r,z) in a plane parallel to the chamber walls and leave on a surface parallel to the drain wall, this description of the acceleration effects on the transport velocity is clearly nonphysical. However, this description can be used to discuss to a first-order approximation the total viscous losses in the tangential component near the corner.

Note first that in the tangential momentum equation the acceleration across this curve is zero if there is no dissipation. The nonphysical description of the transport component of velocity influences the tangential equation only in that it arbitrarily sharpens the manner in which the transport velocity changes from the chamber function to the drain function. If the change is smooth and monotonic in the actual case, as it is near the points (R_1, $\pm$ h/2), then the error is second order. If the fluid stagnates in going from one region to the next, as it does near (0, 0), then the error may not be small. This approach can then be used to examine the viscous loss in the tangential component near (R_1, $\pm$ h/2).

The tangential velocity in the chamber in the region near F(r,z) is given approximately by

$$v_\theta = \left[\left(\frac{g_1}{r} + r\right) g_2 - \sum_n C_n (f_1)_n \psi_n + \sum_n D_n (f_2)_n \psi_n\right] \Omega_o e^{i\omega t} \tag{84}$$

where g_1, g_2, $(f_1)_n$ and ψ_n are found by setting $k_1 = k_o$. In the drain the tangential velocity is given (app H) by

$$v_\theta = \left[R_1 \frac{I_1\left(\sqrt{\frac{i\omega'}{S_\ell^2}}\,\frac{r}{R_1}\right)}{I_1\left(\sqrt{\frac{i\omega'}{S_\ell^2}}\right)} + \sum_n C_n' (f_1)_n' \psi_n' \right] \Omega_o e^{i\omega t} \tag{85}$$

where

$$(f_1)_n' = \frac{r}{R_1} e^{\frac{-\delta_n}{2}\left(\frac{r}{R_1}\right)} M\left[\left(1 + \frac{i\omega'}{S_\ell^2 \delta_n} + \frac{\delta_n^3}{16 Re_1^2} - \frac{\delta_n}{4}\right), 2, \delta_n \left(\frac{r}{R_1}\right)^2\right] \tag{86}$$

$$\psi_n' = e^{-\frac{2(\delta_n)^2}{Re_1}\frac{z}{R_1}} \tag{87}$$

$$S_\ell = \frac{h}{R_1} \tag{88}$$

$$Re_1 = \frac{[v_{z\,drain}]_{avg} R_1}{\nu} = \frac{\dot{m}}{\pi R_1 \mu} \tag{89}$$

and $\dot{m}$ = mass flow rate. I_1 is the modified first-order Bessel function of the first kind and the δn's are the ordered set of values that satisfy the relationship

$$M\left[\left(1+\frac{i\omega'}{4S_1^2\delta_n}+\frac{\delta_n^3}{16Re_1^2}-\frac{\delta_n}{4}\right),2,\delta_n\right]=0 \qquad (90)$$

The coefficients C_n are specified by the boundary conditions at some boundary upstream of the drain (since $(f_2)_n$ is effectively zero just upstream of R_1) while C_n' and D_n are chosen so that the tangential velocity and the shear are continuous across F(r,z). Some general features of this matching can be discussed without going into explicit detail.

Consider the tangential velocity profile in the chamber sufficiently far upstream of F(r,z) to eliminate the influences of $(f_2)_n$. If the tangential profile decreases evenly from a maximum at the centerline to a minimum at the wall, then the values found for the coefficients D_n are small, and the coefficients C_n' are nearly equal to those that are chosen simply to match V_θ at F(r,z). However, if the profile is significantly blunted, the shear generated by this matching condition will be large.

In the real sensor, the matching region may well span most of the region $|z| < h/2$, $r < R_1$, as well as include a significant stagnation region about the point (0,0) and a separation region around the corner. In addition, the drain may distort the radial profile upstream of the corner and cause a small V_z to exist. However, to a first order approximation this distortion will not change the axisymmetric propagation of tangential shear along a given streamline. The field will only be distorted. Therefore, the net effect of the viscous dissipation at the corner on the output characteristics should be about the same as that predicted by this description, that is, that the losses near the corner will be relatively high if the tangential velocity profile is somewhat blunted.

Consider what happens for the case when $\omega = 0$ as Re_o' is reduced (by decreasing h, for instance) from a large value to the value Re_{ocrit}', the point at which the flow becomes fully developed. The tangential velocity profile near the corner changes from nearly uniform (for nearly inviscid flow) to nearly parabolic (g_1 at $\omega = 0$ is the parabolic profile if $k_1 = k_o$). The bluntness of the tangential profile is then reduced considerably. Although a pickoff mounted in the chamber would see a decrease in G_o as Re_o' is reduced, due to the increased chamber losses, one mounted in the drain would see at

best a small change. Because little of the information destroyed by the boundary layer can be recovered by a pickoff in the drain due to the bluntness of the tangential profile, changing the relative boundary layer size should not greatly change the sensor gain relative to the inviscid case.

Consider next the effect of the corner losses on the frequency response of the sensor. Since the magnitude of $g_2(z)$ near the wall relative to the value at the center plane increases as ω' increases, the profile is reduced more at the center plane with increasing ω'. Because this effect leads directly to a blunting of the tangential profile, the pickoff will recover a smaller portion of the total time-dependent information as ω' increases. This implies that the attenuation predicted by this analysis will not be as large as that measured with the experimental model. As ω' increases the pickoff will also recover a smaller portion of the information near the wall, which is in the closest phase agreement with the sensor motion. This implies that the phase shift predicted by this analysis will not be sufficiently large.

It is possible to make two other observations about the losses in the corner-drain region. The magnitude of the lower order eigenvalues of (90) is of the order of 10. Since Re_1 is of the order of 10^4 in this experiment, ψ_n' is very nearly one for the lower order eigenfunctions if z is of the order of R_1. In addition, the term δ_n^3/Re^2_1 in the first coefficient of the hypergeometric function can then be ignored. Only a few terms should be needed to describe the tangential profile in the drain, so the first result states that the losses in the drain tube can be ignored. The second result implies that the losses in the corner region are independent of Re_1, for this parameter does not appear in either (84) or in the simplified version of (85). This latter result is important and will be discussed in the experimental phase of the study.

3. EXPERIMENT

3.1 Approach

It is possible to obtain some important information about the viscous effects in the chamber and in the corner region by comparing this analysis with data obtained for a properly chosen set of conditions.

3.1.1 Determination of G_o

The accuracy of the analysis in predicting G_o when only the chamber losses are varied is first examined. Data

relating G_o to Re_o' was obtained by changing h, since this is the only parameter that can be easily varied in Re_o' to cause the gain to approach some constant at large Re_o' (for the purpose of normalizing the data to compare it with theory). Viscosity could also be varied, but such an experiment would surely be unmanageable.

Since Re_1 is independent of h, the accuracy of predicting chamber losses can be tested independently of testing the prediction that corner losses are not a function of Re_1.

If the previous test is repeated for various values of $\dot{m}$ (and thus various values of Re_1), then curves can be obtained that examine ranges of Re_o' that have differing upper limits. The degree of correlation of these curves would reveal some information about the dependence on Re_1 of the losses at the corner, as will be discussed later.

3.1.2 Determination of G, $G_{i\omega}$, and the Corner Losses due to Re_1

3.1.2.1 Influence of Re_1 on G and $G_{i\omega}$

It is of great interest to examine the accuracy of this analysis in predicting $G_{i\omega}$ as well as the dimensional d-c sensor gain (that is, not divided by inviscid gain), G, if Q_o and ν are varied. But since these latter variations would lead to a change in Re_1, it is necessary to carefully choose the experimental conditions in order that accurate conclusions can be drawn.

In the range $Re_o' < 1$, even the first terms in the series portions of the solutions for G_o and $G_{i\omega}$ can be ignored. This is equivalent to stating that the contributions due to the entrance conditions are negligible, or that the features of V_θ near the pickoff are specified by u_1.

It will now be shown that in this range of Re_o' not only can one conduct tests that predict G for changing Q_o and ν as well as tests that predict $G_{i\omega}$, but that these same tests can investigate in different manners whether the losses at the corner depend on Re_1. It is not unreasonable to restrict the range of Re_o' to values less than one, particularly in the first planned experimental study of the fully developed range, since this limited range is just that which was previously specified by intuitive means to the most advantageous range, the range in which entrance conditions have no effect on signal output.

3.1.2.2 $G_{i\omega}$ and the Dependence of the Corner Losses on Re_1

Suppose that an experiment were conducted in this range of Re_o' to predict $G_{i\omega}$ for various values of Re_o' obtained

by varying $\dot{m}$. Because Re_1 is also a function of $\dot{m}$, any influence of Re_1 on the losses at the corner could appear and confuse the results.

For each value of Re'_o, data would be reduced for comparison to the analytical expression for $G_{i\omega}$ by comparing the magnitude of the signal at various values of ω' to that d-c. Thus, this data would not be influenced by the magnitude of u_1 at d-c or any dependence on Re_1 of the manner in which the magnitude of the tangential velocity profile is altered at the corner, since those dependences are eliminated when the signal is compared to d-c.

However, the data could be influenced by any dependence on Re_1 of the manner in which the shape of the tangential profile is altered at the corner. It has already been predicted in section 2.4.3 that the losses at the corner depend upon the bluntness of the profile. Because the shape of u_1 is a function of ω', an error should be expected in the analytical expression for $G_{i\omega}$ that is a function of ω'. However, since the shape of u_1 is not a function of Re'_o, the shape of the velocity profile at the corner is the same for a given ω' for all values of Re_1 tested. As a result, the shape effects at the corner are independent of Re_1 if the error in predicting $G_{i\omega}$ is a function of only ω' for values of Re'_o less than one that are obtained by changing $\dot{m}$.

3.1.2.3 G and the Dependence of the Corner Losses on Re_1

For $Re'_o < 1$, G_o is proportional to Re'_o in both the uniform and parabolic radial profile solutions. It can then be shown that this analysis predicts that, for a pickoff in the drain and $Re'_o < 1$, G is given by

$$G = K_3 \frac{\dot{m}^2 h}{\mu R_1^3} \qquad (91)$$

where K_3 is a function of pickoff design and location as well as the losses at the corner.

It should be recalled that only the magnitude of u_1 varies if $\dot{m}$ and μ are changed for $\omega = 0$. The outcome of an experiment conducted to predict G will then be influenced by the dependence on Re_1 of the manner in which the magnitude of the tangential profile is altered by the viscous losses at the corner. The degree to which K_3 depends on Re_1 can be demonstrated by tests that show how curves for G versus $\dot{m}$ correlate for various gases. Since Re_1 changes for a given $\dot{m}$ when μ is changed, the magnitude effects will be independent of Re_1 if the experimental curves correlate when (91) is used.

These tests should show whether the corner losses are independent of Re_1 and should demonstrate the accuracy of this analysis in predicting the effects of any design change other than a change in the pickoff-drain configuration.

3.2 Apparatus

Data points were obtained from the experimental model shown in figure 4. For the frequency response data, the chamber height was fixed at 0.035 in.

Data points relating G_o to Re_o' were obtained by varying the chamber height between 0.250 and 0.004 in. Mass flow rate was held constant in obtaining a single curve, but was varied in a series of such tests, as previously discussed.

The predictions of (91) were tested by varying $\hat{m}$ at a fixed chamber configuration. The gain was measured using three different gases: carbon dioxide, air, and helium.

In every test the output of each channel of the pickoff could be monitored. A miniature hot-wire probe was used to measure flow rate, and a strain gauge transducer was used to measure pressure. The load resistance in each channel could be varied by changing a valve downstream of the transducer cavity.

Only the data points for an infinite load resistance are presented in this paper, because it was decided that the characteristics of the sensor for a blocked load should be analyzed before the sensor's load sensitivity is discussed. With an infinite load resistance, the frequency response of the readout system was high compared with that of the rate sensor. Direct measurement with the pickoff and readout assembly indicated that the amplitude was down about 1 dB relative to d-c at 100 Hz.

4. RESULTS

4.1 Data and Theory for G_o

Data points relating G_o to Re_o' are shown in figure 7. Solutions of (64) and (78) are also shown in this same figure. The data have been normalized to fall midway between the two theoretical curves so that the shapes of these curves can be compared. The actual value of G_o for each data point can be obtained by multiplying the value shown by 1.49, or by regarding the value of the data point at $Re_o' = 7$ as having a value $G_o = 1.00\ (\pm\ 0.02)$.

Data obtained at a very high Re_1 (over a range of Re'_o up to 20) showed that the curve was flat within an experimental accuracy of several percent for values of Re'_o above 7. The data for the largest Re_1 shown here were therefore normalized with respect to its value near $Re'_o = 7$, the largest value of Re'_o that could be obtained at that value of Re_1.

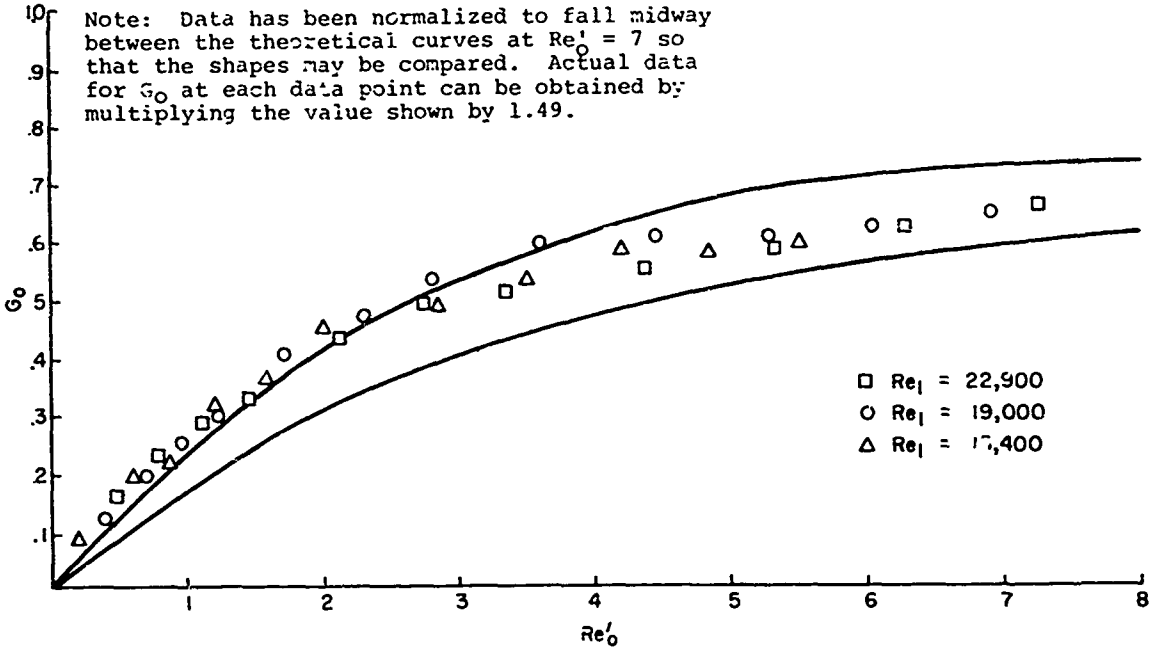

Figure 7. Nondimensional gain.

Since the curves for the smaller values of Re_1 did not have that great a range of Re'_o, they were normalized to fit the curve for the largest Re_1 at their outer data point.

This method of fitting the data curves together is in a sense artificial, but it can reveal some information. It should be noted that the shape of V_θ does depend on Re'_o in this range, since u_2 cannot be neglected. Then if the manner in which the losses near the corner change the shape of the tangential profile were to depend on Re_1, the shapes of these curves would be different. They would not be superimposed on each other when normalized in this manner.

The information that is lost through this method is the dependence on Re_1 of the alteration of the magnitude of the tangential profile near the corner, since the information about the magnitude of the curve is lost. However, this question is explored in the next comparison.

4.2 Data and Theory for G

Two series of tests were conducted to investigate the dependence of K_3 in (91) on Re_1. The results of the first series are shown in figure 8. The gain of the sensor as a function of standard volumetric flow rate is plotted for two different gases: air and carbon dioxide. A parabolic curve was drawn to intersect the empirical curve for air somewhere in the middle of its range. Deviations of the data from this curve can be considered to arise from a change in the value of K_3. This parabolic curve and (91) were then used to obtain a similar curve through the data points for carbon dioxide by assuming K_3 is constant.

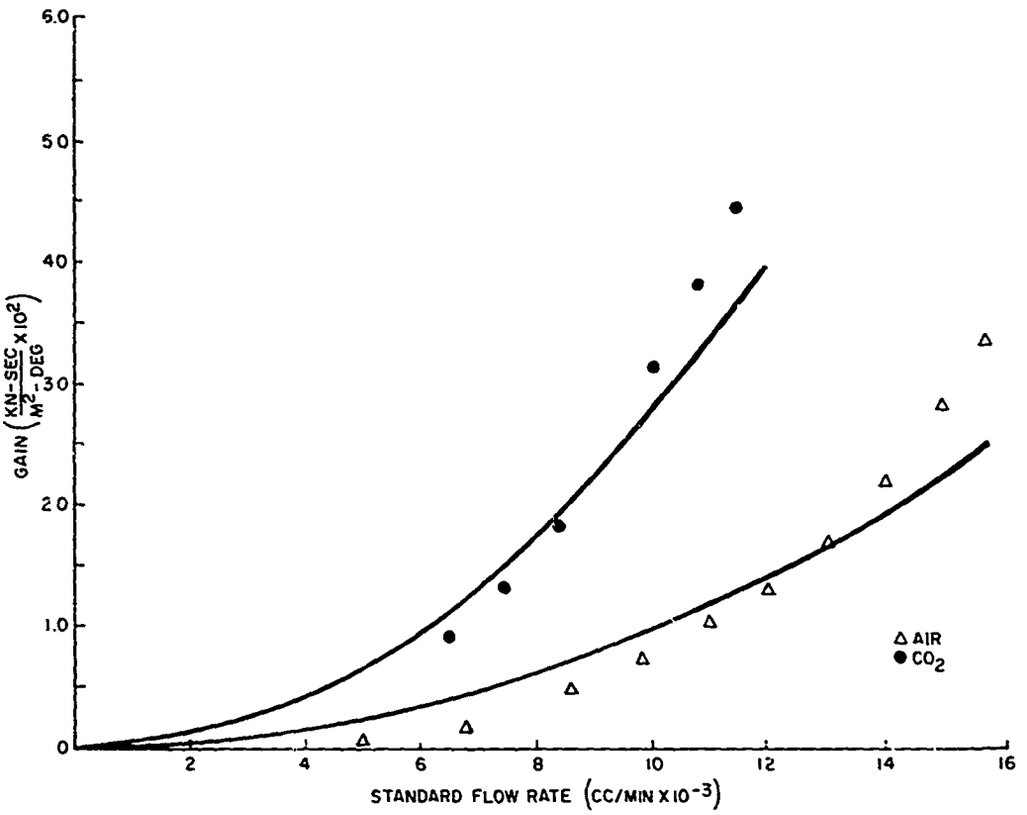

Figure 8. Sensor Gain vs Standard Volumetric Flow Rate - Air and Carbon Dioxide.

Theory indicates that K_3 is independent of Re_1. However, it may depend on some other parameter. An effort is made here to correlate the variations in K_3 to the Mach number at the exit of the drain. Since the pickoff is downstream of a sudden enlargement of drain diameter in the model tested (see figure 4), the output may vary as the Mach number changes due to the associated change in streamline pattern.

The percentage deviation of the empirical values from the parabolic curves is plotted for both gases in figure 9 as a function of Mach number at the pickoff. The Mach number was calculated by assuming the flow was isentropic and the exit pressure was one atmosphere. Therefore,

$$M = \sqrt{\frac{2}{\gamma-1}\left[\left(\frac{P_c}{P_a}\right)^{\frac{\gamma-1}{\gamma}} - 1\right]} \qquad (92)$$

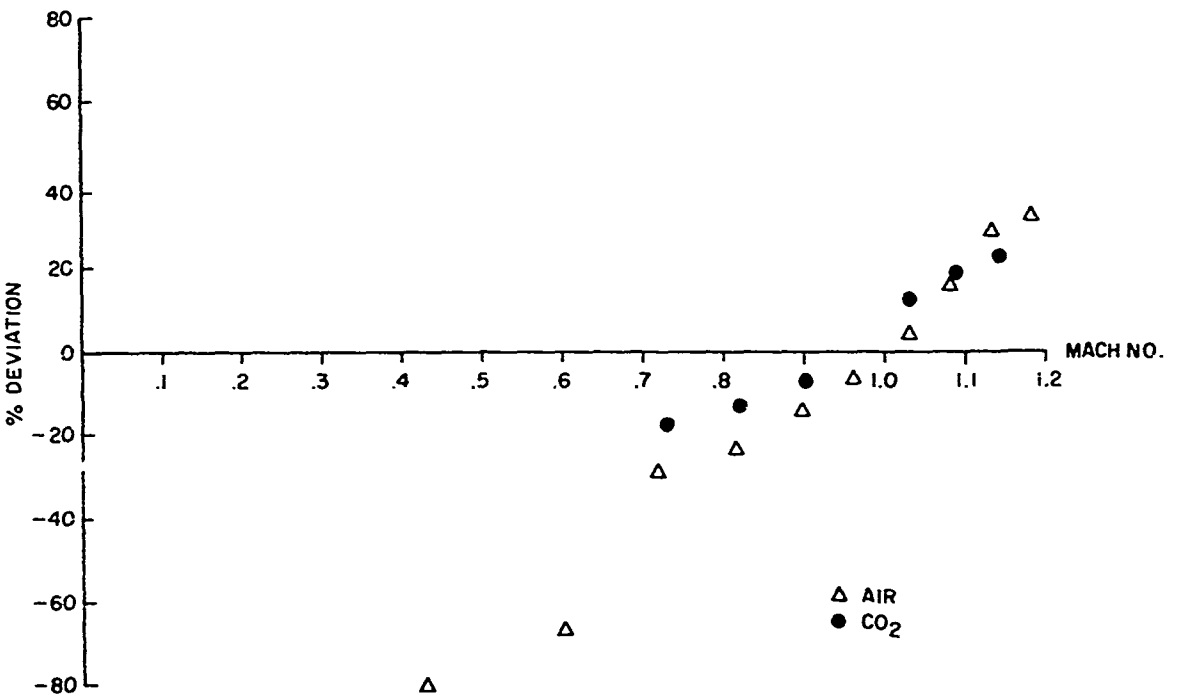

Figure 9. Percent Deviation of Empirical Values from Parabolic Curves of Figure 8.

where γ = ratio of specific heats, P_c = chamber pressure, and P_a = atomspheric pressure. Although the flow in the chamber is clearly not isentropic in this case, the error in (92) should not be large. In a direct test, no change in the chamber pressure for fixed flow rate was detected when the chamber height was varied over the widest possible range, indicating that the acceleration effects dominate in determining the pressure distribution.

This test was repeated with helium and air, as shown in figure10 and 11(note scale difference between figures 8 and 10). The shapes of the curves in figures 9 and 11 are different because the pick off position was changed before the latter test was conducted, causing the effect brought on by a changing streamline pattern to vary.

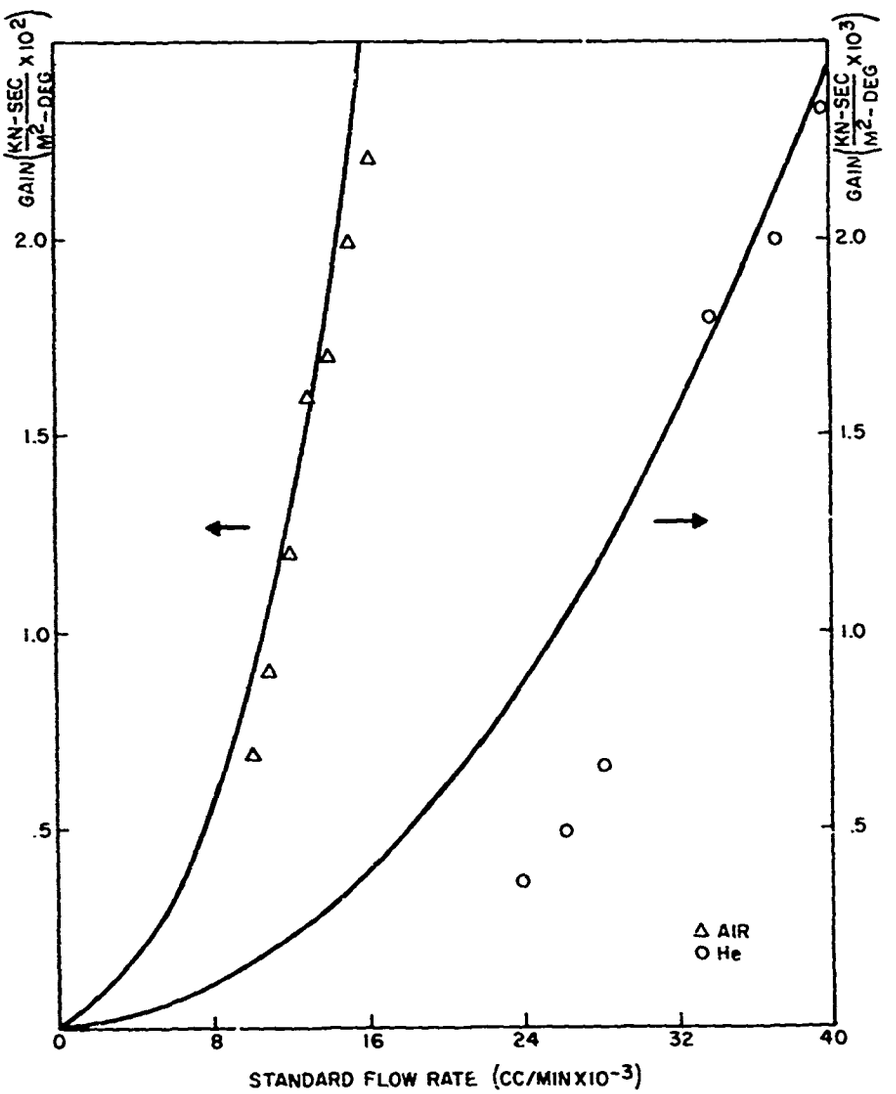

Figure10. Sensor Gain versus Standard Volumetric Flow Rate--Air and Helium.

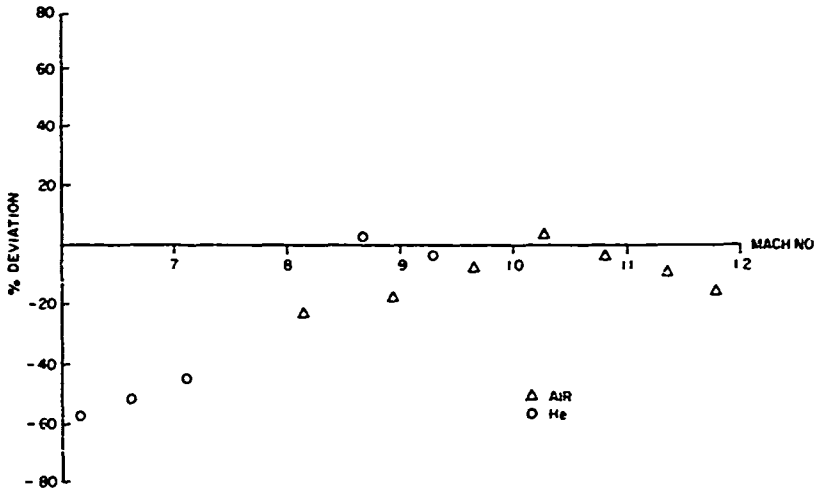

Figure 11. Percent Deviation of Empirical Values from Parabolic Curves of Figure 10.

4.3 Data and Theory for $G_{i\omega}$

Numerical solutions of (65) and (79) are plotted with the data in figures 12 through 15. The difference (in decibels) between the magnitude given by (65) and the empirical amplitude ratio is plotted in figure 16. The difference in phase is plotted in figure 17. The magnitude and phase of (65) are plotted in figures 18 and 19, respectively, for a wider range of Re'_o.

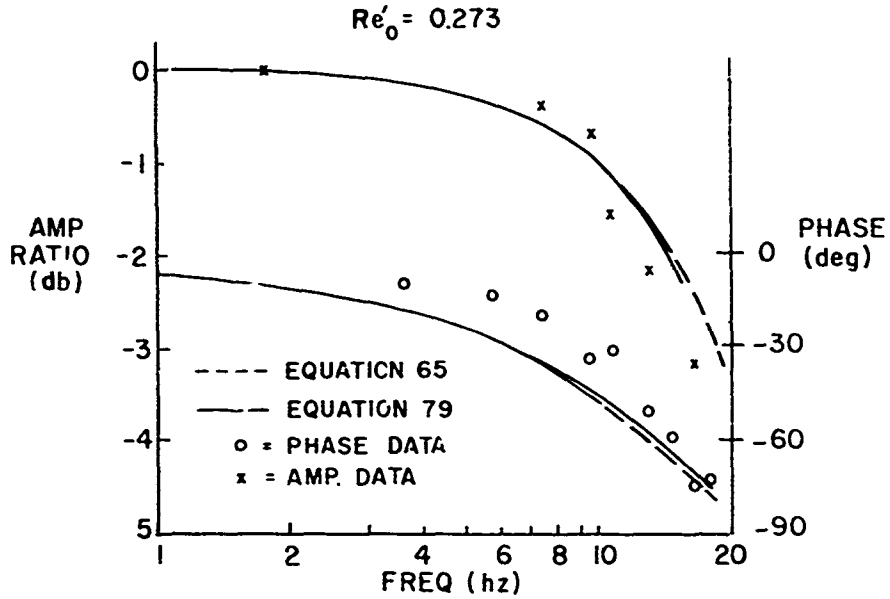

Figure 12. Numerical Solutions of Equations (65) and (79)--Re'_o = 0.273

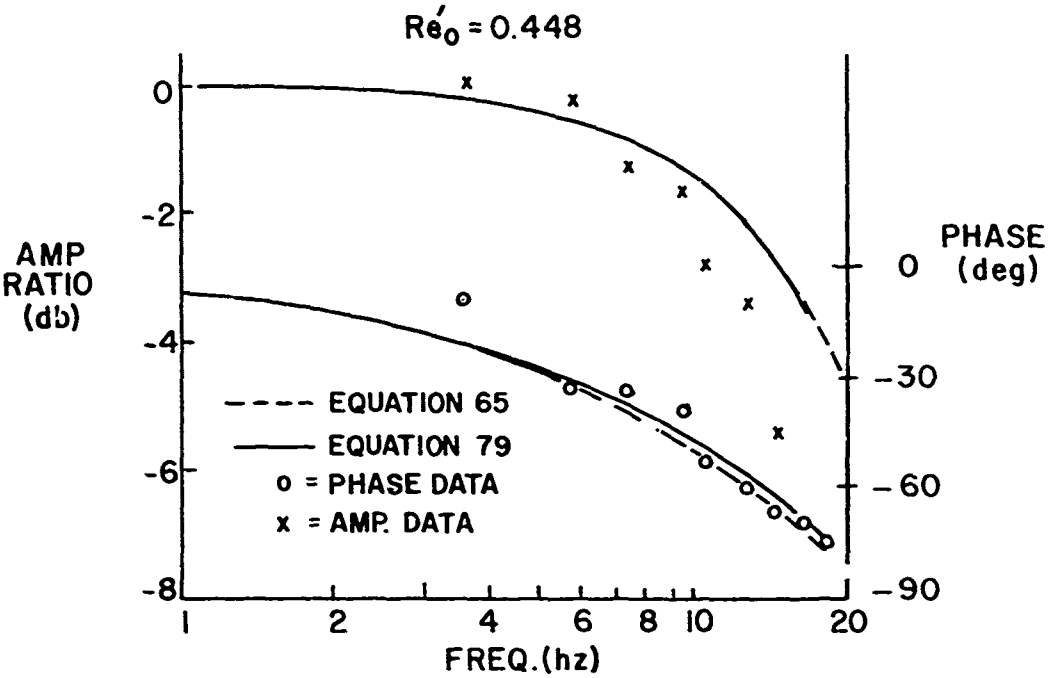

Figure 13. Numerical Solutions of Equations (65) and (79)--Re'_o = 0.448.

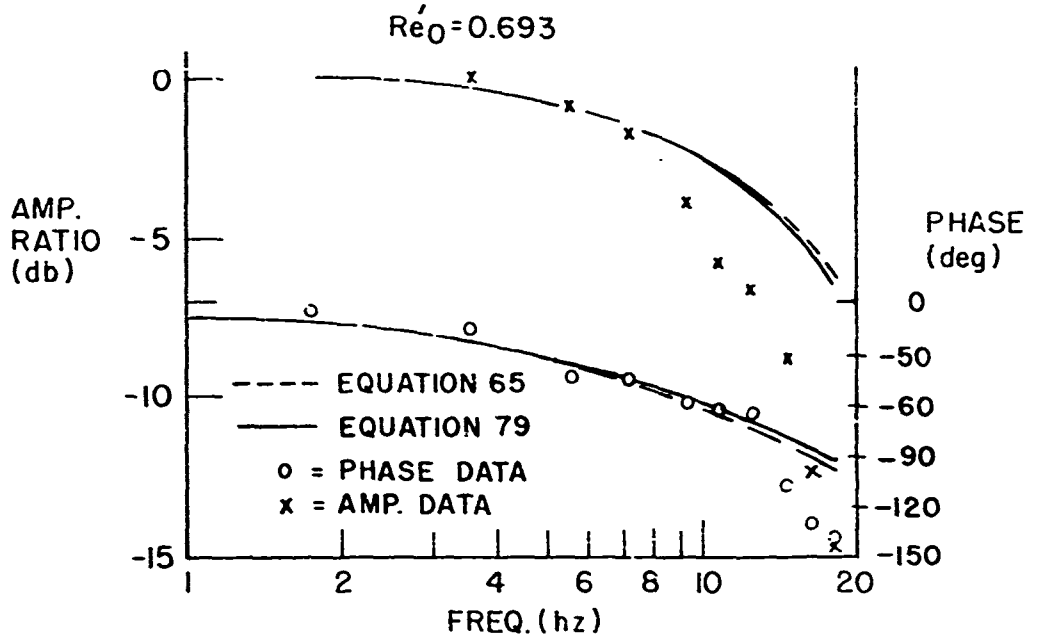

Figure 14. Numerical Solutions of Equations (65) and (79)--Re'_o = 0.693.

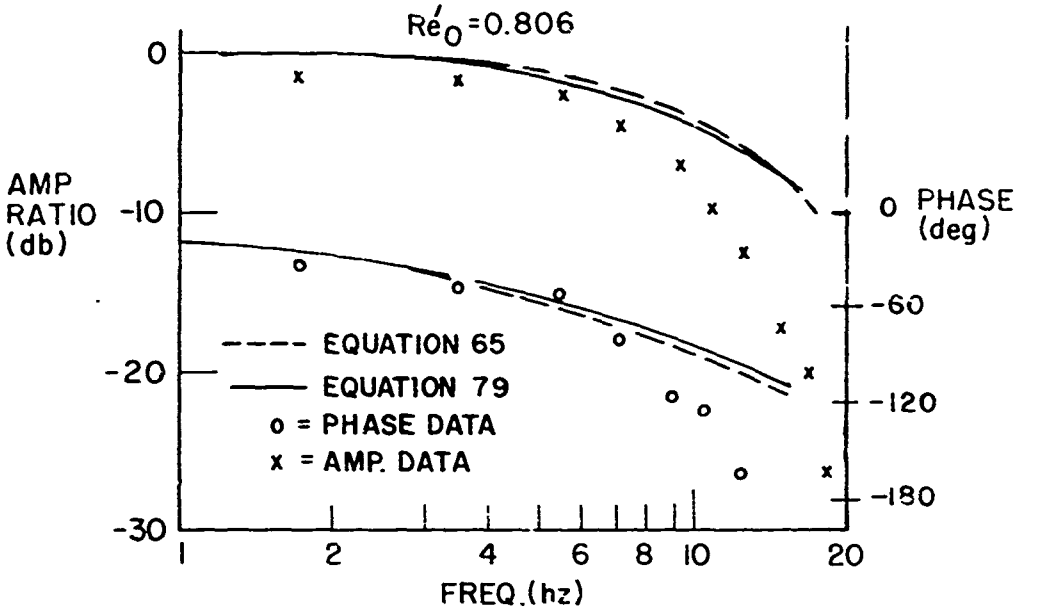

Figure 15. Numerical Solutions of Equations (65) and (79)--Re'_o = 0.806 .

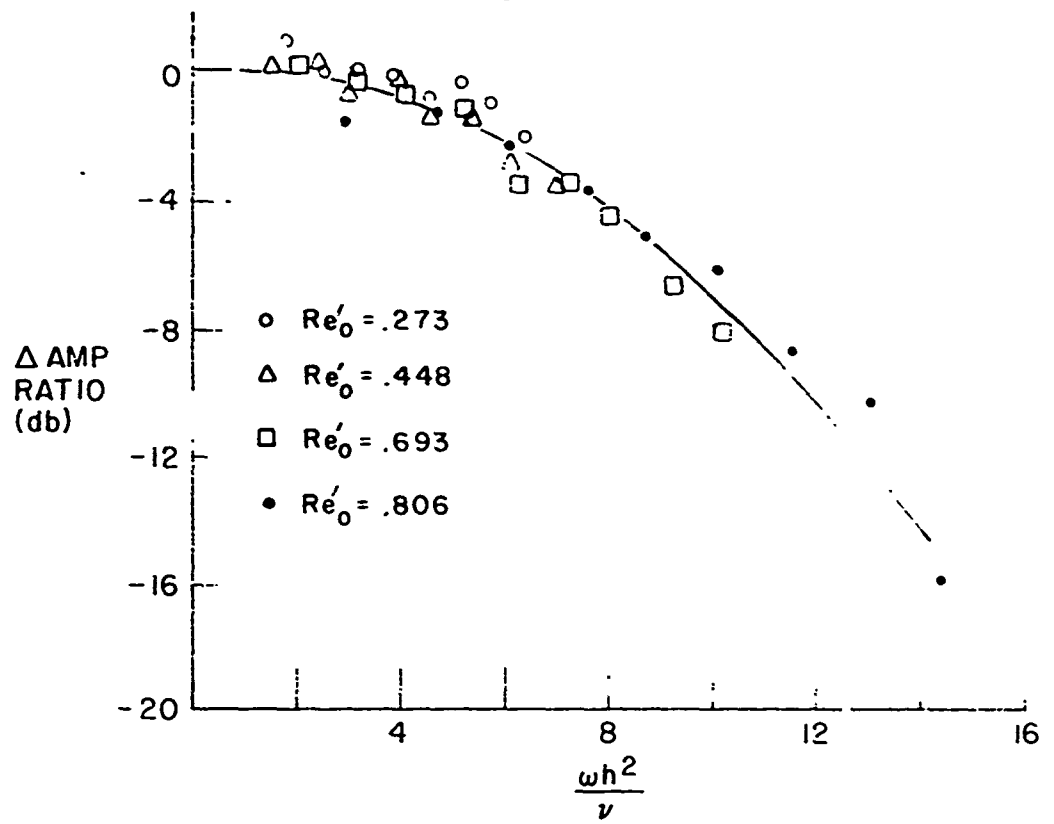

Figure 16. Difference in Amplitude Ratio Between Equation (65) and Empirical Data.

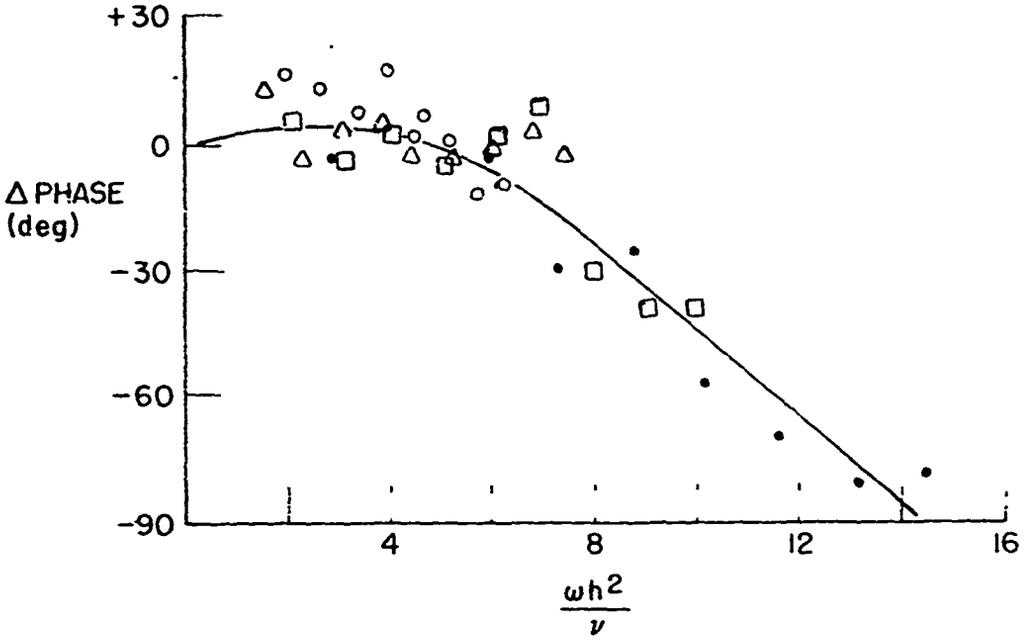

Figure 17. Difference in Phase Between Equation (65) and Empirical Data.

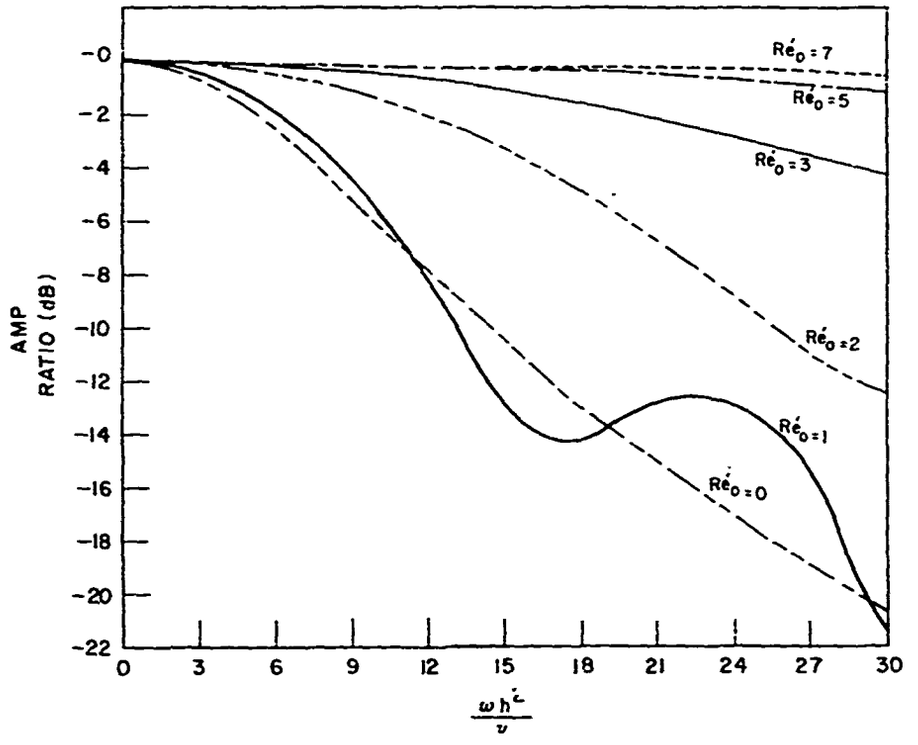

Figure 18. Amplitude Ratio Magnitude of Equation (65).

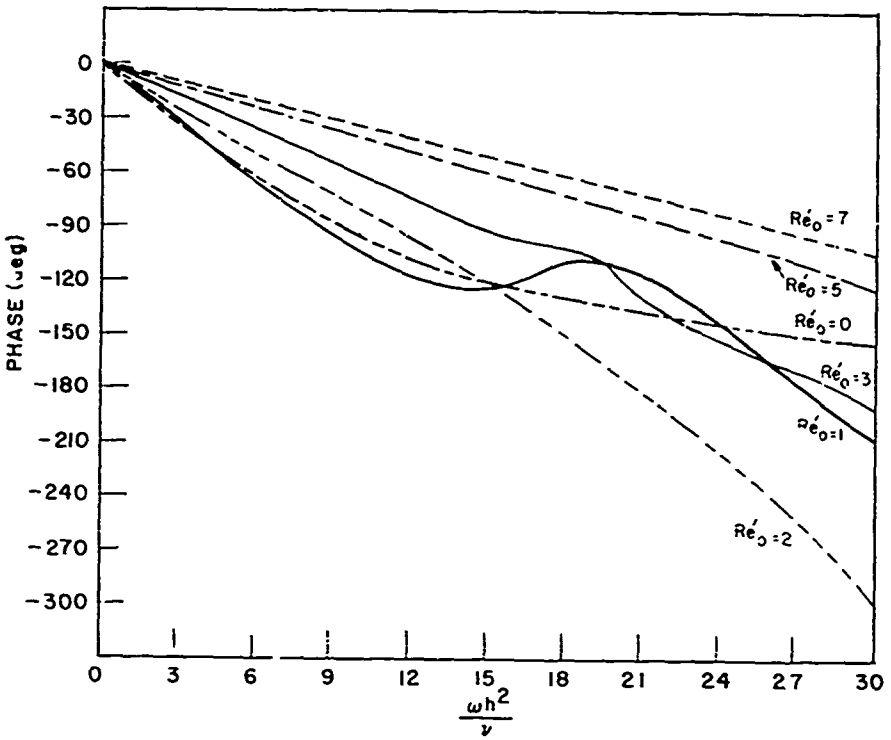

Figure 19. Phase of Equation (65).

5. DISCUSSION

5.1 Prediction of G_o

The analysis predicts rather well the behavior of G_o as a function of Re'_o. The shapes of the data curve and the two theoretical curves in figure 7 are quite similar except that the empirical curve is somewhat flatter in the range of Re'_o between 2 and 7, as anticipated in section 4.2. It was also expected that the empirical curve would be nearly flat above Re'_{ocrit}, even though the chamber losses change in that region, because little of the signal destroyed by the boundary layers is recovered by a pickoff in the drain. This latter effect makes the empirical value of G_o at Re'_{ocrit} greater than the theoretical value when both the theoretical and empirical curves are normalized with respect to their values in the inviscid range.

No significant difference in the shape of the data curves taken for the three different values of Re_1 is evident. A more careful experiment might disclose differences in the range of Re'_o between 3 and 5, for there does seem to be slight difference in trend of the three data curves in this region. This difference is so small, however, that it is unimportant with regard to the immediate task of designing a greatly improved rate sensor.

5.2 Prediction of G

It is obvious from figures 8 and 10 that K_3 does change. However, figures 9 and 11 indicate that this is due in great part to a change in the Mach number at the pickoff. A slight effect is present that cannot be correlated with a change in Mach number, because the error in the data points does not completely coincide in figures 9 and 11. This may have been caused by an inaccuracy in (92) or by the way in which gain was measured from the rough data. Gain was defined as the slope in the linear portion of the plot of pressure output versus angular rate. Since the shape of the output curve was at times somewhat distorted, and was generally not identical for two different gases at the same Mach number, it is possible that the manner in which the linear range was selected graphically could introduce a small error.

It is extremely unlikely that the lack of correlation in figures 9 and 11 is caused by a dependence of the drain losses upon Re_1. In both figures, the air data is about 10 percent lower than that of the other gas near M = 0.9, for example, even though Re_1 for carbon dioxide was about twice that for air in the region and Re_1 for helium was an order of magnitude smaller. Any dependence on Re_1 would be expected to be monotonic.

5.3 Prediction of $G_{i\omega}$

Figures 12 through 15 indicate that the differences between (65) and (79) are slight and that qualitatively both predict the frequency response. Figures 16 and 17 indicate that the error in this data is independent of Re_1. These figures imply that the viscous loss near the corner is a function of the shape of the tangential velocity profile upstream of the corner. In particular, the blunter the tangential profile, the greater the loss will be, as discussed in section 2.4.3.

5.4 Use of Semiempirical Equations

Some very simple design equations that are valid in the range $Re_1' < 1$ can be formulated on the basis of the discussion in the two previous sections. In section 5.2 it was shown that (91) is valid to within about 10 percent if a single experiment is first conducted to establish the functional dependence of K_3 on M. In section 5.3, it was shown that the error in predicting $G_{i\omega}$, is a function only of ω in this range of Re_o'. Again, only a single experiment need to be conducted to establish this dependence.

Although such results are semiempirical, they provide a very useful design tool, because the effect of any design change other than the pickoff-drain design can be predicted to within at least 10 percent.

These results can be used to demonstrate the effect on frequency response of changing h while holding the other design quantities constant, as shown in figure 19. Phase lag for $Re_0' = 10$ was calculated from (1). For $Re_0' < 1.4$,

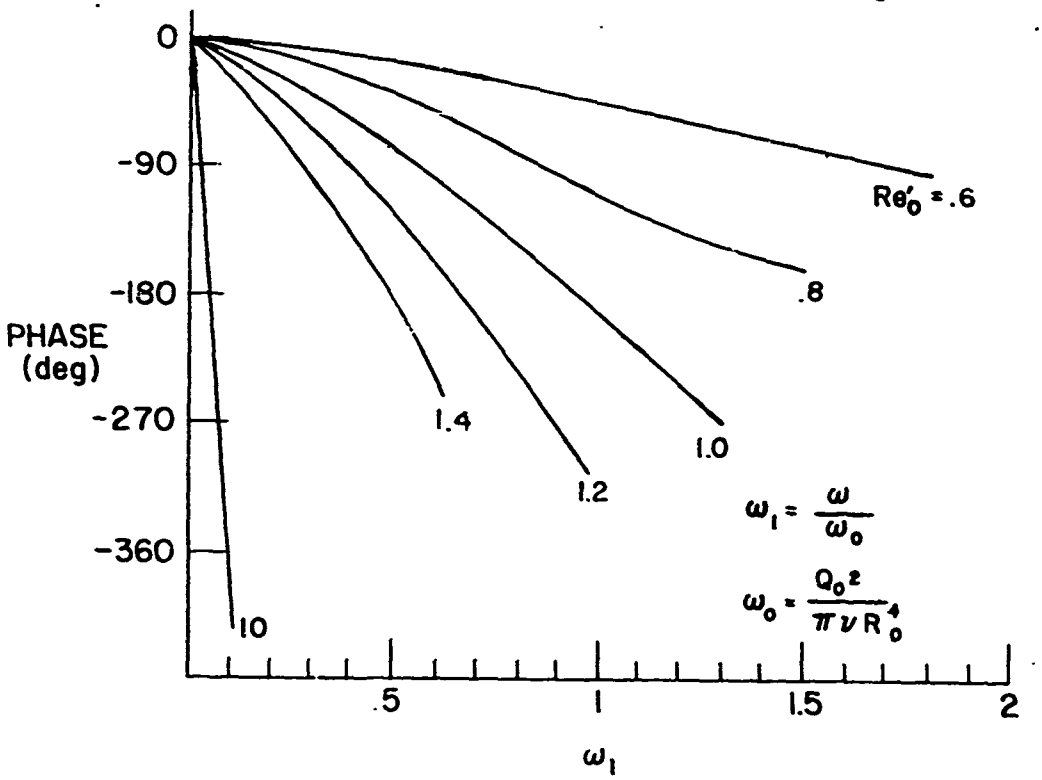

Figure 20. Effect of Changing Chamber Height.

values were used from figure 18 corrected by figure 17. Notice that decreasing Re_0' (a linear function of h in this case) significantly decreases the phase lag. In particular, by changing h so that Re_0' decreases from 10 to 1 the frequency at which the phase lag is 90 degrees increases by a factor of about 20. However, figure 6 indicates that the gain would be reduced by only a factor of about 2.

An increase in frequency response is not the only benefit derived from operating in the fully developed range. If the boundary layers in the chamber are small compared with h, the signal that reaches the drain can have significant phase shift without appreciable attenuation. If the drain

corner has a large radius of curvature (to reduce viscous losses), the attenuation due to the corner will not be as large as that indicated by figure 16. This could lead to a slender stability margin in a control system, since the phase shift is not accompanied by significant attenuation. It would be easier to design a stable system using a sensor with fully developed flow because, for example, the amplitude in such a design would be down about 20 dB when the phase lag is 180 degrees.

5.5 Variation with r of the Shape of the Radial Profile

The change in shape of the radial velocity profile as the fluid flows toward the drain does not appear to affect the sensor characteristics significantly. The most significant variation in the two solutions obtained is in the magnitude of the curves for G_o. The shape of the two theoretical curves for G_o agree quite closely as do both the magnitude and shape of the curves for $G_{i\omega}$.

It appears on first reflection that the shape of the curve of G_o versus Re'_o obtained from the stepwise procedure need not be similar to that obtained from either hypothetical solution. Since the ratio of the acceleration term to the viscous term in (30) is proportional to Re'_o, as indicated by (31), the acceleration effects will decrease as Re'_o decreases and the profile will become more nearly parabolic throughout the chamber. The results of the stepwise procedure might then be expected to yield a solution for G_o that agrees more closely with the solution for a parabolic radial profile as Re'_o decreases. However, this tendency is opposed by another effect.

The opposing effect can be shown by first examining some features of u_1 and u_2 where $\omega = 0$. As indicated by (53), g_1 is proportional to Re'_o. As k_1 becomes more nearly uniform, the proportionality constant decreases slightly. Consequently, in the stepwise procedure outlined, the u_1 in each annular region contributes a positive portion to the u_2 in the next inner region.

This implies that if the stepwise solution were known for infinite R_o, the magnitude of the tangential velocity relative to the wall predicted by the stepwise solution would be greater everywhere than the solution obtained by assuming $k_1 = k_o$ everywhere. But most importantly, the ratio of the former to the latter at R_i increases as the

changes in k_1 upstream become more significant. Now since the change in the radial profile between R_o and R_1 is greater with increasing Re_o', this implies that the ratio of G_o predicted by the stepwise analysis to the G_o predicted by everywhere setting $k_1 = k_o$ will increase as Re_o' increases. This effect then causes the stepwise curve to attempt to approach the parabolic curve as Re_o' increases, in direct opposition to the former effect.

Since these effects oppose each other, the shape of the curve obtained from the stepwise procedure is probably close to that obtained for either of the theoretical cases; only its magnitude is not well defined. This poses no problem for the use of these results as design equations, for it contributes only to an uncertainty in K_3 in (91), a constant which must be measured empirically anyway.

5.6 Temperature Effects

No effort was made in this experiment to investigate whether the temperature dependence of the sensor is influenced if the suggested change in viscous effects is pursued. However, this problem can now be discussed from an analytical viewpoint.

Since the shape of the stepwise curve for G_o will be very nearly similar to that of either (64) or (78), (61), (63) and (78) can be used to show that for $Re_o' < 7$, the dimensional gain, G , is given by

$$G = K_4 \dot{m} \left[K_5 \frac{\dot{m}}{\mu} \left(1 - \frac{96}{\pi^4} e^{-\frac{\pi^3 R_o^2 \mu}{A \dot{m}}} \right) \right] \tag{93}$$

where the product of K_4 and K_5 is a function of h, R_1, the pickoff design, and the corner losses. The portion of the right of (93) contained in the brackets is just the contribution due to G_o. Clearly $\dot{m}/\mu$ goes as Re_o' if temperature changes. Then from figure 7, the change in G_o with temperature is a minimum near $Re_o' = 7$, and a maximum at small Re_o' .

Now consider the full expression for G. If the change in $\dot{m}$ with respect to temperature has the same sign as that of $\dot{m}/\mu$, then decreasing Re_o' below 7 increases the temperature sensitivity of G. If the sign of the changes is opposite, however, this can lead to a reduction of temperature effects, and possibly even temperature insensitivity. This point deserves further elaboration.

If the temperature changes by some small amount ΔT, then it can be shown that the change in gain, ΔG, is given by

$$\Delta G = K_4 K_5 \frac{\dot{m}_\delta^2}{\mu_o} \left\{ \frac{1}{\dot{m}_o} \frac{\partial \dot{m}}{\partial T} \left[2\left(1 - \frac{96}{\pi^4} e^{-\frac{\pi^2}{2Re_o'}} \right) - \frac{48}{\pi^2 Re_o'} e^{-\frac{\pi^2}{2Re_o'}} \right] - \frac{1}{\mu_o} \frac{\partial \mu}{\partial T} \left[\left(1 - \frac{96}{\pi^4} e^{-\frac{\pi^2}{2Re_o'}} \right) - \frac{48}{\pi^2 Re_o'} e^{-\frac{\pi^2}{2Re_o'}} \right] \right\} \Delta T \tag{94}$$

where the subscripts on $\dot{m}$ and μ refer to the respective values at the initial temperature.

If the flow is inviscid (that is, if Re'_0 is large), then

$$\frac{\Delta G}{G} = \frac{\Delta \dot{m}}{\dot{m}_0} \tag{95}$$

If Re'_0 is very small, (94) can be used to show that

$$\frac{\Delta G}{G} = 2\frac{\Delta \dot{m}}{\dot{m}_0} - \frac{\Delta \mu}{\mu_0} \tag{96}$$

Since (96) describes the greatest possible contribution of G_0 to the temperature effects, it can then be shown from (95) and (96) that temperature sensitivity can be reduced below that for inviscid flow if

$$\frac{\Delta \dot{m}}{\dot{m}_0} < \frac{\Delta \mu}{\mu_0} \tag{97}$$

Let us then define the quantity

$$N \equiv \frac{\Delta \mu}{\mu_0} \Big/ \frac{\Delta \dot{m}}{\dot{m}_0} \tag{98}$$

It can then be shown from (97) that the temperature sensitivity increases as Re'_0 is decreased if $N<1$. (96) can be used to show that if $1<N<2$, the temperature sensitivity decreases as Re'_0 is decreased. If $N>2$, (94) can be used to show that gain is insensitive to small changes in temperature at some value of Re'_0. In the fully developed range this value can be approximated by solving the expression

$$Re'_0 \left(\frac{\pi^2}{4\beta} e^{\frac{\pi^2}{2Re'_0}} - \frac{2}{\pi^2}\right) = \frac{N-1}{N-2} \tag{99}$$

Two typical cases can be considered to discuss these effects. Suppose first that a sensor using a hydraulic fluid is powered by a constant pressure source. If the sensor design is that of a plenum, chamber, and a drain in series, then the source sees the sensor as a series combination of an orifice and a laminar resistor. The resistance of the orifice does not change appreciably with temperature, but a decrease in viscosity causes a decrease in laminar resistance, and thus an increase in mass flowrate. Therefore, N is negative, and temperature sensitivity increases as Re'_0 decreases.

Now suppose a pneumatic sensor is powered by a gas bottle that supplies fluid to the sensor through a choked orifice. Since the Mach number at this orifice is one for all temperatures, the velocity through the orifice goes as the speed of sound; that is, proportional to the square root of temperature. The density in the bottle does not change with temperature if the volume of the bottle can be considered constant, so that the density at the minimum cross section of the orifice is also independent of temperature if the ratio of specific heats can be considered constant. Therefore, mass flowrate through the sensor increases in proportion to the square root of temperature. If μ is expressed in terms of temperature by a relationship such as Sutherland's formula[14], it can be shown

that for the most commonly used gases operating in the standard military temperature range, N falls in the range $1<N<2$. Therefore, the temperature sensitivity of the sensor decreases as Re_o' decreases.

The slope of $\dot{m}$ as a function of temperature can be made to decrease, thereby increasing N, if the orifice is not choked, but loaded by a laminar resistance. In general, it should be possible to choose a particular combination of orifice and laminar resistance for a given mean operating temperature such that N is equal to 2 for small changes of temperature. At that value of N, the sensor gain is insensitive to temperature for values of Re_o' that are sufficiently small to cause the contributions of u_2 to G_o to be negligible. If a value of Re_o' less than 0.1 were chosen, for instance, the temperature could increase without limit and decrease by at least two orders of magnitude without causing any significant contribution from u_2 to be felt. The degree of temperature insensitivity would therefore be specified by the degree to which N could be held constant over the temperature range.

5.7 Other Observations

It is apparent that u_2 affects G_o and $G_{i\omega}$ at values of Re_o' significantly less than 7, the value at which, it was argued, the radial velocity profile becomes fully developed. However, deviations in G_o caused by the entrance effects on the radial profile, as discussed in sections 2.4.2 and 5.1, appear slight. The entrance lengths for the two components of velocity thus appear different, but since G_o is not very sensitive to the shape of the radial profile, a more careful analysis of the development of the radial velocity profile is needed to establish formally the influence of the entrance conditions on that profile for this range of Re_o'.

It should be noted that the chamber pressure in the frequency response test for which $Re_o' = 0.806$ was 22 psig, while for $Re_o' = 0.273$, it was 4 psig, causing a significant change in compressible effects in this experiment. Since these effects would necessarily be localized in or very near the drain, they could be lumped with the other drain effects as a matter to be ignored in this analysis in order to establish their significance. They clearly have no effect on the dynamic characteristics, as shown by figures 16 and 17. Their effect on dc gain has been discussed in section 4.2.

It is also interesting to note that the signs of the contribution in $G_{i\omega}$ due to u_2 is negative, while that due to u_1 is positive. It may then be possible to choose conditions in which the two contributions are nearly 180 degrees out of phase and of equal amplitude, so that the combined signal is very small. (65) can be used, for instance, to show that for $Re_o' = 1.3$, as ω' increases from 15 to 21 the amplitude drops from -9db to -28 db and then recovers to -12db at $\omega' = 30$. A similar phenomenon occurs at slightly larger values of Re_o' and ω' if (79) is used. It would therefore appear that a sensor with a very simple design could be made to have a notched frequency response.

6. CONCLUSIONS ABOUT PRESENT MODEL

The nature of the gain and frequency response of the present rate sensor design in the fully developed range can be closely predicted through the use of this chamber analysis and a single test. Tests carried out in the range of $Re_o' < 1$ demonstrate that the error in this analysis is not a function of Re_1, which implies that losses at the corner and in the drain are independent of Re_1. This also indicates that once a single test is made on the present sensor to specify those losses, the results of making any design change other than one in the pickoff-drain configuration can be predicted to within at least 10 percent.

The change in shape of the radial velocity profile as the fluid flows toward the drain does not significantly affect the sensor characteristics. The only significant uncertainty created by the approximate method used in this analysis appears in the magnitude of the sensor gain at Re_{ocrit}'. This gain must be measured anyway in the semi-empirical design equations presented because of the incomplete analysis of the pickoff-drain region. There is some uncertainty in the prediction of $G_{i\omega}$ at values of ω' near 15 and Re_o' near 1, since the solutions do not provide bounds in those ranges of the governing parameters. However, in the present design with the pickoff in the drain, the attenuation at the corner is so great that this uncertainty is not of great consequence.

In summary, from a control systems point of view the dynamic characteristics of a rate sensor operating in the fully developed range are significantly more favorable than those of an inviscid sensor. Not only can the phase lag in the output be much less, but this lag is accompanied by an attenuation in amplitude.

If only the height of the present design is changed to induce the viscous effects, the gain is reduced and the temperature sensitivity may increase or decrease, depending on the

initial design. However, other new design alternatives can then be used which appear beforehand to allow improvement of sensor performance in all areas, as will be discussed next.

7. FUTURE MODELS

7.1 Experimental Work

7.1.1 Chamber Height

Sensors can currently be fabricated with chamber heights as small as several thousandths of an inch. Analysis indicates these sensors should have corner frequencies in excess of 1 kHz. Models are being fabricated to test this prediction.

7.1.2 Pickoff Location

In the future models, the signal pickoff will be located in the chamber just upstream of the drain with its longitudinal axis parallel to the drain axis. This change has a wide impact on sensor performance. Some of these effects will be discussed.

7.1.2.1 Noise Reduction

The effect of drain turbulence on the output can be reduced if the pickoff is located in the chamber upstream of the disturbance. In addition, the problem of designing a drain in which the flow is stable can then be isolated from problems relating to the pickoff fabrication and mounting.

If the flow separates on the surface of a probe in the chamber even though the undisturbed field is accelerating, the problem of pickoff turbulence can be attacked. This turbulence could be suppressed with the top and bottom walls if the chamber is sufficiently thin at the pickoff location.

A pickoff in the chamber could be bonded to the top and bottom walls, so that a pickoff-drain insert could be fabricated that does not respond to thermal or mechanical disturbances. The signal null must then be adjusted by some mechanism external to the pickoff. If this can be achieved the problem of adjusting the null will be isolated from problems concerning the pickoff design.

It then appears that the problem of pickoff-drain noise and null shift could be attacked systematically if the pickoff is located in the chamber.

7.1.2.2 Frequency Response

Relocating the pickoff upstream of the corner would eliminate corner losses. Figures 16 through 19 indicate that frequency response would be about doubled for ω' of the order of 15 or less. This may make the use of the fully developed sensor in a control system even more attractive.

It can be shown (App. I) that if there are no corner losses, for small Re_o' and large ω' the phase lag approaches a limit, ϕ_{max}, where $135° < \phi_{max} < 225°$. This maximum could probably be reduced by changing the pickoff design to respond more strongly to the information near the wall.

7.1.2.3 Signal Gain

The relocation of the pickoff in the chamber just upstream of the drain will result in a change of gain. Equation(61) indicates that, for a pickoff in the chamber, gain is a linear function of ρV_r and V_θ in the undisturbed flow field at the pickoff's longitudinal axis, as it is of ρV_z and V_θ for a pickoff in the drain. The ratio of ρV_r (at the chamber location) to ρV_z (at the drain location) might realistically be slightly more than one-half if the average transport velocity component is nearly constant in the vicinity of the corner, as it is in the typical design. The ratio of the tangential velocities might also be about one-half. The significant viscous effect at the center of the drain account for the difference between this value and a smaller value that would be predicted by inviscid analysis. The combined effect is a gain reduction by about 4 for a typical design.

This initial reduction of gain must be considered a loss in sensor effectiveness, even when the increased frequency response is considered. However, this design change

sets the stage for other changes which can result in an increased effectiveness, the first step of which is to reduce chamber height. The effect that this latter change has on signal gain will be discussed first. For sake of a clear comparison, the gain will be expressed in terms of that of a typical present sensor operating at the lower limit of the inviscid range with a pickoff in the drain.

The gain before and after the relocation is indicated by points A and B respectively in figure 21. Now let h be reduced while the rest of the geometry is held fixed. The restrictions on power supply must now be considered in order to relate $\dot{m}$ to h.

Suppose first that $\dot{m}$ is held fixed while h is reduced with the pickoff in the chamber. If inviscid gain for these conditions is multiplied by G_0 from the analysis, it can be shown that actual gain increases, approaches a limit, and is nearly constant for $Re_0'<1$, as indicated in figure 21. In the latter range the gain is nearly equal to that obtained from a pickoff in the drain with $Re_0' = 7$.

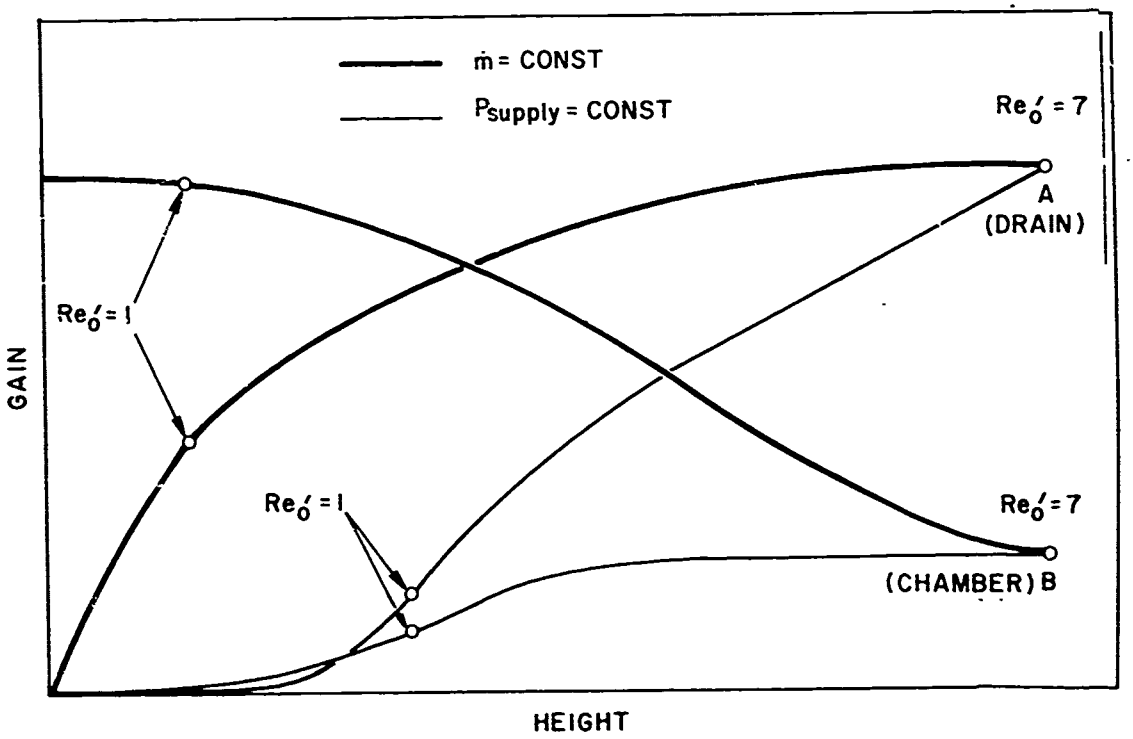

Figure 21. Effect on Gain of Relocating Pickoff and Reducing h.

Consider next that the supply pressure is held constant while h is reduced with the pickoff in the next chamber. If one assumes that the curtain area (that is, $2\pi R_1 h$) is the dominant restriction, then it can be shown that gain is nearly independent of h for Re_0' nearly 7 and proportional to h^2 for Re_0' less than 1. The curve representing any other type of power supply or system specification on consumption must lie between these two curves.

The curves for the same two cases with the pickoff in the drain are represented in this same figure by the curves that meet point A. It appears that if h is made very small on a model with a pickoff in the chamber, the gain will be reduced below point A for any power supply that responds to downstream pressure. However, this reduction is less than would have occurred if the pickoff had remained in the sink. In addition, this sacrifice in gain has resulted in an appreciable increase in frequency response, as will be discussed next.

7.1.2.4 Gain-Bandwidth Product

A quantity which is often of interest to the designer of a control system is the gain-bandwidth product (or sensitivity-frequency response product, since this is a sensor). The gain-bandwidth product before and after the transfer of the pickoff are presented in figure 22 by points A and B, respectively. For the present typical design, the reduction might well be a factor of about two.

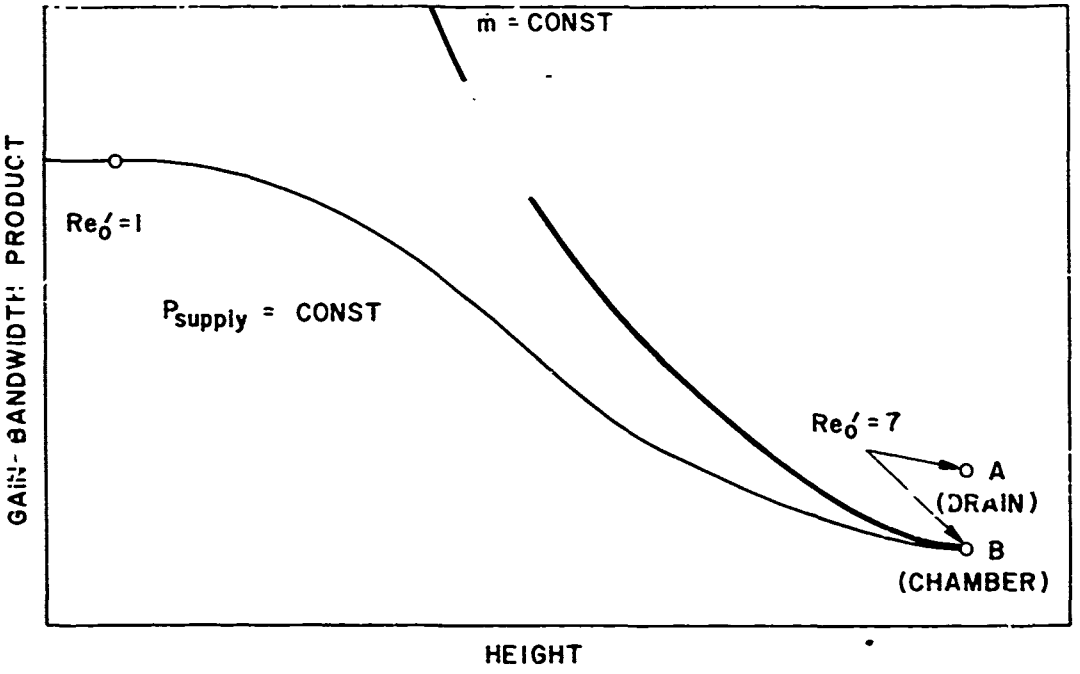

Figure 22. Effect on Gain-bandwidth Product of Relocating Pickoff and Reducing h.

Consider first the case in which $\dot{m}$ is held fixed while h is reduced. It can be shown that frequency response increases by about a factor 20 while Re_o' is reduced from 7 to 1 and is proportional to $1/\rho h^2$ for $Re_o' < 1$. Figure 21 can then be used together with this information to show that the gain-bandwidth product at $Re_o' = 1$ is about 30 times the value at point A. For $Re_o' < 1$, it increases as $1/\rho h^2$.

For the case when supply pressure is held constant, the gain-bandwidth product increases and approaches a limit as h is reduced. It can be shown that the value for $Re_o' < 1$ is about three times the value at point A.

Clearly, then, for any type of power supply conditions the gain-bandwidth product can be increased significantly over the value in the present inviscid sensor by placing the pickoff in the chamber and reducing the height. For small h, the gain-bandwidth product is greater for a pickoff in the chamber than for one in the drain regardless of the power supply used. The improvement is especially large if the mass flowrate is not a strong function of the load that the curtain area at the drain entrance represents.

7.1.2.5 Airfoil Gain and Output Impedance

Although the transfer of the pickoff initially results in a loss of gain if nothing else is changed, changes in the pickoff design that may improve performance can then be made.

Since a strong faborable pressure gradient exists in the flow field near the sink due to acceleration, pickoff designs are not as severely restricted by flow separation. It may be possible to use a pickoff then whose gain is higher than those presently used; perhaps a pickoff design that takes an appreciable amount of flow through the sensing ports could be used without destroying the nearby pressure field. This would increase the gain and decrease the output impedance.

7.1.3 Supply Distribution System

A model is being designed at HDL that has a flow distribution system upstream of the working chamber that should reduce the magnitude of upstream nonaxisymmetric disturbances significantly more than the present design. This should allow the influence on the sensor output noise level of disturbances near the drain and changes in the mean power level to be studied.

7.1.4 Multiple Pickoffs

It can be shown from the solution for V_θ obtained in this analysis that for $Re'_o < 1$ the lines connecting points near the pickoff that have the same phase with respect to the wall motion are nearly parallel to the wall or, in other words, that the signal propagates into the fluid in a direction normal to the walls. Since the noise propagates in a direction normal to that of the signal, then the time history of the wall motion could possibly be traced independently of that of the noise.

It can be shown that the output of n pickoffs, each of which measures the signal at a different elevation in the chamber, can measure by simple arithmetical operations the first through the nth time derivative of angular motion. In addition, the shape of the frequency response curve for $\dot{\theta}$ can be shaped. The output of two pickoffs could be used, for instance, to measure both $\dot{\theta}$ and $\ddot{\theta}$, with the amplitude of the angular rate signal relative to d-c made arbitrarily small at a phase lag of about 120 degrees.

Some careful design may be required to extract the information at different levels in the fluid. Placing in the fluid a multi-channeled probe that has a number of pickoff ports at various points along its length would probably cause such a severe local disturbance that the variation of information across the channel is washed out, and the output from any port along the probe may be nearly the same. However, there may be some other method a clever designer might propose that can extract a flueric signal. In addition, other methods such as anemometry provide ready access to this information if the systems specifications allow an immediate interface to electronics.

7.1.5 Chamber Design

Present plans also call for the testing of an axisymmetric model in which the chamber is something other than cylindrical. There are several objectives to this effort, one of which is to design a model whose gain does not change for small excursions of the environmental temperature or power supply level, or some combination of these two parameters. The finer details of this design will hopefully be specified by a theoretical program presently in progress.

7.2 Theoretical Studies

It can presently be shown that the approximate governing equations used in this analysis can also be solved

for a thin chamber in which the height varies in any monotonic fashion with r. This solution will be pursued.

It can also be shown that for the cylindrical chamber, the growth or decay with radius of perturbations with respect to z, θ and t can be treated analytically. In addition, stability in the supply distribution system and in the drain is being studied.

8. ACKNOWLEDGEMENTS

The author wishes to thank the following members of the HDL staff who have contributed toward this publication: Norman Eisenberg for his insight and patience throughout many discussions of this analysis, John M. Goto for the unpublished analytical results that are plotted in figure 2, Jean Kiernan for writing the computer program in appendix D, and John Burke for designing the particular model tested in this experiment. This analysis is the direct result of an attempt to theoretically describe the behavior of a rate sensor that Mr. Burke designed, rather than an early insight into the problem by the author.

9. REFERENCES

1. Burke, J. and Roffman, G. L., "A Pickoff Element for an Angular Sensor (U)", Fluid Amplification Symposium, Vol. V, May 1964 (Confidential Report).

2. Egli, W. H., Kizilos, A. P., and Reilly, R. J., "Study of Vortex Gyro (U)", Honeywell, Inc., Tech. Doc. No. AL-TD4-64-50, June 1964 (Confidential Report).

3. Manion, F. M., and Dexter, E. M., "Investigation of Fluid Inertial Device for Missile Control Systems (U)", Bowles Engineering Corp., R-2-1-65, January 1965 (Confidential Report).

4. Sarpkaya, T., "A Theoretical and Experimental Investigation of the Vortex-Sink Angular Rate Sensor", Proceedings of the HDL Fluid Amplification Symposium, Vol. II, October 1965.

5. Burke, J. F., "Evaluation of a Flueric Angular-Rate Sensor with High Sensitivity", ASME Publication 67-WA/FE-36.

6. Egli, W. H., Moynihan, F. A., and Sampson, R. L., "Investigation of Noise and Null Uncertainty in the Vortex Rate Sensor (U)", Honeywell, Inc., Final Report on HDL Contract DA-49-186-AMC-226 (D), March 1967 (Confidential Report).

7. Feibig, M., "On the Motion Within Fluid Gyroscopes", AIAA J., Vol. 4, No. 4, April 1966.

8. DeSantis, M. J. and Rakowsky, E. L., "Vortex Flow Field Study" Singer-General Precision, Inc., HDL-TR-033-1, May 1970.

9. Sarpkaya, T., Goto, J. M., and Kirshner, J. M., "A Theoretical and Experimental Study of Vortex Rate Gyro", Advances in Fluidics, May 1967.

10. Schlichting, H., "Boundary Layer Theory", Fourth Ed., McGraw-Hill Book Company, 1960, p. 121.

11. Ibid, p. 171.

12. Ibid, p. 295.

13. Ibid, pp. 53-54.

14. Chapman, A. J., "Heat Transfer", MacMillan Co., 1960, p. 34.

15. Kirshner, J. M., "Fluid Amplifiers", McGraw-Hill, 1966, p. 141.

16. Rouse, H., "Fluid Mechanics for Hydraulic Engineers", Dover, 1961, pp. 76-82.

17. Binder, R. C., "Fluid Mechanics", Second Ed., Prentice-Hall, 1949, p. 160.

18. Liusternik, L. A., and Sobolev, V. J., "Elements of Functional Analysis", Frederick Ungar Pub. Co., 1961, p. 74.

19. Friedman, B., "Principles and Techniques of Applied Math", John Wiley & Sons, Inc., 1956, p. 199.

20. Abramowitz, M., and Stegun, I. A., "Handbook of Mathematical Functions", National Bureau of Standards Applied Mathematics Series 55, June 1964, pp. 358-360.

21. Gradshteyn, I. S., and Ryzhik, I. M., "Tables of Integrals, Series and Products", Academic Press, 1965.

22. Abramowitz, M., and Stegun, I. A., op cit., pp. 504-515.

23. Ibid, pp. 374-375.

10. LIST OF SYMBOLS

A_∞ = $3Q_o/4\pi h$

A_o = $Q_o/2\pi h$

a = $\sqrt{i\omega/\nu}$

B = ratio of terms in two series

f_1 = function that describes the propagation of information from the coupler

f_2 = function that describes the propagation of information upstream from the drain

f_1' = eigenfunction in the drain

F_θ, F_r, F_z = body forces

G = d-c gain

G_o = d-c gain relative to inviscid case

$G_{i\omega}$ = a-c gain relative to d-c level

h = chamber height

$k\ (r,z)$ = normalized radial velocity profile

l_e = entrance length

$\dot{m}$ = mass flow rate through the sensor

p = pressure

Q_o = volumetric flow rate in the outer portion of the chamber

r = radial distance

R_o = chamber radius

R_1 = drain radius

Re_o = chamber Reynolds number = $U_o R_o/\nu$

Re_o' = modified Reynolds number = $(U_o R_o/\nu)\ (h^2/R_o^2)$

Re_1 = $\left(V_{z_{drain}}\Big|_{avg}\right) R_1/\nu$

S_n = nth eigenvalue

T = transport time

u_1 = function describing the propagation of information from the top and bottom plates

u_2 = function describing the propagation of information from the coupler and drain into the chamber

U_o = average radial velocity at R_o

U_∞ = free stream velocity

V_r = radial velocity

V_z = axial velocity

V_θ = tangential velocity

$V_{\theta rel}$ = tangential velocity relative to the wall

x_1 = distance from leading edge

z = distance from the centerplane of the chamber

α = angle between a streamline and radial line

β_n = nth eigenvalue

ϵ_1 = sink tube radius

δ = boundary layer thickness

δ^* = displacement thickness

δ_n = nth eigenvalue

θ = momentum thickness

λ_n = nth eigenvalue

Λ = shape factor

μ	= dynamic viscosity
ν	= kinematic viscosity
ρ	= density
ϕ	= output of rate sensor
ψ_n	= eigenfunction in the chamber
ψ'_n	= function that describes propagation of information down the drain
ω	= oscillatory frequency of rate sensor
ω'	= $\omega h^2/\nu$
Ω_o	= angular rate amplitude

APPENDIX A. VISCOUS CORE OF A 2-D VORTEX-SINK FLOW FIELD

The existence of a rigid body core in two-dimensional vortex-sink flow is usually not questioned. Two arguments imply its existence. The first involves discussion of the isentropic energy equation, in which the existence of a limit circle is described. The second is a description of an observed Rankine (or combined forced and free) vortex.[16]

The first discussion indicates that energy limitations exist in a potential field. If a set of stagnation conditions is established and the strength of the sink and vortex is specified, this approach shows that a radius exists at which the absolute pressure is zero. The region inside this limiting radius is therefore inaccessible to the fluid and is often assigned a rigid body nature.

What this approach does point out is that if the outlet is placed inside the limit circle, no such flow field can exist. If the specified features of the external flow are somehow established with the outlet placed inside the limit circle, the flow rate cannot be maintained and therefore is reduced. The field eventually adjusts to a new sink strength as defined by the pressure specified in the outlet and the stagnation conditions in the external field. The fact that the radius of the limit circle changes if a swirl is introduced in the external field indicates that the imposed vortex throttles the flow, a well-known phenomenon.

The nature of the flow field in the interior of the limit circle is then at best academic because such a field cannot exist in reality. The fact that it is often assigned a rigid-body nature may lead some readers to believe that a rigid-body core does exist near the center of a two-dimensional sink flow field.

The discussion of a Rankine vortex, often accompanied by photographs of the region above the outlet of a hydraulic sink-vortex flow field, may lead to confusion if it is not made quite clear that this rigid-body core is necessarily a feature of the three-dimensional nature of the flow field over the outlet.

---

* For references, see pp. 72-73.

Quite often, the two-dimensional vortex-sink field is discussed without any apparent concern about the manner in which the fluid exists at the center of the field. The popular description[17] is that the field is a combination of free vortex in the outer region, a solid body core in the center, and a transition region between. If this description is applied to a truly two-dimensional vortex-sink field, then it poses several physical and mathematical absurdities. Instead of discussing these, however, it might be best to attack the problem directly.

In order to understand the two-dimensional vortex-sink field more clearly, consider the field shown in figure A-1. The physical boundaries consist of two very long concentric cylinders that have porous walls. The outer one turns at a rate Ω_0; the inner one at a rate Ω_2. Fluid enters the region between the two in an axisymmetric fashion from the outer wall and leaves through the inner wall. The tangential velocity relative to either bounding wall is zero at the wall. A purely two-dimensional vortex-sink field can be described by first finding the solution to the incompressible momentum equations for the region between these two cylinders and by then examining the features of this solution as the radius of the inner cylinder is allowed to approach zero. The implications of this inner radius being infinitesimal (in relation to the previous discussion of the limit circle), as well as the consequences of the assumption of incompressibility will be discussed after the solution is found so that the ramifications will be more apparent.

Equations (17), (18), (19), and (20) become

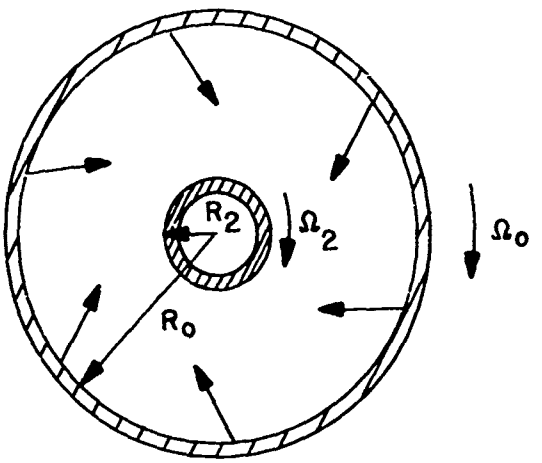

Figure A-1. Two-dimensional Vortex-sink Field.

$$\rho\left(V_r\frac{\partial V_r}{\partial r}-\frac{V_\theta^2}{r}\right)=\frac{\partial p}{\partial r}+\mu\frac{\partial}{\partial r}\left(\frac{\partial V_r}{\partial r}+\frac{V_r}{r}\right) \tag{A-1}$$

$$\rho V_r\left(\frac{\partial V_\theta}{\partial r}+\frac{V_\theta}{r}\right)=\mu\frac{\partial}{\partial r}\left(\frac{\partial V_\theta}{\partial r}+\frac{V_\theta}{r}\right) \tag{A-2}$$

$$\frac{\partial p}{\partial z}=0 \tag{A-3}$$

$$\frac{\partial V_r}{\partial r}+\frac{V_r}{r}=0. \tag{A-4}$$

From (A-1), (A-3), and (A-4), it can be shown that the pressure gradient is given by

$$\frac{dp}{dr}=\rho\left(\frac{V_r^2+V_\theta^2}{r}\right). \tag{A-5}$$

Since the flow field is axisymmetric and also independent of z, the partial derivative in (A-4) becomes a total derivative. Therefore

$$V_r=\frac{-q}{2\pi}\frac{1}{r}, \tag{A-6}$$

where q is the volumetric flow rate per unit length of z.

Equations (A-2) and (A-6) can then be combined to obtain

$$-Re\,\frac{1}{r}\left(\frac{dV_\theta}{dr}+\frac{V_\theta}{r}\right)=\frac{d}{dr}\left(\frac{dV_\theta}{dr}+\frac{V_\theta}{r}\right), \tag{A-7}$$

where

$$Re\equiv\frac{\rho q}{2\pi\mu},$$

This equation has the solution

$$V_\theta=\frac{A}{r}+\frac{B}{rRe-1}\qquad(Re\neq 2) \tag{A-8}$$

$$V_\theta=\frac{A'}{r}+\frac{B'\ell nr}{r}\qquad(R_e=2). \tag{A-9}$$

If the boundary conditions

$$V_\theta(R_0)=R_0\Omega_0 \tag{A-10}$$

and

$$V_\theta(R_2)=R_2\Omega_2 \tag{A-11}$$

are imposed, these solutions become

$$V_\theta = \frac{R_0\Omega_0}{\left[\left(\frac{R_2}{R_0}\right)-\left(\frac{R_2}{R_e}\right)^{Re-1}\right]}\left[\left(\frac{R_2}{r}\right)-\left(\frac{R_2}{r}\right)^{Re-1}\right]$$

$$+\frac{R_2\Omega_2}{\left[\left(\frac{R_0}{R_2}\right)-\left(\frac{R_0}{R_2}\right)^{Re-1}\right]}\left[\left(\frac{R_0}{r}\right)-\left(\frac{R_0}{r}\right)^{Re-1}\right], (Re\neq 2) \qquad \text{(A-12)}$$

$$V_\theta = -\frac{R_i^2\Omega_0}{r}\frac{\ell n\left(\frac{r}{R_2}\right)}{\ell n\left(\frac{R_0}{R_2}\right)}+\frac{R_2^2\Omega_2}{r}\frac{\ell n\left(\frac{r}{R_0}\right)}{\ell n\left(\frac{R_2}{R_0}\right)} \qquad (Re=2) \qquad \text{(A-13)}$$

Let us examine the case when $\Omega_2 = 0$. This case describes the most severe viscous effects that occur under typical physical requirements if a tube is inserted in the field to extract the fluid.

Let us define the viscous core (not necessarily a rigid body core) as the region inside R_3, the radius at which the tangential velocity is a maximum. Then, from (A-12) with $\Omega_2 = 0$,

$$\left.\frac{\partial V_\theta}{\partial r}\right|_{R_3} = 0 \Rightarrow \left[-\frac{R_2}{r^2}+\frac{Re-1}{r}\left(\frac{R_2}{r}\right)^{Re-1}\right]_{R_3} = 0. \qquad \text{(A-14)}$$

Thus,

$$\frac{R_3}{R_2} = (Re-1)^{\frac{1}{Re-2}} \qquad (Re\neq 2). \qquad \text{(A-15)}$$

In addition, (A-13) with $\Omega_2 = 0$ can be used to show that

$$\left.\frac{\partial V_\theta}{\partial r}\right|_{R_3} = 0 \Rightarrow \left[1-\ell n\left(\frac{r}{R_2}\right)\right]_{R_3} = 0.$$

Thus

$$\frac{R_3}{R_2} = e \quad (Re=2). \qquad \text{(A-16)}$$

If one lets

$$Re = 2 \pm \epsilon$$

then from (A-15)

$$\frac{R_3}{R_2} = (1 \pm \epsilon)^{\pm \frac{1}{\epsilon}}$$

But since $\lim_{\epsilon \to 0} (1 \pm \epsilon)^{\pm \frac{1}{\epsilon}} = e$

(A-15) also shows that $\frac{R_3}{R_2} = e$ at $Re = 2$

Thus, (A-15) can be used for all Re.

This relationship can be used to show that R_3/R_2 is bounded for all $Re > 1$. In particular,

$$\lim_{Re \to \infty} \left(\frac{R_3}{R_2} \right) = 1$$

because

$$\lim_{Re \to \infty} \left[(Re-1)^{\frac{1}{Re-2}} \right] = e^{\lim_{Re \to \infty} \ell n \left[(Re-1)^{\frac{1}{Re-2}} \right]}$$

$$= e^{\lim_{Re \to \infty} \left[\frac{\ell n (Re-1)}{Re-2} \right]} = e^{\left(\frac{\lim_{Re \to \infty} \frac{d}{dRe} \left[\ell n (Re-1) \right]}{\lim_{Re \to \infty} \frac{d}{dRe} \left[Re-2 \right]} \right)}$$

$$= e^{\lim_{Re \to \infty} \left(\frac{1}{Re-1} \right)} = 1.$$

The core size thus approaches that of the sink tube as Re becomes large. In the experiment that is the subject of this report, Re is of the order of 10^4.

If R_2 is reduced, then Re will change unless specific supply and sink conditions are maintained. If the pressure drop between the two cylinders is maintained, for instance, the flow rate will gradually decrease. (A-6) and (A-12) with $\Omega_2 = 0$ can be used in (A-5) to show that at some R_2 the flow stops if the pressure drop is less than $\frac{R_0^2 \Omega_0^2}{2}$. If R_2 is decreased, the flow is then outward.

If R_2 is made to approach zero while Re is held constant, (A-15) shows that R_3 also approaches zero if $Re > 1$. If $Re \leq 1$, $\partial V_\theta / \partial r$ is not zero at any point between the two cylinders. Thus, as R_2 approaches zero, the viscous core either gradually shrinks to zero or continues to fill the entire flow region. The behavior of the fluid in the core is definitely not that of a rigid-body. Notice that the only case in

which a term linear in r does appear in (A-12) is for the case Re = 0, or when the flow rate is zero. Even in that case, though, the 1/r dependence makes its strongest contribution near the center of the vortex, and the rigid-body behavior is strongest in the outer portion of the region, just the opposite of a free vortex with a rigid-body core.

For given values of R_0, R_2, Re and Ω_0, a value for Ω_2 exists such that the fluid very near the sink wall behaves as a rigid-body. However, this value increases without limit as R_2 is decreased. Thus, it is not possible to construct a situation in which the fluid near the center approaches a specific rigid-body field as R_2 is decreased.

It was specified in the previous discussion that Re be constant. This is equivalent to assuming that the strength of the sink and that the stagnation conditions remain constant, the requirements which should be made if one were to consider only the effect of shrinking the sink tube. Re can be maintained constant simply by adjusting the pressure difference between R_0 and R_2 (in keeping with the solution of (A-5)) as R_2 is changed so that the mass flow rate through the region remains constant.

If the pressure ratio between R_0 and R_2 varies significantly from 1 while increasing this pressure difference and decreasing R_2, compressible effects must be considered. The continuity equation will require

$$\frac{\partial}{\partial r}\left(\rho V_r\right)+\frac{\rho V_r}{r}=0 \qquad \text{(A-17)}$$

The term (ρV_r) on the left side of (A-2) remains unchanged, because (A-17) requires

$$\rho V_r = \frac{\text{constant}}{r}$$

the same result which is obtained if ρ is constant. However, two additional effects must be considered in the viscous term on the right of (A-2). In deriving the incompressible equations, it is assumed that μ is constant and that div $\bar{V} = 0$. The continuity equation requires that div $(\rho\bar{V}) = 0$, so that div $\bar{V}$ is not zero if ρ is not constant. Also, μ changes with radius due to a change in temperature induced by compressible effects. However, since the flow can at best become sonic at R_2 if Ω_0 is small, these two effects will not be severe and thus will not drastically alter the results. One should expect the previous results to predict the qualitative behavior of the viscous core even in this extreme case.

APPENDIX B. ORTHOGONALITY OF EIGENFUNCTIONS

The complex space composed of functions whose square is integrable in the sense of Lebesgue over the range $a \le z \le b$ becomes a Hilbert space if the scalar product of two elements $u(z)$ and $v(z)$ is defined[18] as

$$\langle u, v \rangle = \int_a^b u v^* dz \tag{B-1}$$

where the star indicates a complex conjugate. This implies that any function that is Lebesgue integrable can be represented by a convergent sequence of eigenfunctions generated by a complex differential operator L, of the type appearing in (56). In order to find the coefficients of such a sequence, one needs to find the eigenfunctions of the adjoint operator, L^+, which must satisfy the condition[19]

$$\langle u_m, L v_n \rangle = \langle L^+ u_m, v_n \rangle \tag{B-2}$$

where $u_m \varepsilon \bar{E}$, the set of solutions of L^+, and $v_n \varepsilon E$, the set of solutions of L.

It will be shown that if (B-1) is used, (B-2) is satisfied if we choose

$$L^+ = L^* \tag{B-3}$$

Consider first the operator of (56)

$$L v_n \equiv \left(\frac{d^2}{dz^2} - \frac{i\omega}{\nu} \right) v_n = \beta_n k_1(z) v_n \tag{B-4}$$

The conjugate equation is then

$$L^* u_m \equiv \left(\frac{d^2}{dz^2} + \frac{i\omega}{\nu} \right) u_m = \beta'_\eta \, k_1(z) u_m \tag{B-5}$$

Clearly, the two sets are related pairwise such that

$$u_m = v_m^* \tag{B-6}$$

where both sets have been indexed by the same rule. The eigenvalues are also related in the same way; that is,

$$\beta'_m = \beta_m^* \tag{B-7}$$

If (B-4) is multiplied by v_m and this result is subtracted from an equation that is identical except that the indices are exchanged, the result is

$$v_m \frac{d^2 v_n}{dz^2} - v_n \frac{d^2 v_m}{dz^2} = (\beta_n - \beta_m) k_1(z) v_n v_m \tag{B-8}$$

This equation can be integrated once to obtain

$$\left[v_m \frac{d^2 v_n}{dz^2} - v_n \frac{d^2 v_m}{dz^2} \right]_a^b = (\beta_n - \beta_m) \int_a^b k_1(z) v_n v_m dz \tag{B-9}$$

If (B-1) and (B-4) through (B-7) are used, this becomes

$$\left[v_m \frac{d^2 v_n}{dz^2} - v_n \frac{d^2 v_m}{dz^2}\right]_a^b = \langle u_m, Lv_n\rangle - \langle L^* u_m, v_n\rangle \qquad \text{(B-10)}$$

It should be noted that taking the complex conjugate of an integral like that in B-9 is equivalent to reversing the order of the terms in the bracket in B-1.

In that class of boundary conditions for which the left-hand side of B-10 vanishes (in particular for homogeneous boundary conditions, as in the case being considered in this report), (B-2) is satisfied for the relationship chosen in (B-3).

Specifically, then, the complex conjugate of the differential operator of (56) is the adjoint operator, each element of E (the set of solutions of L) is the complex conjugate of one element in $\bar{E}$, and each element of $\bar{E}$ is orthogonal (that is, the scalar product is zero) to every element of E except its conjugate and is not orthogonal to any element of $\bar{E}$ unless $\omega = 0$. When $\omega = 0$, the sets E and $\bar{E}$ coincide and $L^+ = L$.

A function f(z) that is square integrable on the interval (a,b) can then be represented by a sequence

$$f(z) = \sum_n C_n v_n \qquad \text{(B-11)}$$

where

$$C_n = \frac{\int_a^b f(z) k_1(z) v_n \, dz}{\int_a^b v_n k_1(z) v_n \, dz}$$

The function f(z) could also have been represented by a sequence in which all the v's are replaced by u's. Although the coefficients of these two biorthogonal sequences are not identical term by term, the complete series are. This duplicity is a direct result of the fact that L is not self-adjoint, that is, $L^+ \neq L$.

Note also that no solution of the adjoint equation appears in (B-11). Although one must pair the elements of E and $\bar{E}$ to generate an orthogonal series, the conditions that 1) these sets are conjugates of each other and that 2) the complex conjugate of one solution is used in calculating the scalar product combine to cause solutions from only one set to be used in the mechanics of determining the coefficients of the orthogonal series. This is of more than passing interest, since only one equation need be solved. No difficulty arises as it does in matrix problems, where one occasionally must operate on the left and the right of a quantity

using matrices that have different eigenvalues, because the definition of scalar product used here is not analogous to the definition of dot product used in those matrix problems.

APPENDIX C. RELATIONSHIP BETWEEN THE TWO HYPOTHETICAL SOLUTIONS AND THE STEPWISE SOLUTION

What will be discussed here are the ranges of the governing parameters for which the two hypothetical solutions can be considered as bounding expressions for the stepwise solution. Before this is undertaken, it is necessary first to discuss some features of the profile k_1.

Consider the flow in the annular region about a typical r_1 used in the stepwise solution. The k_1 valid there is a solution of (30). The nature of this equation is such that the value of this particular k_1 in the range $o<|z|<h/2$ is greater than that of the solution for any r_1' where $r_1'>r_1$ and less than the solution for any r_1'' where $r_1''< r_1$. Furthermore, the shape of this solution changes continuously if r_1 is varied continuously. Therefore, the value of k_1 at a particular z varies continuously and in a monotonic fashion as r is varied over the full extent of its range.

Now consider the annulus that is bounded on the upstream side by the coupler. Suppose that the pickoff were located at the downstream limit of this annulus and further that it can be shown that the output from the pickoff varies in a monotonic fashion as the profile is varied in any arbitrary but monotonic fashion from parabolic to uniform. One solution would then provide an upper bound for the output at the downstream limit of the annulus, and the other a lower bound.

If one were to proceed with the step-wise solution, these solutions could now be used to provide an upper and a lower bound for the upstream boundary condition on the next inner annulus. For instance, the upper bound for sensor output if the pickoff were located at the downstream limit of this second annulus could be obtained if the solution which provided the upper bound in the previous annulus were continued across this second annulus. To understand this, remember that a "maximum" function provides an upper bound for the solution at the downstream limit of a given annulus for a given upstream boundary condition, and that a "minimum" function gives a lower bound. If this lower bound is used in the next inner annulus as the upstream boundary condition for the minimum function, the result obtained is thus the lower bound for the downstream limit of this second annulus. Likewise, the upper bound at the downstream limit of the first annulus can be used with the maximum function to obtain the upper bound at the lower limit of this second annulus. This procedure is equivalent to extending the maximum and minimum functions across both annuli without bothering to evaluate the results at the interface of the annuli.

The same argument can be extended for both bounding expressions through the entire chamber to the pickoff. As a result, it can be seen that these two hypothetical solutions provide bounding expressions for the sensor gain if it can be established that the expression for gain behaves in a monotonic fashion as k_1 varies in any arbitrary but monotonic fashion from parabolic to uniform where k_1 is made to apply over the entire range of r.

This is an unnecessarily strong condition. It does not, for instance, take into account the fact that k_1 varies in a monotonic fashion with r_1. As such, this method could be used to specify output bounds if k_1 were allowed to vary in an arbitrary manner with r_1. The governing equation specifies a specific manner, not an arbitrary one, in which the profile changes from parabolic to uniform as r_1 decreases. But although this condition is not a necessary one for the hypothetical solutions to be bounds, it is certainly a sufficient one. It is the one pursued here because it was felt that no other method could be used which would not require the solving of (30). Such an effort would partially defeat the purpose of this abbreviated approach to finding expressions for the sensor output.

It will not be possible in all cases to establish the monotonic behavior for an arbitrary variation of k_1, particularly because the form of Ψ_n depends on k_1. In those cases, some insight can be gained by allowing k_1 to vary in some convenient manner from parabolic to uniform. This approach is not rigorous, but should be of some value for the purpose of obtaining engineering design equations.

Consider first the expression for G_0 obtained from (63), (29), (38), (43), (46), (52), (53) and (59) with $\omega=0$. Only the first term in the series generated by u_2 will be considered, since it is shown in Section 2.3.2 of the text that the higher order terms are very small. The coefficient C_0 is found here by a technique analogous to that used when $k_1 = k_\infty$. That technique will be explained when equation (D-21) is found in the following appendix.

$$G_0 = \frac{Re_0'}{h}\left[\int_0^{\frac{h}{2}} k_1'(z)\int_z^{\frac{h}{2}}\int_0^{\eta} k_1'(\xi)\,d\xi\,d\eta\,dz - e^{\left[\frac{-2\beta_0'}{Re_0'}\left(\frac{2}{h}\int_0^{\frac{h}{2}} k_1\,dz\right)\right]}\frac{\int_0^{\frac{h}{2}} k_1(z)\psi_0\int_z^{\frac{h}{2}}\int_0^{\eta} k_1(\xi)\,d\xi\,d\eta\,dz\int_0^{\frac{h}{2}} k(z)\psi_0\,dz}{\int_0^{\frac{h}{2}} k(z)\psi_0\psi_0\,dz\int_0^{\frac{h}{2}} k_1(z)\,dz\int_0^{\frac{h}{2}} k_1(z)\,dz}\right] \qquad (C\text{-}1)$$

where

$$k_1' = \frac{k_1}{\int_0^{\frac{h}{2}} k_1 \, dz}$$

and

$$\beta_0' = -\frac{h^2}{4}\beta_0 .$$

When $\omega=0$, the eigenfunction Ψ_0 satisfies the equation

$$\frac{d^2\psi_0}{dz^2} + \frac{4}{h^2}\beta_0' k_1 \psi_0 = 0. \qquad \text{(C-2)}$$

Consider first the case when Re_0' is so small that the exponential term is negligible. (C-1) becomes

$$G_0 = \frac{Re_0'}{h}\int_0^{\frac{h}{2}} k_1'(z)\int_z^{\frac{h}{2}}\int_z^{\eta} k_1'(\xi)\, d\xi\, d\eta\, dz \qquad \text{(C-3)}$$

Let k_2 and k_3 be functions of z that are one at z=0, zero at $z = \pm h/2$, and behave in a monotonic fashion between the centerplane and either wall. Let k_3 be greater than k_2 for for $o<|z|<h/2$. The expression $(k_2'-k_3')$ is then a maximum at $z = 0$, decreases to some negative value, and then increases to zero (fig. C1 and C2).

The two cross hatched areas of figure C2 are equal but opposite since the total area under k_2' is by definition equal to that under k_3'. Therefore,

$$\int_o^{\eta}\left(k_2' - k_3'\right)d\xi > 0, \qquad 0 < \eta < \frac{h}{2}$$

Furthermore,

$$\int_z^{\frac{h}{2}}\int_0^{\eta}\left(k_2' - k_3'\right)d\xi\, d\eta > 0, \qquad 0 < z < \frac{h}{2}$$

or, expressed in another form

$$\int_z^{\frac{h}{2}}\int_0^{\eta} k_2'\, d\xi\, d\eta > \int_z^{\frac{h}{2}}\int_0^{\eta} k_2'\, d\xi\, d\eta \qquad z \neq \frac{h}{2} \qquad \text{(C-4)}$$

Each integral in (C-4) decreases monotonically from some positive value at $z = 0$ tc zero at $z = h/2$. If it is also noted that (1) $(k_2' - k_3')$ is positive at $z = 0$, that (2) $(k_2' - k_3')$ has only one zero between $z = 0$ and $z = h/2$, and that (3) the total hatched area of figure C2 is zero, then it can be shown that

$$\int_0^{\frac{h}{2}}\left(k_2' - k_3'\right)\int_z^{\frac{h}{2}}\int_0^{\eta} k_2'\, d\xi\, d\eta\, dz > 0.$$

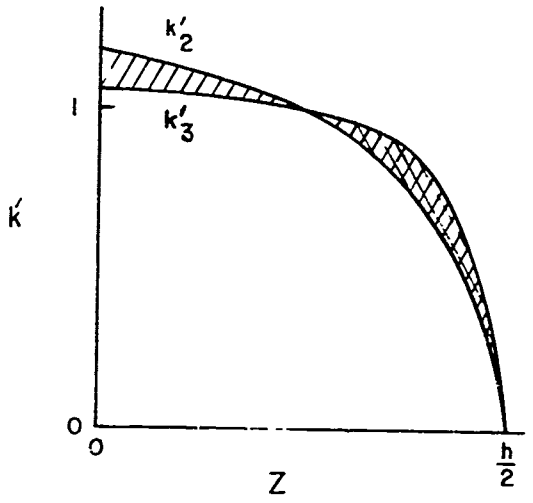

FIGURE C1.- k'_2 AND k'_3 vs Z

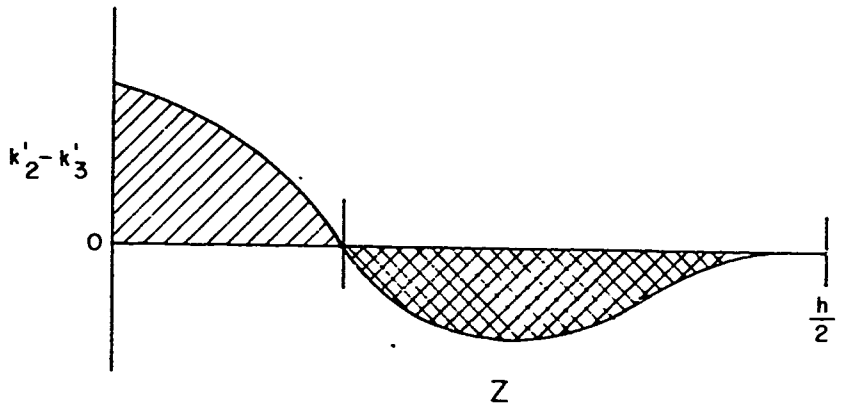

FIGURE C2.- $(k'_2 - k'_3)$ vs Z

If this relationship and (C-4) are combined, one obtains

$$\int_0^{\frac{h}{2}} k_2' \int_z^{\frac{h}{2}} \int_0^{\eta} k_2' \, d\xi d\eta dz$$

$$> \int_0^{\frac{h}{2}} k_2' \int_z^{\frac{h}{2}} \int_0^{\eta} k_2' \, d\xi d\eta dz \qquad \text{(C-5)}$$

$$> \int_0^{\frac{h}{2}} k_3' \int_z^{\frac{h}{2}} \int_0^{\eta} k_3' \, d\xi d\eta dz .$$

Since the limiting expression for k_2 in this case is k_∞, relationship (C-5) establishes that the parabolic solution provides an upper bound for (C-3). Since the limiting expression for k_3 in this case is k_0, the uniform solution provides a lower bound for (C-3).

Therefore, the parabolic solution provides an upper bound for G_0 when Re_0' is small, and the uniform solution a lower bound.

Consider next the range $Re_0' < 7$ where the second term on the right (C-1) is not negligible. If (C-2) is used, the coefficient of the exponential term becomes

$$I_2 \equiv \frac{\int_0^{\frac{h}{2}} \left(\frac{-h^2}{4\beta_0'}\right) \frac{d^2\psi_0}{dz^2} \int_z^{\frac{h}{2}} \int_0^{\eta} k_1(\xi) \, d\xi d\eta dz \int_0^{\frac{h}{2}} \left(\frac{-h^2}{4\beta_0'}\right) \frac{d^2\psi_0}{dz^2} dz}{\int_0^{\frac{h}{2}} \left(\frac{-h^2}{4\beta_0'}\right) \frac{d^2\psi_0}{dz^2} \psi_0 dz \int_0^{\frac{h}{2}} k_1 dz \int_0^{\frac{h}{2}} k_1 dz}$$

$$= \frac{-h^2}{4\beta_0'} \frac{\int_0^{\frac{h}{2}} \frac{d^2\psi_0'}{dz^2} \int_z^{\frac{h}{2}} \int_0^{\eta} k_1(\xi) \, d\xi d\eta dz}{\int_0^{\frac{h}{2}} \frac{d^2\psi_0'}{dz^2} \psi_0' dz \int_0^{\frac{h}{2}} k_1 dz \int_0^{\frac{h}{2}} k_1 dz} \left(\frac{\left.\frac{d\psi_0}{dz}\right|_{z=\frac{h}{2}}}{\left.\psi_0\right|_{z=0}} \right), \qquad \text{(C-6)}$$

where

$$\psi_0' = \frac{\psi_0}{\psi_0|_{z=0}} .$$

After some examination, it is evident that the combined contribution of I_2 and the exponential term diminishes as k_1 changes from parabolic to uniform, as in the case of the first term in (C-1). However, since the signs of the first and second terms are opposite, it is necessary to establish their relative magnitude in order to determine the sign of the net change in G_0 as k_1 is varied.

The non-rigorous method of choosing k_1 equal to some convenient function of z will be used in this effort. This lack of rigor may not be so disturbing if it is recalled that we have established from intuitive means that the most attractive operational range is that in which the entrance effects can be ignored, or that range in which the second term in (C-1) can be ignored.

The solution of (C-2) will now be given for the range $0 \leq z \leq h/2$ when k_1 is chosen to be some convenient function of z. The solution for negative z can be found from this solution by symmetry. The boundary conditions are

$$\left.\frac{d\psi_0}{dz}\right|_{z=0} = 0 \qquad \text{(C-7)}$$

and

$$\psi_0\left(\frac{h}{2}\right) = 0, \qquad \text{(C-8)}$$

Now let

$$k_1 = \left(1 - \frac{2z}{h}\right)^m \qquad \text{(C-9)}$$

where $1/2 \geq m \geq 0$. The upper limit of m has been chosen so that the area under k_1 for $m = 1/2$ is equal to the area under the parabolic profile. The mean deviation of this profile and the parabolic is about 5 percent. Comparable deviations for other k_1's might be expected, yielding an approximation accurate to the first order.

First let

$$y = 1 - \frac{2z}{h} . \qquad \text{(C-10)}$$

Then (C-2) becomes

$$\frac{d^2\psi_0}{dy^2} + \beta_0' y^m \psi_0 = 0 \qquad \text{(C-11)}$$

Now let

$$\psi_0 \equiv U\sqrt{y} \qquad \text{(C-12)}$$

and

$$W \equiv \frac{2\sqrt{\beta_0'}}{m+2} y^{\frac{m+2}{2}} \qquad \text{(C-13)}$$

Equation (C-11) becomes

$$W^2 \frac{d^2U}{dW^2} + W\frac{dU}{dW} + \left[W^2 - \left(\frac{1}{m+2}\right)^2\right] U = 0. \qquad \text{(C-14)}$$

This equation has the solution[20]

$$U \equiv A' J_{\left(\frac{1}{m+2}\right)}(W) + B' Y_{\left(\frac{1}{m+2}\right)}(W), \qquad \text{(C-15)}$$

where A' and B' are constants and J and Y are Bessel functions.

If (C-12) and (C-13) are applied, (C-15) becomes

$$\psi_0 = A' y^{\frac{1}{2}} J_{\left(\frac{1}{m+2}\right)}\left(\frac{2\sqrt{\beta_0'}}{m+2} y^{\frac{m+2}{2}}\right) + B' y^{\frac{1}{2}} Y_{\left(\frac{1}{m+2}\right)}\left(\frac{2\sqrt{\beta_0'}}{m+2} y^{\frac{m+2}{2}}\right) \qquad \text{(C-16)}$$

The boundary conditions are given by

$$\left.\frac{d\psi_0}{dy}\right|_{y=1} = 0 \qquad \text{(C-17)}$$

and

$$\psi_0(0) = 0. \qquad \text{(C-18)}$$

Equation (C-18) requires B' = 0. Equation (C-17) can now be used to determine β_0'.

If the series representation[20] of the Bessel function is used, (C-16) becomes

$$\psi_0 = \left(\frac{\lambda_0}{2}\right)^{\frac{1}{m+2}} y \sum_{\ell=0}^{\infty} \frac{\left(-\frac{1}{4}\right)^{\ell}\left(\lambda_0\right)^{2\ell} y^{\ell(m+2)}}{\ell!\Gamma\left(\frac{1}{m+2}+1+\ell\right)}, \tag{C-19}$$

where

$$\lambda_0 = \frac{2\sqrt{\beta_0'}}{m+2} \tag{C-20}$$

and λ_0 is the first nonnegative root of the expression

$$\sum_{\ell=0}^{\infty} \frac{\left[\ell\left(m+2\right)+1\right]\left(-\frac{1}{4}\right)^{\ell}\lambda^{2\ell}}{\ell!\Gamma\left(\frac{1}{m+2}+1+\ell\right)} = 0. \tag{C-21}$$

To evaluate (C-6), $\frac{d\psi_0}{dz}$ must be evaluated at the wall and ψ_0 must be evaluated at the centerplane. From (C-10) and (C-19),

$$\left[\frac{d\psi_0}{dz}\Big|_{z=\frac{h}{2}}\right] = -\frac{2}{h}\left(\frac{\lambda_0}{2}\right)^{\frac{1}{m+2}} \frac{1}{\Gamma\left(\frac{1}{m+2}+1\right)} \tag{C-22}$$

and

$$\psi_0\Big|_{z=0} = \left(\frac{\lambda_0}{2}\right)^{\frac{1}{m+2}} \sum_{\ell=0}^{\infty} \frac{\left(-\frac{1}{4}\right)^{\ell}\left(\lambda_0\right)^{2\ell}}{\ell!\Gamma\left(\frac{1}{m+2}+1+\ell\right)} \tag{C-23}$$

Next, the expression

$$\int_z^{\frac{h}{2}} \int_0^{\eta} k_1(\xi)\, d\xi\, d\eta$$

in (C-6) can be evaluated using (C-10). This expression becomes

$$\frac{h^2}{4}\int_y^0\int_1^\eta \xi^m\, d\xi\, d\eta = \frac{h^2}{4(m+2)} f'(y)$$

where

$$f'(y) = \frac{m+2}{m+1}\left[y - \frac{y^{m+2}}{m+2}\right] \qquad \text{(C-24)}$$

The function f'(y) has a value of one at the center plane for all m and zero at the wall, but its average decreases over the range of y is less than two percent as m increases from zero to one-half.

Finally

$$\int_0^{\frac{h}{2}} k\, dz = -\frac{h}{2}\int_1^0 y^m\, dy$$

$$= \frac{h}{2(m+1)}. \qquad \text{(C-25)}$$

If (C-6) and (C-22) through (C-25) are used, the second term in (C-1) becomes

$$I_2 e^{-\frac{2\beta_0'}{Re_0'}\left(\frac{2}{h}\int_0^{\frac{h}{2}} k_1 dz\right)} = \frac{h}{4}\left[e^{-\frac{2\lambda_0^2}{Re_0'}\frac{\left(1+\frac{m}{2}\right)^2}{(1+m)}}\right]$$

$$\cdot\cdot\frac{\dfrac{(1+m)^2}{\left(1+\frac{m}{2}\right)^3}\dfrac{\int_0^{\frac{h}{2}}\frac{d^2\psi_0'}{dz^2} f' dz}{\int_0^{\frac{h}{2}}\frac{d^2\psi_0'}{dz^2}\psi_0' dz}}{\lambda_0^2\sum_{\ell=0}^{\infty}\dfrac{\left(-\frac{\lambda_0^2}{4}\right)^\ell \Gamma\left(\frac{1}{m+2}+1\right)}{\ell!\,\Gamma\left(\frac{1}{m+2}+1+\ell\right)}}, \qquad \text{(C-26)}$$

where λ_0 is found from (C-21).

Both ψ_0' and f' are normalized functions whose maximum value is independent of m and whose shape depends only weakly

on m. Thus, the ratio of the integrals may be considered a constant. Since the above approach is identical when m = 0 to the method used to obtain the uniform solution, the value of this ratio can be found from (78) and (C-26) with m = 0. It can be shown that for m = 0,

$$\lambda_0 = \frac{\pi}{2} \tag{C-27}$$

and

$$\frac{\int_0^{\frac{h}{2}} \frac{d^2\psi_0'}{dz^2} f' dz}{\int_0^{\frac{h}{2}} \frac{d^2\psi_0'}{dz^2} \psi_0' dz} = \sum_{\ell=0}^{\infty} \frac{\left(\frac{\pi^2}{16}\right)^{\ell-1} (-1)^{\ell}}{\ell!} \frac{\Gamma\left(\frac{3}{2}\right)}{\Gamma\left(\frac{3}{2}+\ell\right)} \tag{C-28}$$

The behavior of the second term in (C-1) can then be found from (C-26) and (C-28). It was calculated for $Re_0' = 7$, the worst case. It was found to vary from .081 h for m = 0 to .099 h for m = 1/2. The behavior was very nearly linear with m. Although this behavior is somewhat weak, it should be compared to the behavior of the first term in (C-1) to establish whether the entire expression increases as m varies from 0 to 1/2.

Now consider the first term in (C-1). If this is rewritten in terms of k_1, then

$$I_1 \equiv \frac{\int_0^{\frac{h}{2}} k_1(z) \int_z^{\frac{h}{2}} \int_0^{\eta} k_1(\xi)\, d\xi\, d\eta\, dz}{\int_0^{\frac{h}{2}} k_1\, dz \int_0^{\frac{h}{2}} k_1\, dz}, \tag{C-29}$$

If (C-9), (C-10), (C-24) and (C-25) are used, (C-29) becomes

$$I_1 = \frac{\frac{h}{2}\int_0^1 y^m \left[\frac{y}{m+1} - \frac{y^{m+2}}{(m+2)(m+1)}\right] dy}{\left[\frac{h}{2(m+1)}\right]^2} \tag{C-30}$$

$$= h\,\frac{(m+1)^2}{(m+2)(2m+3)}$$

It can be shown that (C-30) behaves in a nearly linear fashion with m, and that this expression varies from .167 h to .225 h as m varies from 0 to 1/2. It can be shown from (78) that (C-30) should be .167 h when the profile is uniform and from (64) that it should be .243 h when the profile is parabolic. This approach would then seem sufficiently accurate. It shows that the increase with m in the first term in (C-1) is about four times greater than the increase in magnitude of the second term. Thus, G_0 very probably increases monotonically as k_1 changes from uniform to parabolic even in the upper limit of the fully developed range.

Let us next consider $G_{i\omega}$ when Re' is very small. If (52) is used, one then has

$$G_{i\omega}\Big|_{R\acute{e}_0 \cong 0} = \frac{\int_0^{\frac{h}{2}} k_1 \frac{\cosh(az)}{\cosh\left(\frac{ah}{2}\right)} \int_z^{\frac{h}{2}} \frac{1}{\cosh^2 a\eta} \int_0^{\eta} k_1 \cosh^2(a\xi)\, d\xi\, d\eta\, dz}{\int_0^{\frac{h}{2}} k_1(z) \int_z^{\frac{h}{2}} \int_0^{\eta} k_1(\xi)\, d\xi\, d\eta\, dz} \qquad \text{(C-31)}$$

For small ω', this may be expressed as

$$G_{i\omega}\Big|_{R\acute{e}_0 \cong 0} = \int_0^{\frac{h}{2}} k_1(z) \left[1 + \frac{i\omega}{2\nu}\left(z^2 - \frac{h^2}{4}\right) - \frac{\omega^2}{\nu^2}\left(\frac{z^4}{24} - \frac{z^2 h^2}{16} + \frac{5h^4}{24 \times 16}\right)\right]$$

$$\times \frac{\int_z^{\frac{h}{2}} \int_0^{\eta} k_1(\xi)\left[1 - \frac{1}{3}\frac{\omega^2}{\nu^2}\left(\xi^4 - \eta^4\right)\right] d\xi\, d\eta}{\int_0^{\frac{h}{2}} \int_0^{\eta} k_1(z) \int_z^{\frac{h}{2}} \int_0^{\eta} k_1(\xi)\, d\xi\, d\eta\, dz} dz \qquad \text{(C-32)}$$

$$= 1 - \frac{i\omega'}{8} \frac{\int_0^{\frac{h}{2}} k_1(z)\left(1 - \frac{4z^2}{h^2}\right) \int_z^{\frac{h}{2}} \int_0^{\eta} k_1(\xi)\, d\xi\, d\eta\, dz}{\int_0^{\frac{h}{2}} k_1(z) \int_z^{\frac{h}{2}} \int_0^{\eta} k_1(\xi)\, d\xi\, d\eta\, dz}$$

$$\frac{-(\omega')^2}{48}\left[\frac{5}{8} \frac{\int_0^{\frac{h}{2}} k_1(z)\left(1 - \frac{4z^2}{h^2}\right)\left(1 - \frac{4z^2}{5h^2}\right) \int_z^{\frac{h}{2}} \int_0^{\eta} k_1(\xi)\, d\xi\, d\eta\, dz}{\int_0^{\frac{h}{2}} k_1(z) \int_z^{\frac{h}{2}} \int_0^{\eta} k_1(\xi)\, d\xi\, d\eta\, dz}\right. \qquad \text{(C-33)}$$

$$\left. - \frac{\int_0^{\frac{h}{2}} k_1(z) \int_z^{\frac{h}{2}} \int_0^{\eta} \left[\left(\frac{2\eta}{h}\right)^4 - \left(\frac{2\xi}{h}\right)^4\right] k_1(\xi)\, d\xi\, d\eta\, dz}{\int_0^{\frac{h}{2}} k_1(z) \int_z^{\frac{h}{2}} \int_0^{\eta} k_1(\xi)\, d\xi\, d\eta\, dz}\right]$$

$$\equiv 1 - \frac{i\omega'}{8} I_3 - \frac{(\omega')^2}{48}\left(\frac{5}{8} I_4 - I_5\right)$$

The phase lag, ϕ, of $G_{i\omega}$ at small ω' is thus given in radians approximately by

$$\phi = \frac{\omega'}{8} I_3 \tag{C-34}$$

and the amplitude, $|G_{i\omega}|$, is given approximately by

$$|G_{i\omega}| = 1-(\omega')^2\left[\frac{1}{48}\left(\frac{5}{8}I_4 - I_5\right) - \frac{I_3^2}{128}\right] \tag{C-35}$$

Consider first (C-34). It can be established intuitively that the value of I_3 decreases as k_1 changes from parabolic to uniform. To see this, it may help to think of I_3 in the form

$$I_3 = \frac{\int_0^{\frac{h}{2}} k_1(z)\rho(z)\int_z^{\frac{h}{2}}\int_0^{\eta} k_1(\xi)\,d\xi\,d\eta\,dz}{\int_0^{\frac{h}{2}} k_1(z)\int_z^{\frac{h}{2}}\int_0^{\eta} k_1(\xi)\,d\xi\,d\eta\,dz} \tag{C-36}$$

where $\rho(z) = 1-\frac{4z^2}{h^2}$ is looked on as a weighting function. If $\rho(z)$ were a constant, then the value of I_3 would be independent of $k_1(z)$. But since $\rho(z)$ decreases monctonically from the centerplane to the wall in this case, the value of I_3 increases if k_1 is weighted more strongly toward the centerplane. Thus, I_3 increases as the profile changes from uniform to parabolic. This implies that the parabolic solution provides an upper bound for the phase lag when ω' and Reδ are small, and the uniform provides a lower bound.

It would appear that (C-35) cannot be handled in any convenient manner for a general k_1. Let us then attack the problem in a less rigorous manner by assuming that

$$k_1(z) = 1 - \left(\frac{2z}{h}\right)^m \qquad \text{(C-37)}$$

where $2 \leq m < \infty$. The upper limit for m represents a uniform profile.

I_4 is then given by

$$I_4 = \frac{\int_0^1 (1-z'^m)(1-z'^2)(1-\frac{1}{5}z'^2)\int_{z'}^1\int_0^{\eta'}(1-\xi'^m)\,d\xi'\,d\eta'\,dz'}{\int_0^1 (1-z'^m)\int_{z'}^1\int_0^{\eta'}(1-\xi'^m)\,d\xi'\,d\eta'\,dz'} \qquad \text{(C-38)}$$

where all the independent variables have been normalized with respect to $h/2$. It can then be shown that

$$I_4 = \left[\frac{178}{525}m^2 + \frac{524m}{525} - \frac{64}{525} - \frac{m^2+3m}{2(m+1)} + \frac{11m^2+33m+20}{10(m+3)} - \frac{7m^2+21m+24}{10(m+5)}\right.$$

$$\left. + \frac{m^2+3m+4}{10(m+7)} - \frac{1}{2m+3} + \frac{6}{5(2m+5)} - \frac{1}{5(2m+7)}\right] \Bigg/ \left[\frac{1}{3}m^2 + m \right. \qquad \text{(C-39)}$$

$$\left. - \frac{1}{3} - \frac{m^2+3m}{2(m+1)} + \frac{1}{m+3} - \frac{1}{2m+3}\right]$$

It can also be shown that if C-37 is used I_5 becomes

$$I_5 = \left[\frac{4}{35}\,\frac{m^2+8m}{(m+1)(m+1)} - \frac{4(m^2+7m)}{(m+1)^2(m+5)(m+6)(2m+7)}\right] \Bigg/ \left[\left(\frac{1}{3}m^2\right.\right. \qquad \text{(C-40)}$$

$$\left.\left. + m - \frac{1}{3} - \frac{m^2+3m}{2m+2} + \frac{1}{m+3} - \frac{1}{2m+3}\right)\frac{1}{(m+1)(m+2)}\right]$$

and that I_3 becomes

$$I_3 = \left[-\frac{1}{15} - \frac{1}{m+1} + \frac{1}{m+3} - \frac{1}{2(m+5)} + \frac{m^2+3m}{3(m+1)(m+2)} - \frac{1}{(m+1)(m+2)(2m+3)}\right.$$

$$\left. - \frac{1}{(m+1)(m+2)(m+5)} + \frac{1}{(m+1)(m+2)(2m+5)}\right] \Bigg/ \left[\left(\frac{1}{3}m^2 + m \right.\right. \qquad \text{(C-41)}$$

$$\left.\left. - \frac{1}{3} - \frac{m^2+3m}{2m+2} + \frac{1}{m+3} - \frac{1}{2m+3}\right)\frac{1}{(m+1)(m+2)}\right]$$

If (C-39), (C-40) and (C-41) are used, (C-35) can be evaluated. It can be shown that the bracket to the right in (C-35) is a weakly increasing function of m. Thus, the attenuation predicted by either expression can be considered as a good estimate of the behavior at small ω' and Re_0', although it would appear that the parabolic solution provides a maximum estimate for the amplitude of $G_{i\omega}$ and the uniform provides a minimum

When Re_0' is very small and ω' is large, (C-32) can then be approximated by

$$G_{i\omega}|_{Re_0' \simeq 0} = \int_0^{\frac{h}{2}} k_1(z)\, e^{\sqrt{\frac{\omega}{2\nu}}\left(z-\frac{h}{2}\right)}\, e^{i\sqrt{\frac{\omega}{2\nu}}\left(z-\frac{h}{2}\right)} \int_z^{\frac{h}{2}} \int_0^{\eta} k_1(\xi)$$

$$\times \frac{e^{\sqrt{\frac{2\omega}{\nu}}(\xi-\eta)}\, e^{i\sqrt{\frac{2\omega}{\nu}}(\xi-\eta)} d\xi\, d\eta\, dz}{\int_0^{\frac{h}{2}} k_1(z) \int_z^{\frac{h}{2}} \int_0^{\eta} k_1(\xi)\, d\xi\, d\eta\, dz} \qquad \text{(C-42)}$$

The influence of the functions of ω in this expression is now more apparent. Clearly, the exponential functions with a real exponent, which may be regarded as weighting functions, cause the integrands to be weighted quite heavily toward the values near the wall. Then if the value of k_1 is made to increase near the wall, the magnitude of the numerator increases more than that of the denominator, which has no such weighting function. Thus, the amplitude of $G_{i\omega}$ increases as the profile changes from parabolic to uniform for large ω' and very small Re_0'.

The phase can be discussed by considering only the numerator, since the denominator is real. For this discussion, it may help to consider the function k_1 as the weighting function. If the value of k_1 near the wall increases, then the contributions due to the exponential that has an imaginary exponent are weighted more heavily near the wall. Since the phase lag relative to the wall decreases as z approaches the wall, this implies that the phase lag decreases as the profile changes from parabolic to uniform.

It has been shown that when Re_0' is very small, the amplitude of $G_{i\omega}$ for small ω' does not vary significantly as the radial profile is changed and that for large ω' the amplitude is bounded above by the uniform solution and below by the parabolic. Since the amplitude of the functions of a (that is, ω') in (C-31) is monotonic with ω', it would then seem reasonable to conclude that for all ω', either the amplitude is bounded above by the uniform solution and below by

the parabolic or the difference in the two expressions for amplitude is negligibly small.

If Re_0' is not small, then the contributions due to u_2 must be considered. Before this problem is attacked head-on, a little discretion can be used. The form of $G_{i\omega}$ can be represented as

$$G_{i\omega} = \frac{G_{i\omega}\big|_{Re_0'=0} - e^{-\frac{\beta_0'}{Re_0'}\left(\frac{2}{h}\int_0^h k_1(z)dz\right)} \cdot F_0\left(Re_0', \omega'\right)}{G_0} \qquad \text{(C-43)}$$

where β_0' is the first eigenvalue of the equation

$$\frac{d^2\psi_n}{d\left(\frac{2z}{h}\right)^2} + \left[\frac{-i\omega'}{4} + \beta_n' k_1(z)\right]\psi_n = 0 \qquad \text{(C-44)}$$

The function $F_0(Re_0', \omega')$ represents the output due to the ψ_0 contribution to the boundary condition at the coupler, and the exponential term specifies the attenuation and phase shift that results when this signal is transported to the pickoff. The function $F_0(Re_0', \omega')$ will be discussed later.

First consider equation (C-44). The only significant variation in $k_1(z)$ occurs near the wall, where ψ_0 is small. The effect in this equation of changing the radial profile from parabolic to uniform is then small. Thus, the shape of ψ_0 and the value of β_0' are relatively independent of the shape of k_1. The solution for a uniform radial profile (to be shown later in appendix F) can be used then to show that the imaginary part of β_0' is positive and nearly a linear function of ω' and that the real part is positive and nearly independent of ω'.

Some features of $F_0(Re_0', \omega')$ can now be discussed. First, since the shape of ψ_0 does not change greatly with $k_1(z)$, $F_0(Re_0', \omega')$ does not depend significantly on $k_1(z)$ either. Its behavior can then be treated simultaneously for all $k_1(z)$. To treat it, we must understand what the contributions due to u_2 represent.

Notice that the boundary conditions on ψ_n are homogeneous. It is as if some signal were introduced at R_0 in a stationary sensor and made to propagate toward the pickoff. The time dependent motion of the sensor would effect the output due to this signal only in that the input

signal would vary due to a change in the function which u_2 must satisfy at the coupler. This input signal is just the value of u_1 relative to the wall.

Now consider u_1, as given by (46), (52) and (53). If ω' is very large, (53) becomes

$$g_1(z)=\frac{2A_1}{\nu}\int_z^{\frac{h}{2}}\int_0^{\eta} k_1(\xi)e^{\sqrt{\frac{\omega'}{2}}\left(\frac{2\xi}{h}-\frac{2\eta}{h}\right)}e^{-i\sqrt{\frac{\omega'}{2}}\left(\frac{2\xi}{h}-\frac{2\eta}{h}\right)}d\xi d\eta \qquad \text{(C-45)}$$

Since the dummy variable η is the upper limit for the dummy variable ξ, the value of $\sqrt{\frac{\omega'}{2}}\left(\frac{2\xi}{h}-\frac{2\eta}{h}\right)$ is always negative, and in particular, increases in magnitude as ω' increases. The exponential function with the real exponent then causes the integrand to diminish rapidly as ω' increases. Thus, g_1 vanishes for large ω', and u_1 takes on the behavior

$$u_1 \cong r g_2(z) \cong r e^{-\sqrt{\frac{\omega'}{8}}\left(1-\frac{2z}{h}\right)}e^{-i\sqrt{\frac{\omega'}{8}}\left(1-\frac{2z}{h}\right)} \qquad \text{(C-46)}$$

For $z \neq h/2$, g_2 vanishes for large ω'. For points away from the wall, then, u_1 goes to zero as ω' increases. In that case, u_2 must then take on the value R_0 at the coupler for points away from the wall.

It will be shown in appendix D that if the radial profile is assumed parabolic throughout the chamber when $\omega'=0$, u_1 is given by

$$u_1=\left[\frac{5Re_0'}{16}\left(1-\frac{4z^2}{h^2}\right)\left(1-\frac{4z^2}{5h^2}\right)\frac{R_0}{r}+\frac{r}{R_0}\right]R_0 \qquad \text{(C-47)}$$

In appendix F it will be shown that if the radial profile is assumed uniform when $\omega'=0$

$$u_1=\left[\frac{Re_0'}{4}\left(1-\frac{4z^2}{h^2}\right)\frac{R_0}{r}+\frac{r}{R_0}\right]R_0 \qquad \text{(C-48)}$$

Thus, the magnitude of the boundary condition at the centerplane which u_2 must satisfy, changes from about $\left(\frac{-Re_0'}{4}\right)R_0$ for small ω' to R_0 for very large ω'.

These facts can be used to approximate the magnitude of $F_C(Re_0', \omega')$, as indicated in Figure C3. The magnitude at small ω' is a linear function of Re_0', but approaches a value of 1 at large ω' for all Re_0'.

Now consider the exponential term It was noted

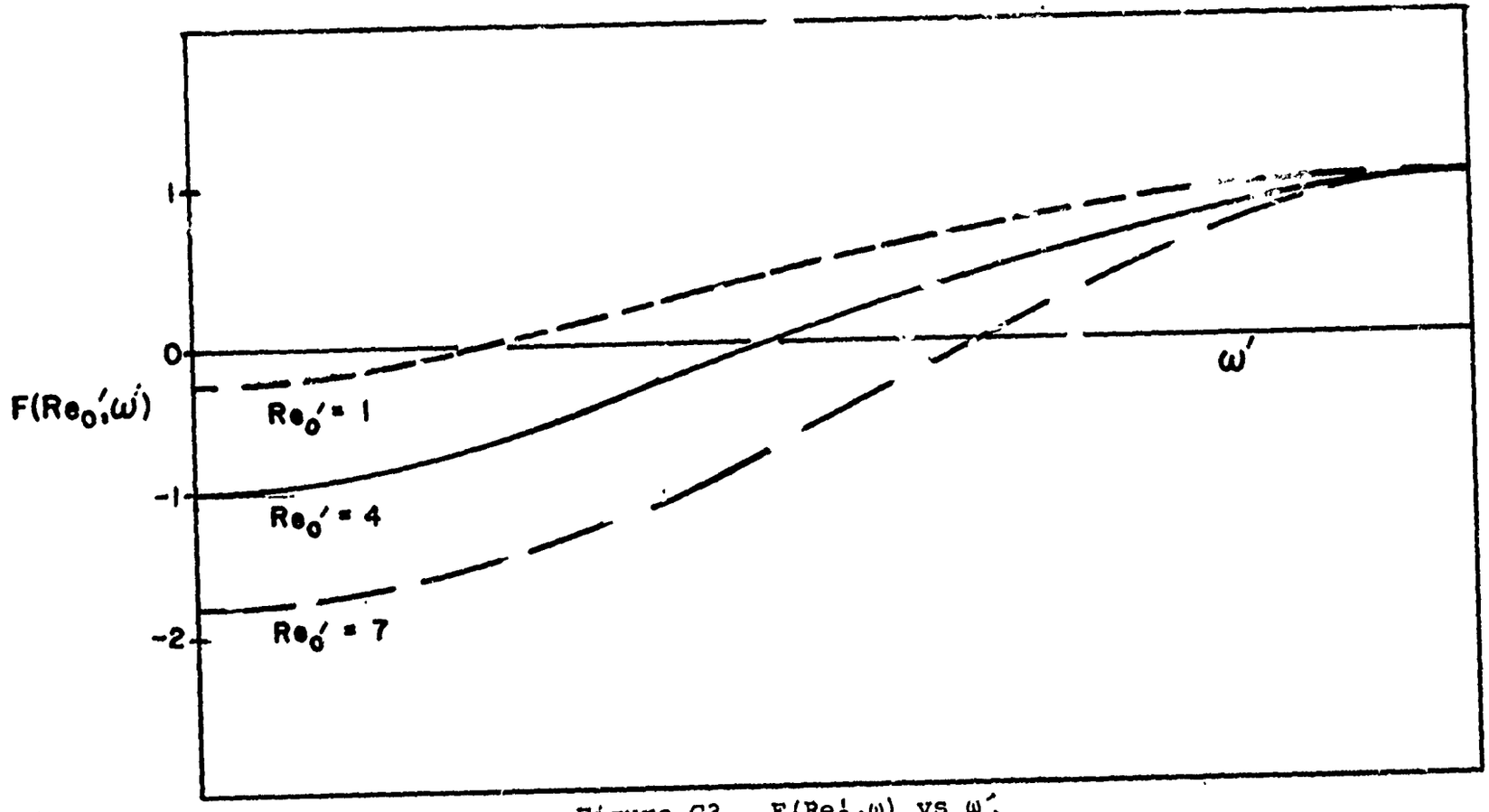

Figure C3. $F(Re_0', \omega)$ vs ω'.

previously that the real part of β_0' is nearly independent of ω'. Then the magnitude of the product of the exponential and $F_C(Re_0', \omega')$ approaches a constant value as ω' increases. Thus, the signal contribution due to u_2 vanishes for large ω' only if the exponential term vanishes. This implies that Re_0' must be sufficiently small to ensure sufficient transport attenuation to reduce the signal contribution below the noise level for all ω'.

Since both β_0' and ψ_0 are nearly independent of $k_1(z)$, the behavior of the signal contribution due to u_2 can be discussed simply by noting the effect on the exponential term of changing the integral in the exponent. The integral increases monotonically as $k_1(z)$ changes from parabolic to uniform.

If the behavior of β_0' with ω' is recalled, it can then be shown that the parabolic solution provides a minimum expression for phase lag and a maximum for amplitude in the signal contribution due to u_2. The uniform solution has the complementary features.

It should be noted that the sign of the contribution due to u_2 is negative, while that due to u_1 is positive. This fact must be recalled carefully when the behavior of $G_{i\omega}$ is discussed in a range where both contributions must be considered.

Now the behavior of $G_{i\omega}$ can be discussed if several other points are mentioned. As ω' increases, the amplitude due to u_1 diminishes relative to dc. and approaches zero, while the phase lag increases and approaches some finite limit. The phase of the signal due to u_2 increases without limit as ω' increases, and the amplitude approaches a finite limit. This value may be either greater or less than the value at dc, depending on the value of Re_0.

These results can be summarized by the statement in Section 2.3 of the main text.

APPENDIX D. SOLUTION FOR A PARABOLIC RADIAL PROFILE

If (33) is used, (53) can be found by evaluating the integral

$$I_1 = \int_z^{\frac{h}{2}} \frac{1}{\cosh^2(a\eta)} \int_0^{\eta} \left(1 - \frac{4\xi^2}{h^2}\right) \left[\cosh^2(a\xi)\right] d\xi\, d\eta. \qquad \text{(D-1)}$$

The following evaluations* are needed

*The number to the right of each evaluation identifies the equation in reference 21.

$$\int \cosh^2 w \, dw = \frac{w}{2} + \frac{1}{4}\left[\sinh(2w)\right], \qquad \text{2.414 \#9}$$

$$\int w^2 \cosh^2 w \, dw = \frac{1}{4}\left(w^2 + \frac{1}{2}\right)\left[\sinh(2w)\right] \qquad \text{2.474 \#6}$$

$$-\frac{w}{4}\left[\cosh(2w)\right] + \frac{w^3}{6},$$

$$\int \frac{w^3 dw}{\cosh^2 w} = w^3 \tanh w - 3\sum_{K=1}^{\infty} \frac{2^{2K}(2^{2K}-1)B_{2k} w^{2k+2}}{(2+2k)[(2k)!]}, \qquad \text{2.477 \#8}$$

where B_{2k} is Bernoulli's coefficient,

$$\int \frac{w\,dw}{\cosh^2 w} = w \tanh w - \ell n\left[\cosh w\right], \qquad \text{2.477 \#18}$$

$$\int \tanh w \, dw = \ell n(\cosh w), \qquad \text{2.423 \#17}$$

$$\int w^2 \tanh w \, dw = \sum_{k=1}^{\infty} \frac{2^{2k}\,(2^{2k}-1)\,B_{2k}\, w^{2k+2}}{(2k+2)[(2k)!]}, \qquad \text{2.479 \#7}$$

as well as the relationships

$$\sinh(2w) = 2\sinh(w)\cosh(w),$$

$$\cosh(2w) = 2\cosh^2(w) - 1.$$

It can be shown that

$$I_2 \equiv \int_0^{\eta}\left(1 - \frac{4\xi^2}{h^2}\right)\left[\cosh^2(a\xi)\right] d\xi$$

$$= \frac{1}{2}\eta - \frac{2}{3h^2}\eta^3 + \left(\frac{1}{4a} - \frac{1}{2a^3h^2}\right)\left[\sinh(2a\eta)\right] \qquad \text{(D-2)}$$

$$- \frac{1}{ah^2}\eta^2\left[\sinh(2a\eta)\right] + \frac{\eta}{a^2h^2}\left[\cosh(2a\eta)\right].$$

From (D-1) and (D-2), as well as the relationships and evaluations above, it can be seen that

$$I_1=\left\{\left[\eta\left(\frac{1}{2a}-\frac{1}{a^3h^2}\right)-\frac{2\eta^3}{3ah^2}\right]\left[\tanh(a\eta)\right]+\frac{\eta^2}{a^2h^2}\right\}_z^{\frac{h}{2}}. \tag{D-3}$$

If this result and (34) are used, (53) becomes

$$g_1=\frac{3Q_0}{2\pi h\nu}\left\{\left[z\left(\frac{1}{a^3h^2}-\frac{1}{2a}\right)+\frac{2z^3}{3ah^2}\right]\left[\tanh(az)\right]\right.$$
$$+\frac{1}{4a^2}\left(1-\frac{4z^2}{h^2}\right) \tag{D-4}$$
$$\left.+\left(\frac{h}{6a}-\frac{1}{2a^3h}\right)\left[\tanh\left(\frac{ah}{2}\right)\right]\right\}$$

The value of ${}_0g_1$, that is, the value of g_1 as ω goes to zero, can be found by reevaluating I_1 with

$$\cosh^2(a\eta)=\cosh^2(a\xi)=1,$$

The result is

$${}_0g_1=\frac{5\Omega'_{e_0}}{16}R_0^2\left(1-\frac{4z^2}{h^2}\right)\left(1-\frac{4z^2}{5h^2}\right). \tag{D-5}$$

Equation (D-4) can be checked by showing that (D-5) can be obtained also by finding the limit of g_1 as a approaches zero. in (D-4). In this limiting process, only the first two terms of the series representation of the hyperbolic tangent need be considered as significant:

$$\tanh x\simeq x-\frac{x^3}{3},$$

In order to solve (56) when k_1 is given by (33), consider the substitution

$$\psi_n=e^{\gamma_n z^2}(g_3)_n \tag{D-6}$$

where γ_n is some constant as yet unspecified. If (D-6) is differentiated twice with respect to z, the result is

$$\frac{d^2\psi_n}{dz^2}=\left[\left(2\gamma_n+4\gamma_n^2z^2\right)(g_3)_n+4\gamma_n z\frac{d(g_3)_n}{dz}+\frac{d^2(g_3)_n}{dz^2}\right]e^{\gamma_n z^2} \tag{D-7}$$

Equation (56) will be satisfied if

$$\frac{d^2(g_3)_n}{dz^2}+4\gamma_n z\frac{d(g_3)_n}{dz}=\xi_n(g_3)_n \tag{D-8}$$

$$\beta_n + a^2 = 2\gamma_n + \xi_n \tag{D-9}$$

and

$$\gamma_n^2 = \frac{-\beta_n}{h^2}\,, \tag{D-10}$$

where ξ_n is another constant as yet unspecified. It will be seen that it is the eigenvalue of (D-8) defined by the boundary condition.

$$(g_3)_n\left(\pm\frac{h}{2}\right) = 0\,. \tag{D-11}$$

Equations (D-9) and (D-10) can be used to find β_n and γ_n in terms of a and ξ_n. The result is

$$\beta_n = -\left[a^2 - \xi_n + \frac{2}{h^2}\left(1 + \sqrt{1 + h^2(a^2 - \xi_n)}\right)\right] \tag{D-12}$$

$$\gamma_n = -\frac{1}{h^2}\left(1 + \sqrt{1 + h^2(a^2 - \xi_n)}\right) \tag{D-13}$$

The positive sign has been chosen in front of the radical in (D-12) and (D-13) for convenience. The solution obtained in this manner must be unique, since the original problem is well posed. The solution obtained for $(g_3)_n$ does depend on the sign chosen; however, when the accompanying change of γ_n is considered in (D-6), the solution obtained for ψ_n by either method should be formally identical. No effort is made to pursue this point, though.

Now consider (D-8). If the substitution

$$x = -2\gamma_n z^2 \tag{D-14}$$

is used, this equation becomes

$$x\frac{d(g_3)_n}{dx^2} + \left(\frac{1}{2} - x\right)\frac{d(g_3)_n}{dx} + \frac{\xi_n}{8\gamma_n}(g_3)_n = 0. \tag{D-15}$$

This equation is the confluent hypergeometric equation. The general solution is given[22] by

$$g_3 = K'M\left[-\frac{\xi_n}{8\gamma_n}, \frac{1}{2}, x\right] + K''x^{\frac{1}{2}}M\left[\left(-\frac{\xi_n}{8\gamma_n} + \frac{1}{2}\right), \frac{3}{2}, x\right] \tag{D-16}$$

where

$$M\left[a_1, a_2, x\right] = \sum_{m=0}^{\infty} \frac{\Gamma(a_1+m)\Gamma(a_2)x^m}{\Gamma(a_2+m)\Gamma(a_1)\ m!} \qquad \text{(D-17)}$$

Since the boundary conditions are symmetric with respect to the centerplane, $K'' = 0$.

Equation (D-11) can now be used to find the eigenvalues of (D-16). It is then found that

$$\psi_n = e^{\frac{\gamma_n'}{4}\left(\frac{2z}{h}\right)^2} M\left[-p_n, \frac{1}{2}, -\frac{\gamma_n'}{2}\left(\frac{2z}{h}\right)^2\right] \qquad \text{(D-18)}$$

where

$$\gamma_n' = -\left(1+\sqrt{1+i\omega'+S_n}\right)$$

$$S_n = -\xi_n h^2$$

$$P_n = \frac{S_n}{8\left(1+\sqrt{1+i\omega'+S_n}\right)}$$

$$\omega' = \frac{\omega h^2}{\nu}$$

and the S_n are the ordered set of values of S which satisfy the equation

$$M\left[-\frac{S}{8\left(1+\sqrt{1+i\omega'+S}\right)}, \frac{1}{2}, \frac{1}{2}\left(1+\sqrt{1+i\omega'+S}\right)\right] = 0, \qquad \text{(D-19)}$$

If (40), (43), (46), (52), (59), and (D-12) are used, it can be seen that

$$R_0\Omega_0 e^{i\omega t} = \left[\left(\frac{g_1}{R_0}+R_0\right)\frac{\cosh(az)}{\cosh\left(\frac{ah}{2}\right)} + \frac{1}{R_0}\sum_n C_n e^{\frac{\nu\lambda_n R_0^2}{2A\omega h^2}}\psi_n\right]\Omega_0 e^{i\omega t} \qquad \text{(D-20)}$$

where

$$\lambda_n = i\omega' + S_n + 2\left(1+\sqrt{1+i\omega'+S_n}\right).$$

If both sides of (D-20) are multiplied by $(1-4z^2/h^2)\psi_n$ and integrated with respect to z from 0 to h/2, the orthogonality condition provides an evaluation for C_n, namely

$$C_n = -R_0^2 \, e^{\frac{-\lambda_n}{3Re_0'}} \frac{\int_0^{\frac{h}{2}} \left[\frac{\cosh(az)}{\cosh\left(\frac{ah}{2}\right)}\left(\frac{g_1}{R_0^2}+1\right)-1\right]\left(1-\frac{4z^2}{h^2}\right)\psi_n \, dz}{\int_0^{\frac{h}{2}}\left(1-\frac{4z^2}{h^2}\right)\psi_n^2 \, dz} \tag{D-21}$$

To find G_0 and $G_{i\omega}$, one must first evaluate the integral in (61):

$$I_3 \equiv \int_0^{\frac{h}{2}} \left[V_{\theta_{rel}} V_r\right]_{r=R_1} dz. \tag{D-22}$$

One has

$$V_{\theta_{rel}}\Big|_{r=R_1} = \left\{\frac{g_1 \cosh(az)}{R_1 \cosh\left(\frac{ah}{2}\right)} + R_1\left[\frac{\cosh(az)}{\cosh\left(\frac{ah}{2}\right)}-1\right] + \frac{1}{R_1}\sum C_n e^{\frac{\lambda_n R_1^2}{3Re_0' R_0^2}} \psi_n\right\} \Omega_0 e^{iwt}. \tag{D-23}$$

Since $(R_1^2/3Re_0'R_0^2)$ is of the order of 10^{-4}, the exponential in the series above can be set equal to 1 if λ_n is of the order of 10^2 or less. Since it will be seen later that only the first term in this series need be considered and that λ_0 is about 11 when $\omega'=0$, the exponential in (D-23) is set equal to 1. The term linear in R_1 can be neglected, and thus (D-23) becomes

$$V_{\theta_{rel}}\Big|_{r=R_1} = \frac{1}{R_1}\left[g_1 \frac{\cosh(az)}{\cosh\left(\frac{ah}{2}\right)} + \sum C_n \psi_n\right]. \tag{D-24}$$

If (28), (33), (34), and (D-24) are used in (D-22), one has

$$I_3 = \frac{-3Q_0}{4\pi h R_1^2}\left[\frac{1}{\cosh\left(\frac{ah}{2}\right)}\int_0^{\frac{h}{2}} g_1 \cosh(az)\left(1-\frac{4z^2}{h^2}\right)dz + \sum_n C_n \int_0^{\frac{h}{2}}\left(1-\frac{4z^2}{h^2}\right)\psi_n dz\right] \tag{D-25}$$

Now let

$$I_4 \equiv \int_0^{\frac{h}{2}} g_1\left[\cosh(az)\right]\left(1-\frac{4z^2}{h^2}\right)dz. \tag{D-26}$$

From (D-4)

$$\begin{aligned}\frac{2\pi h_1}{3Q_0} I_4 = &\left(\frac{1}{a^3h^2}-\frac{1}{2a}\right)\int_0^{\frac{h}{2}} z\left[\sinh(az)\right]dz \\ &+\left[-\frac{4}{h^2}\left(\frac{1}{a^3h^2}-\frac{1}{2a}\right)+\frac{2}{3ah^2}\right]\int_0^{\frac{h}{2}} z^3\left[\sinh(az)\right]dz \\ &+\left(-\frac{8}{3ah^4}\right)\int_0^{\frac{h}{2}} z^5\left[\sinh(az)\right]dz \\ &+\left\{\frac{1}{4a^2}+\left(\frac{h}{6a}-\frac{1}{2a^3h}\right)\left[\tanh\left(\frac{ah}{2}\right)\right]\right\}\int_0^{\frac{h}{2}}\left[\cosh(az)\right]dz \\ &+\left\{-\frac{4}{h^2}\left[\frac{1}{4a^2}+\left(\frac{h}{6a}-\frac{1}{2a^3h}\right)\tanh\left(\frac{ah}{2}\right)\right]-\frac{1}{a^2h^2}\right\}\int_0^{\frac{h}{2}} z^2\left[\cosh(az)\right]dz \\ &+\left(\frac{4}{a^2h^4}\right)\int_0^{\frac{h}{2}} z^4\left[\cosh(az)\right]dz.\end{aligned} \tag{D-27}$$

The following evaluations[21] are needed:

$$\int w\sinh w\,dw = w\cosh w - \sinh w, \qquad 2.472\ \#7$$

$$\int w^3\sinh w\,dw = 6\left[\left(w+\frac{w^3}{6}\right)\cosh w-\left(1+\frac{w^2}{2}\right)\sinh w\right], \qquad 2.472\ \#4$$

$$\int w^5\sinh w\,dw = 120\left[\left(w+\frac{w^3}{6}+\frac{w^5}{120}\right)\cosh w-\left(1+\frac{w^2}{2}+\frac{w^2}{24}\right)\sinh w\right], \qquad 2.472\ \#4$$

$$\int \cosh w\,dw = \sinh w,$$

$$\int w^2 \cosh w\,dw = (2+w^2)\sinh w - 2w\cosh w, \qquad 2.472\ \#10$$

$$\int w^4 \cosh w\,dw = 24\left[\left(1+\frac{w^2}{2}+\frac{w^4}{24}\right)\sinh w-\left(w+\frac{w^2}{6}\right)\cosh w\right]. \qquad 2.472\ \#5^*$$

If the above substitutions are made in (D-27) and the results grouped in powers of $\tanh(ah/2)$, one obtains

$$I_4=\frac{3Q_0}{2\pi h\gamma}\left[\cosh\left(\frac{ah}{2}\right)\right]\left\{\frac{4}{3a^2h}\left(1-\frac{165}{a^2h^2}\right)\right.$$
$$+\frac{32}{a^5h^2}\left(1+\frac{55}{4a^2h^2}\right)\left[\tanh\left(\frac{ah}{2}\right)\right] \qquad \text{(D-28)}$$
$$\left.-\frac{4}{3a^4h}\left(1-\frac{3}{a^2h^2}\right)\left[\tanh^2\left(\frac{ah}{2}\right)\right]\right\}$$

Equation (D-28) can be checked if the solution obtained by substituting (D-5) for g_1 in (D-26) is compared with the solution obtained by letting a approach zero in (D-28). In this latter process, the expressions

$$\tanh x = x-\frac{1}{3}x^3+\frac{2}{15}x^5-\frac{17}{315}x^7+\ \ldots$$

$$\tanh^2 x = x^2-\frac{2}{3}x^4+\frac{17}{45}x^6+\ \ldots$$

are needed. By both methods

$$\lim_{a\to 0} I_4=\frac{3Q_0}{2\pi h\gamma}\,\frac{17h^3}{630} \qquad \text{(D-29)}$$

The first half of the solution of (D-25) has now been found. The second half will now be found. If (D-21) is used,

---

* The lower index on the first summation in 2.472 #5 was changed from k=1 to k=0 in this evaluation. This is necessary for 2.472 #5 to be consistent with 2.472 #10.

one obtains

$$C_n \int_0^{\frac{h}{2}} \left(1-\frac{4z^2}{h^2}\right)\psi_n dz = -\frac{R_0^2 h}{2} e^{\frac{-\lambda_n}{3Re_0'}}$$

$$\int_C^1 \left\{\frac{\cosh\left(\frac{w}{2}\sqrt{i\omega'}\right)}{\cosh\left(\frac{1}{2}\sqrt{i\omega'}\right)}\left[\frac{3Re_0'}{2}\phi_2(w,\omega')+1\right]-1\right\}\left(1-w^2\right)\psi_n dw \qquad \text{(D-30)}$$

$$\frac{\int_0^1 \left(1-w^2\right)\psi_n dw}{\int_0^1 \left(1-w^2\right)\psi_n^2 dw},$$

where

$$\phi_2(w,\omega') = \left[-\left(\frac{1}{2}+\frac{i}{\omega'}\right)w+\frac{w^3}{6}\right]\frac{\tanh\left(\frac{w}{2}\sqrt{i\omega'}\right)}{\sqrt{i\omega'}}$$

$$-\frac{i}{2\omega'}\left(1-w^2\right)+\left(\frac{1}{3}+\frac{i}{\omega'}\right)\tanh\frac{\left(\frac{1}{2}\sqrt{i\omega'}\right)}{\sqrt{i\omega'}}.$$

and ψ_n is given by (D-18) with the substitution $W = \frac{2z}{h}$.

If (D-18), (D-22), (D-25), (D-26), (D-28) and (D-30) are used, (61) can be evaluated. If the limit for this expression as ω approaches zero is found (with the help of (D-29)) (63) can be evaluated. This evaluation is given by (64). If (63) used to specify K_1 such that Φ approaches 1 as ω goes to zero, then (65) is obtained.

APPENDIX E. COMPUTER PROGRAMS FOR EQUATIONS (64) AND (65)

The following are the computer programs used to evaluate (64) and (65) numerically.

The program to evaluate G_0 is listed first. One data card is required to specify REZS (starting value of Re_o'), REZF (final value of Re_o'), and DR (the increment between the values desired). Total running time of this program for thirteen values of Re_o', for instance, was 1.4 minutes on an IBM 7094. The results will be plotted by a CalComp plotter if the cards calling for the subroutines PLOT, PLOTS, SCALE, AXIS, and FLINE are retained.

The program to evaluate $G_{i\omega}$ is listed next. Double precision is required in evaluating $\phi_2(w,\omega')$ because the series representation for the hyperbolic tangent must be carried out to an equivalent of at least the ninth degree of the polynomial expression to obtain any contributions to $G_{i\omega}$. The subroutine HOME searches for the first eigenvalue of (D-19).

Two data cards are required, one for the title (called "Frequency Response" here) and one to specify REZERO (value of Re_o'), WPS (starting value of ω'), and DWP (the increment between the values desired). The results will be plotted by a CalComp if the call cards for the same subroutines previously mentioned and also the subroutine SYMBOL are retained.

Typical running time of this program is about 3 minutes on an IBM 7094.

```
C     PROGRAM TO PLOT GO VS REZERO
C
      DIMENSION IBUF(1024),R(100),GO(100)
      CALL PLOTS(IBUF,1024)
      CALL PLOT(0.,-30.,-3)
      CALL PLOT(1.,.75,-3)
      REAL LAMDAO
      LAMDAO=11.311052
      V6=.08936417
      V7=.5054014
      V8=.4208766
      C6=.026984127
    9 READ (5,10) REZS,REZF,DR
   10 FORMAT (3F10.0)
C
C     REZS IS STARTING VALUE OF REZERO
C     REZF IS FINAL VALUE OF REZERO
C     DR IS THE INCREMENT FOR REZERO
C
C     INSERT A BLANK CARD AFTER LAST DATA CARD
C
      IF(DR.EQ.0.) GO TO 50
      N=(REZF-REZS)/DR+1.5
      DO 20 I=1,N
      R(I)=REZS+FLOAT(I-1)*DR
      C1=3.*R(I)
      C3=EXP(-LAMDAO/C1)
      C4=C3*V6*(V7/V8)
      C5=C4*.25
      C7=C6-C5
   20 GO(I)=R(I)*9.*C7
      WRITE (6,21) (R(I),GO(I),I=1,N)
   21 FORMAT(1H1,5X,7HRE-ZERO,9X,6HG-ZERO//(1X,1P2E15.5))
C
C     PLOT SECTION
C
      CALL SCALE(R,8.,N,1)
      CALL SCALE (GO, 9.,N,1)
      CALL AXIS(0.,0.,7HRE-ZERO,-7,8.,0.,R(N+1),R(N+2))
      CALL AXIS(0.,0.,6HG-ZERO, 6, 9.,90.,GO(N+1),GO(N+2))
      CALL FLINE(R,GO,-N,1,0,0)
      CALL PLOT(10.,0.,-3)
      GO TO 9
   50 CALL PLOT(0.,0.,999)
      STOP
      END
```

```
C     PROGRAM TO PLOT DB AND THETA VS OMEGA
C
      DIMENSION IBUF(1024),WP(100),R(100),DEGREE(100)
      CALL PLOTS(IBUF,1024)
      CALL XMAX(125.)
      CALL PLOT(0.,-30.,-3)
      CALL PLOT(1.,.75,-3)
      EXTERNAL EVAL
      COMPLEX Z1,Z2,Z3,Z4,Z5,Z6,Z7,LAMBDA,P,GAMMA,Z8,Z9,Z10,Z11,Z12,M
      COMPLEX Z13,Z14,PSI,Z15,Z37   ,Z16,Z17,Z18,Z19,CCOSH,Z20,Z21,Z22
      COMPLEX Z23,PHI2,Z24,Z25,Z26,Z27,Z28,Z29,Z30,Z31,Z32,Z33,Z34,Z35
      COMPLEX PH11,THETA
      COMPLEX Z36
      COMPLEX S
      COMMON SPART
      COMMON OMEGA
      COMMON A1,A2
      REAL LAMDA0
      DIMENSION SPART(2),DELTA(2)
      DIMENSION LABEL(6)
      DIMENSION Y1(101),Y2(101),Y3(101),Y4(101),Y5(101),Z(101)
      DIMENSION Y9(101)
   51 FORMAT (6A6)
   52 FORMAT (1H1,48X,6A6///////)
   53 FORMAT (1H )
   54 FORMAT (1X,57X,8HREZERO =,F10.6)
   55 FORMAT (1X,36X,5HOMEGA,8X,1HX,11X,1HY,10X,3HRHO,8X,2HDB7X,5HPHASE/
     2/)
   56 FORMAT (1X,35X,F6.3,3F12.5,F10.3,F10.1)
   10 FORMAT (8F10.0)
      H=0.01
      LAMDA0=11.311052
      V6=.08936417
      V7=.5054014
      V8=.4208766
      C6=.026984127
      READ (5,51) LABEL
    9 READ (5,10) REZERO,WPS,WPF,DWP
C
C     WPS IS STARTING VALUE OF OMEGA
C     WPF IS THE FINAL VALUE OF OMEGA
C     DWP IS THE INCREMENT FOR OMEGA
C
C     INSERT A BLANK CARD AFTER LAST DATA CARD
C
      IF (DWP   .EQ.0.0) GO TO 100
   11 C1=3.0*REZERO
      C2=2.0/C1
      C3=EXP(-LAMDA0/C1)
      C4=C3*V6*(V7/V8)
      C5=C4/4.0
      C7=C6-C5
      WRITE (6,52) LABEL
      WRITE (6,54) REZERO
      WRITE (6,53)
      WRITE (6,55)
      L=(WPF-WPS)/DWP+1.5
      DO 8 J=1,L
      WP(J)=WPS+FLOAT(J-1)*DWP
      OMEGA=WP(J)
      SPART(1)=4.584669
      SPART(2)=0.0
      DELTA(1)=0.1
      DELTA(2)=0.1
```

```
      Q=1.0E+36
      N=2
      I=3000
      CALL HOME(EVAL,SPART,DELTA,N,I,Q)
      S=CMPLX(A1,A2)
      Z1=CMPLX(0.0,OMEGA)
      Z2=Z1+S
      Z3=1.0+Z2
      Z4=CSQRT(Z3)
      Z5=1.0+Z4
      Z6=2.0*Z5
      Z7=8.0*Z5
      LAMBDA=Z2+Z6
      P=S/Z7
      GAMMA=-Z5
      Z8=-P
      Z9=-GAMMA/2.0
      Z10=-Z9/2.0
      I=1
      W=0.0
    5 W2=W**2
      W3=1.0-W2
      Z11=Z9*W2
      Z12=M(Z8,0.5,Z11)
      Z13=Z10*W2
      Z14=CEXP(Z13)
      PSI=Z12*Z14
      Z15=W3*PSI
      Y1(I)=REAL(Z15)
      Y2(I)=AIMAG(Z15)
      Z16=Z15*PSI
      Y3(I)=REAL(Z16)
      Y9(I)=AIMAG(Z16)
      Z17=CSQRT(Z1)
      Z18=Z17/2.0
      Z19=CCOSH(Z18)
      Z20=Z18*W
      Z21=CCOSH(Z20)
      Z22=Z21/Z19
      Z23=Z22*PHI2(W,OMEGA)
      Z24=Z22-1.0
      Z25=C2*Z24
      Z26=Z23+Z25
      Z27=Z26*W3*PSI
      Y4(I)=REAL(Z27)
      Y5(I)=AIMAG(Z27)
      IF (I.EQ.101) GO TO 6
      I=I+1
      W=W+H
      GO TO 5
    6 CALL QSF(H,Y1,Z,101)
      V1=Z(101)
      CALL QSF(H,Y2,Z,101)
      V2=Z(101)
      CALL QSF(H,Y3,Z,101)
      V3=Z(101)
      CALL QSF(H,Y4,Z,101)
      V4=Z(101)
      CALL QSF(H,Y5,Z,101)
      V5=Z(101)
      CALL QSF(H,Y9,Z,101)
      V9=Z(101)
      Z28=CMPLX(V1,V2)
      Z37=CMPLX(V3,V9)
      Z29=LAMBDA/C1
      Z30=CEXP(-Z29)
      Z31=Z28/Z37
      Z32=CMPLX(V4,V5)
```

```
      Z33=Z30*Z32*Z31
      Z34=Z33/4.0
      Z35=PHI1(OMEGA)
      Z36=Z35-Z34
      THETA=Z36/C7
      X=REAL(THETA)
      Y=AIMAG(THETA)
      RHO=CABS(THETA)
      R(J)=20.0*ALOG10(RHO)
      ANGLE=ATAN2(Y,X)
      DEGREE(J)=57.2957795*ANGLE
      IF(ANGLE.GE.0.) DEGREE(J)=DEGREE(J)-360.
    8 WRITE (6,56) OMEGA,X,Y,RHO,R(J),DEGREE(J)
C
C     PLOT SECTION
C
      CALL SCALE (WP,8.,L,1)
      CALL SCALE (R, 9.,L,1)
      CALL SCALE (DEGREE, 9.,L,1)
      CALL AXIS (0.,0.,5HOMEGA,-5,8.,0.,WP(L+1),WP(L+2))
      CALL AXIS (0.,0.,2HDB,2, 9.,90.,R(L+1),R(L+2))
      CALL AXIS (8.,0.,5HPHASE,-5,9. ,90.,DEGREE(L+1),DEGREE(L+2))
      CALL FLINE(WP,R,-L,1,1,0)
      CALL FLINE(WP,DEGREE,-L,1,1,11)
      CALL SYMBOL (.5,9.8,.1,0,0.,-1)
      CALL SYMBOL (999.,999.,.1,3H DB,0.,3)
      CALL SYMBOL (.5,9.5,.1,11,0.,-1)
      CALL SYMBOL (999.,999.,.1,6H PHASE,0.,6)
      CALL SYMBOL(2.,9.8,.1,LABEL,0.,36)
      CALL SYMBOL (2.,9.5,.1,8HREZERO= ,0.,8)
      CALL NUMBER (999.,999.,.1,REZERO,0.,6)
      CALL PLOT(10.,0.,-3)
      GO TO 9
  100 CALL PLOT(0.,0.,999)
      STOP
      END
```

EVALK - EFN SOURCE STATEMENT - IFN(S) -

```
      SUBROUTINE EVAL(QA,QB,*)
      COMMON SPART
      COMMON OMEGA
      COMMON A1,A2
      DIMENSION SPART(2)
      COMPLEX G
      COMPLEX S,T
      S=CMPLX(SPART(1),SPART(2))
      T=G(S,OMEGA)
      QB=CABS(T)
      IF (QB.GE.QA) RETURN
      A1=SPART(1)
      A2=SPART(2)
      RETURN 1
      END
```

HOMEJK - EFN SOURCE STATEMENT - IFN(S) -

```
      SUBROUTINE HOME(QSET,EX,DS,N,IMAX,Q)
      DIMENSION EX(1),      DS(1),P(9),DD(9),XTEM(9),PP(9),MUG(9)
      IF (N.LE.0) RETURN
      IMAX7=IMAX
      FACT=.5/FLOAT(N)
      DO 10 I=1,N
```

```
      MUG(I)=0
      P(I)=DS(I)
   10 DD(I)=4.*DS(I)
      I2 = 3
      I3 = N
      I=1
      DO 150 I7=1,IMAX7
      IMAX=I7
      DELQ=0.
      DO 90 I6=1,N
      I = I-1
      IF(I.EQ.0) I=N
      IF(MUG(I) .EQ. 0 .OR. N .EQ. 1) GO TO 15
      MUG(I)=0
      GO TO 55
   15 XTEM(I) = EX(I)
      IF(I2.NE.3) GO TO 20
      DS(I) = .25*DD(I)
      DD(I) = 0.
   20 P(I)=SIGN(DS(I),P(I))
      NCYC=1
   40 XP=XTEM(I)+P(I)
      IF(XP.EQ.XTEM(I)) GO TO 50
      EX(I)=XP
      CALL QSET(Q,QT,$60)
      GO TO (35,70,25),NCYC
   25 EX(I)=XTEM(I)
      GO TO 90
   35 Q1 = QT
      P(I) = -P(I)
      NCYC=2
      GO TO 40
   70 P(I)=P(I)*.5*(Q1-QT)/(Q1+QT-2.*Q)
      NCYC=3
      GO TO 40
   50 MUG(I)=1
      IF(NCYC.EQ.3) GO TO 90
   55 I3=I3-1
      IF(I3.EQ.0) RETURN
      GO TO 90
   60 IF(QT.EQ.0.) RETURN
      I3=N
      IF(Q-QT.LE.DELQ.OR.N.EQ.1) GO TO 80
      DELQ = Q-QT
      II = I
   80 Q = QT
   90 DD(I) = DD(I)+ABS(FLOAT (4-I2)*P(I))
      I3=N
      I2 = I2-1
      IF(I2.EQ.0) I2=3
      IF(N.EQ.1) GO TO 150
      PROD=1.
      DO 100 I5=1,N
      PP(I)=P(I)*PROD
      PROD=PROD-FACT
      IF(I.EQ.N) I=0
  100 I=I+1
      DO 140 I5=1,10
      DO 120 I=1,N
  110 XTEM(I)=EX(I)
  120 EX(I) = EX(I)+PP(I)
      CALL QSET(Q,QT,$130)
      DO 145 I=1,N
  145 EX(I) = XTEM(I)
      GO TO 150
  130 IF(QT.EQ.0.) RETURN
      IF(Q-QT.GT.DELQ) GO TO 140
```

```
      Q=QT
      GO TO 150
  140 Q=QT
  150 I=II
      RETURN
      END
```

CCOSHK - EFN SOURCE STATEMENT - IFN(S) -

```
      COMPLEX FUNCTION CCOSH(Z)
      COMPLEX Z
      CCOSH=(CEXP(Z)+CEXP(-Z))/2.0
      RETURN
      END
```

HYPER - EFN SOURCE STATEMENT - IFN(S) -

```
      COMPLEX FUNCTION M(AZERO,BZERO,ZZERO)
      COMPLEX AZERO,ZZERO,A,Z,C,LOGZRO,LOGA,LOGZ,LOGC,LOGX,X,CLOG
      COMPLEX CT
      REAL LOGK,LOGB,LOGD,LOGN
      REAL K,N
      REAL IMAGA,IMAGC
      M=1.0
      K=1.0
      J=0
      A=AZERO
      B=BZERO
      Z=ZZERO
      IF (CABS(ZZERO).EQ.0.0) RETURN
      X=(A*Z)/B
      M=M+X
      C=A+1.0
      D=B+1.0
      N=2.0
      GO TO 2
    4 M=M+X
      IF (CABS(X).LT.1.0E-09) RETURN
      N=N+1.0
      C=C+1.0
      D=D+1.0
      GO TO 3
    2 LOGZRO=CLOG(ZZERO)
      IF (CABS(A)) 12,13,12
   12 REALA=REAL(A)
      IMAGA=AIMAG(A)
      IF (REALA.LT.0.0) GO TO 16
   18 LOGA=CLOG(A)
      LOGK=ALOG(K)
      LOGB=ALOG(B)
      LOGZ=CLOG(Z)
    3 LOGN=ALOG(N)
      IF (CABS(C)) 14,13,14
   14 REALC=REAL(C)
      IMAGC=AIMAG(C)
      IF (REALC.LT.0.0) GO TO 17
      LOGC=CLOG(C)
   19 LOGD=ALOG(D)
      LOGA=LOGA+LOGC
   15 LOGB=LOGB+LOGD
      LOGZ=LOGZ+LOGZRO
      LOGK=LOGK+LOGN
```

```
      LOGX=LOGA+LOGZ-LOGB-LOGK
      X=CEXP(LOGX)*((-1.0)**J)
      GO TO 4
   16 REALA=-REALA
      IMAGA=-IMAGA
      A=CMPLX(REALA,IMAGA)
      J=J+1
      GO TO 18
   17 CREAL=-REALC
      IMAGC=-IMAGC
      CT=CMPLX(CREAL,IMAGC)
      LOGC=CLOG(CT)
      J=J+1
      GO TO 19
   13 X=0.0
      GO TO 4
      END
```

GOFS - EFN SOURCE STATEMENT - IFN(S) -

```
      COMPLEX FUNCTION G(S,OMEGA)
      COMPLEX IOMEGA,Z1,P,Z2,Z3,GAMMA,M
      COMPLEX S
      B=0.5
      IOMEGA=CMPLX(0.0,OMEGA)
      Z1=1.0+(CSQRT(1.0+IOMEGA+S))
      P=S/(8.0*Z1)
      Z2=-P
      GAMMA=-Z1
      Z3=(-GAMMA)/2.0
      G=M(Z2,B,Z3)
      RETURN
      END
```

PHI1K - EFN SOURCE STATEMENT - IFN(S) -

```
      COMPLEX FUNCTION PHI1(OMEGA)
      DOUBLE PRECISION DOMEGA,X1,X2,X3,X4,X5,X6,X7,U1,V1,U2,V2,U3,V3,X
      DOUBLE PRECISION TWOX,X8,X9,X10,X11,X13,U7,X14,V7,U8,V8,U4,V4,U9
      DOUBLE PRECISION V9,U10,V10,U11,V11,U5,U6,V6,U12,V12,U13,V13
      DOUBLE PRECISION X12,V5
      DOMEGA=DBLE(OMEGA)
      X=DSQRT(DOMEGA)/2.828427124746190 1
      TWOX=2.0*X
      U5=TWOX
      V5=TWOX
      X1=DOMEGA**2
      X2=3.0*X1
      X3=4.0/X2
      X4=165.0/DOMEGA
      X5=32.0/X1
      X6=-55.0/(4.0*DOMEGA)
      X7=3.0/DOMEGA
      U1=1.0
      V1=X4
      U2=X3*U1
      V2=X3*V1
      U3=1.0
      V3=X6
      X8=DEXP(TWOX)
      X9=DEXP(-TWOX)
```

```
      X10=(X8-X9)/2.0
      X11=(X8+X9)/2.0
      X12=DCOS(TWOX)
      X13=X11+X12
      U7=X10/X13
      X14=DSIN(TWOX)
      V7=X14/X13
      U8=((U7*U5)+(V7*V5))/((U5**2)+(V5**2))
      V8=((U5*V7)-(U7*V5))/((U5**2)+(V5**2))
      U4=X5*U3
      V4=X5*V3
      U9=(U4*U8)-(V4*V8)
      V9=(U4*V8)+(U8*V4)
      U10=1.0
      V10=X7
      U11=(U7*U7)-(V7*V7)
      V11=(U7*V7)+(U7*V7)
      U6=X3*U10
      V6=X3*V10
      U12=(U6*U11)-(V6*V11)
      V12=(U6*V11)+(U11*V6)
      U13=-U2-U9+U12
      V13=-V2-V9+V12
      U14=SNGL(U13)
      V14=SNGL(V13)
      PHI1=CMPLX(U14,V14)
      RETURN
      END
```

PHI2K - EFN SOURCE STATEMENT - IFN(S) -

```
      COMPLEX FUNCTION PHI2(W,OMEGA)
      DOUBLE PRECISION DOMEGA,U1,V1,U2,V2,U3,V3,U4,V4,U5,V5,U7,V7,U8,V8
      DOUBLE PRECISION U9,V9,X,TWOX,X8,X9,X10,X11,X12,X13,X14,U10,V10
      DOUBLE PRECISION U11,V11,U12,V12,U13,V13,U14,V14,U15,V15,U16,V16
      DOUBLE PRECISION U17,V17,U18,V18,U19,V19
      DOMEGA=DBLE(OMEGA)
      U1=0.0
      V1=1.0
      U2=U1/OMEGA
      V2=V1/OMEGA
      U3=0.5+U2
      V3=V2
      U4=U3*W
      V4=V3*W
      U5=-U4+((W**3)/6.0)
      V5=-V4
      U7=DSQRT(DOMEGA)/1.4142135623730950
      V7=U7
      U8=U7/2.0
      V8=V7/2.0
      U9=U8*W
      V9=V8*W
      J=1
      X=U9
    3 TWOX=2.0*X
      X8=DEXP(TWOX)
      X9=DEXP(-TWOX)
      X10=(X8-X9)/2.0
      X11=(X8+X9)/2.0
      X12=DCOS(TWOX)
      X13=X11+X12
      X14=DSIN(TWOX)
      GO TO (1,2),J
    1 U10=X10/X13
```

```
      V10=X14/X13
      J=2
      U11=((U10*U7)+(V10*V7))/((U7**2)+(V7**2))
      V11=((U7*V10)-(U10*V7))/((U7**2)+(V7**2))
      U12=(U5*U11)-(V5*V11)
      V12=(U5*V11)+(U11*V5)
      U13=U1/(2.0*OMEGA)
      V13=V1/(2.0*OMEGA)
      U14=U13*(1.0-(W**2))
      V14=V13*(1.0-(W**2))
      U15=.3333333333333333+U2
      V15=V2
      X=U8
      GO TO 3
    2 U16=X10/X13
      V16=X14/X13
      U17=((U16*U7)+(V16*V7))/((U7**2)+(V7**2))
      V17=((U7*V16)-(U16*V7))/((U7**2)+(V7**2))
      U18=(U15*U17)-(V15*V17)
      V18=(U15*V17)+(U17*V15)
      U19=U12-U14+U18
      V19=V12-V14+V18
      U20=SNGL(U19)
      V20=SNGL(V19)
      PHI2=CMPLX(U20,V20)
      RETURN
      END
```

MS243 - EFN SOURCE STATEMENT - IFN(S) -

```
C                                                                       QSF  001
C     .................................................................QSF  002
C                                                                       QSF  003
C        SUBROUTINE QSF                                                 QSF  004
C                                                                       QSF  005
C        PURPOSE                                                        QSF  006
C           TO COMPUTE THE VECTOR OF INTEGRAL VALUES FOR A GIVEN        QSF  007
C           EQUIDISTANT TABLE OF FUNCTION VALUES.                       QSF  008
C                                                                       QSF  009
C        USAGE                                                          QSF  010
C           CALL QSF (H,Y,Z,NDIM)                                       QSF  011
C                                                                       QSF  012
C        DESCRIPTION OF PARAMETERS                                      QSF  013
C           H      - THE INCREMENT OF ARGUMENT VALUES.                  QSF  014
C           Y      - THE INPUT VECTOR OF FUNCTION VALUES.               QSF  015
C           Z      - THE RESULTING VECTOR OF INTEGRAL VALUES. Z MAY BE  QSF  016
C                    IDENTICAL WITH Y.                                  QSF  017
C           NDIM   - THE DIMENSION OF VECTORS Y AND Z.                  QSF  018
C                                                                       QSF  019
C        REMARKS                                                        QSF  020
C           NO ACTION IN CASE NDIM LESS THAN 3.                         QSF  021
C                                                                       QSF  022
C        SUBROUTINES AND FUNCTION SUBPROGRAMS REQUIRED                  QSF  023
C           NONE                                                        QSF  024
C                                                                       QSF  025
C        METHOD                                                         QSF  026
C           BEGINNING WITH Z(1)=0, EVALUATION OF VECTOR Z IS DONE BY    QSF  027
C           MEANS OF SIMPSONS RULE TOGETHER WITH NEWTONS 3/8 RULE OR A  QSF  028
C           COMBINATION OF THESE TWO RULES. TRUNCATION ERROR IS OF      QSF  029
C           ORDER H**5 (I.E. FOURTH ORDER METHOD). ONLY IN CASE NDIM=3  QSF  030
C           TRUNCATION ERROR OF Z(2) IS OF ORDER H**4.                  QSF  031
C           FOR REFERENCE, SEE                                          QSF  032
C           (1) F.B.HILDEBRAND, INTRODUCTION TO NUMERICAL ANALYSIS,     QSF  033
C               MCGRAW-HILL, NEW YORK/TORONTO/LONDON, 1956, PP.71-76.   QSF  034
```

```
C           (2) R.ZURMUEHL, PRAKTISCHE MATHEMATIK FUER INGENIEURE UND      QSF  035
C               PHYSIKER, SPRINGER, BERLIN/GOETTINGEN/HEIDELBERG, 1963,    QSF  036
C               PP.214-221.                                                QSF  037
C                                                                          QSF  038
C     ..................................................................   QSF  039
C                                                                          QSF  040
      SUBROUTINE QSF(H,Y,Z,NDIM)                                           QSF  041
C                                                                          QSF  042
C                                                                          QSF  043
      DIMENSION Y(1),Z(1)                                                  QSF  044
C                                                                          QSF  045
      HT=.3333333*H                                                        QSF  046
      IF(NDIM-5)7,8,1                                                      QSF  047
C                                                                          QSF  048
C     NDIM IS GREATER THAN 5. PREPARATIONS OF INTEGRATION LOOP             QSF  049
C                                                                          QSF  050
    1 SUM1=Y(2)+Y(2)                                                       QSF  051
      SUM1=SUM1+SUM1                                                       QSF  052
      SUM1=HT*(Y(1)+SUM1+Y(3))                                             QSF  053
      AUX1=Y(4)+Y(4)                                                       QSF  054
      AUX1=AUX1+AUX1                                                       QSF  055
      AUX1=SUM1+HT*(Y(3)+AUX1+Y(5))                                        QSF  056
      AUX2=HT*(Y(1)+3.875*(Y(2)+Y(5))+2.625*(Y(3)+Y(4))+Y(6))              QSF  057
      SUM2=Y(5)+Y(5)                                                       QSF  058
      SUM2=SUM2+SUM2                                                       QSF  059
      SUM2=AUX2-HT*(Y(4)+SUM2+Y(6))                                        QSF  060
      Z(1)=0.                                                              QSF  061
      AUX=Y(3)+Y(3)                                                        QSF  062
      AUX=AUX+AUX                                                          QSF  063
      Z(2)=SUM2-HT*(Y(2)+AUX+Y(4))                                         QSF  064
      Z(3)=SUM1                                                            QSF  065
      Z(4)=SUM2                                                            QSF  066
      IF(NDIM-6)5,5,2                                                      QSF  067
C                                                                          QSF  068
C     INTEGRATION LOOP                                                     QSF  069
    2 DO 4 I=7,NDIM,2                                                      QSF  070
      SUM1=AUX1                                                            QSF  071
      SUM2=AUX2                                                            QSF  072
      AUX1=Y(I-1)+Y(I-1)                                                   QSF  073
      AUX1=AUX1+AUX1                                                       QSF  074
      AUX1=SUM1+HT*(Y(I-2)+AUX1+Y(I))                                      QSF  075
      Z(I-2)=SUM1                                                          QSF  076
      IF(I-NDIM)3,6,6                                                      QSF  077
    3 AUX2=Y(I)+Y(I)                                                       QSF  078
      AUX2=AUX2+AUX2                                                       QSF  079
      AUX2=SUM2+HT*(Y(I-1)+AUX2+Y(I+1))                                    QSF  080
    4 Z(I-1)=SUM2                                                          QSF  081
    5 Z(NDIM-1)=AUX1                                                       QSF  082
      Z(NDIM)=AUX2                                                         QSF  083
      RETURN                                                               QSF  084
    6 Z(NDIM-1)=SUM2                                                       QSF  085
      Z(NDIM)=AUX1                                                         QSF  086
      RETURN                                                               QSF  087
C     END OF INTEGRATION LOOP                                              QSF  088
C                                                                          QSF  089
    7 IF(NDIM-3)12,11,8                                                    QSF  090
C                                                                          QSF  091
C     NDIM IS EQUAL TO 4 OR 5                                              QSF  092
    8 SUM2=1.125*HT*(Y(1)+Y(2)+Y(2)+Y(2)+Y(3)+Y(3)+Y(3)+Y(4))              QSF  093
      SUM1=Y(2)+Y(2)                                                       QSF  094
      SUM1=SUM1+SUM1                                                       QSF  095
      SUM1=HT*(Y(1)+SUM1+Y(3))                                             QSF  096
      Z(1)=0.                                                              QSF  097
      AUX1=Y(3)+Y(3)                                                       QSF  098
      AUX1=AUX1+AUX1                                                       QSF  099
      Z(2)=SUM2-HT*(Y(2)+AUX1+Y(4))                                        QSF  100
      IF(NDIM-5)10,9,9                                                     QSF  101
    9 AUX1=Y(4)+Y(4)                                                       QSF  102
      AUX1=AUX1+AUX1
```

```
      Z(5)=SUM1+HT*(Y(3)+AUX1+Y(5))                          QSF  103
   10 Z(3)=SUM1                                              QSF  104
      Z(4)=SUM2                                              QSF  105
      RETURN                                                 QSF  106
C                                                            QSF  107
C     NDIM IS EQUAL TO 3                                     QSF  108
   11 SUM1=HT*(1.25*Y(1)+Y(2)+Y(2)-.25*Y(3))                 QSF  109
      SUM2=Y(2)+Y(2)                                         QSF  110
      SUM2=SUM2+SUM2                                         QSF  111
      Z(3)=HT*(Y(1)+SUM2+Y(3))                               QSF  112
      Z(1)=0.                                                QSF  113
      Z(2)=SUM1                                              QSF  114
   12 RETURN                                                 QSF  115
      END                                                    QSF  116
```

APPENDIX F. SOLUTION FOR A UNIFORM RADIAL PROFILE

If (36) and (37) are used with the same procedure as that described in Appendix D one finds that

$$g_1 = \frac{Q_0}{2\pi h \nu a}\left\{\frac{h}{2}\left[\tanh\left(\frac{ah}{2}\right)\right] - z\left[\tanh(az)\right]\right\} \qquad \text{(F-1)}$$

and

$$\sigma g_1 = \frac{Re_0' R_0^2}{4}\left(1 - \frac{4z^2}{h^2}\right). \qquad \text{(F-2)}$$

Equation (F-1) can be checked by comparing its limit as a approaches zero (let tanh x=x) with (F-2).

Now consider (56):

$$\frac{d^2\psi_n}{dz^2} = \left(a^2 + \beta_n\right)\psi_n \qquad \text{(F-3)}$$

This has a solution

$$\psi_n = K_n'''\left[\sin(\xi_n z)\right] + K_n''''\left[\cos(\xi_n z)\right], \qquad \text{(F-4)}$$

where

$$\xi_n^2 = -\left(a^2 + \beta_n\right).$$

The boundary conditions given by (57) require that K''' = 0, and

$$\xi_n = \frac{2n+1}{h}\pi. \qquad \text{(F-5)}$$

Therefore

$$\beta_n = -\xi_n^2 - a^2 = -\frac{(2n+1)^2\pi^2}{h^2} - a^2 \tag{F-6}$$

Thus, one has from (59), (F-4) and (F-5) that for $k_1 = k_0$

$$u_2 = \sum_n C_n \frac{1}{r} e^{\frac{\nu r^2}{2A_0}\left(\xi_n^2 + a^2\right)} \left[\cos(\xi_n z)\right] \tag{F-7}$$

From (40), (43), (46), (52), and (F-7) one has

$$R_0 \Omega_0 e^{i\omega t} = \left[\left(\frac{g_1}{R_0} + R_0\right) \frac{\cosh(az)}{\cosh\left(\frac{ah}{2}\right)}\right] + \sum_n C_n \frac{1}{R_0} e^{\frac{h^2}{2Re_0'}(\xi_n^2 + a^2)} \left[\cos(\xi_n z)\right] . \tag{F-8}$$

The orthogonality condition ,(F-1), and (F-8) can then be used to show that

$$\begin{aligned} &-\frac{C_n}{R_0} e^{\frac{h^2}{2Re_0'}(\xi_n^2 + a^2)} \int_0^{\frac{h}{2}} \left[\cos(\xi_n z)\right]^2 dz \\ &= \left[\frac{Q_0}{4\pi\nu a R_0} \frac{\sinh\left(\frac{ah}{2}\right)}{\cosh^2\left(\frac{ah}{2}\right)} + \frac{R_0}{\cosh\left(\frac{ah}{2}\right)}\right] \int_0^{\frac{h}{2}} \left[\cosh(az)\right]\left[\cos(\xi_n z)\right] dz \\ &- \frac{Q_0}{2\pi h \nu a R_0} \frac{1}{\cosh\left(\frac{ah}{2}\right)} \int_0^{\frac{h}{2}} z \left[\sinh(az)\right]\left[\cos(\xi_n z)\right] dz \\ &- R_0 \int_0^{\frac{h}{2}} \left[\cos(\xi_n z)\right] dz \end{aligned} \tag{F-9}$$

The coefficients C_n can then be found if four integrals (a, b, c, d) are evaluated* .

Integral (a) is given by

$$\int_0^{\frac{h}{2}} \left[\cosh(az)\right]\left[\cos(\xi_n z)\right]dz = \left\{\frac{a}{a^2+\xi_n^2}\left[\sinh(az)\right]\left[\cos(\xi_n z)\right] + \frac{\xi_n}{a^2+\xi_n^2}\left[\cosh(az)\right]\left[\sin(\xi_n z)\right]\right\}_0^{\frac{h}{2}} \qquad \text{(F-10)}$$

$$= \frac{\xi_n}{a^2+\xi_n^2}\left[\cosh\left(\frac{ah}{2}\right)\right](-1)^n \cdot \qquad \text{2.671 \#4}$$

Integral (b) is given by

$$\int_0^{\frac{h}{2}} z\left[\sinh(az)\right]\left[\cos(\xi_n z)\right]dz = uz\Big|_0^{\frac{h}{2}} - \int_0^{\frac{h}{2}} u\,dz\,, \qquad \text{(F-11)}$$

where

$$u \equiv \int \left[\sinh(az)\right]\left[\cos(\xi_n z)\right]dz = \frac{a}{a^2+\xi_n^2}\left[\cosh(az)\right]\left[\cos(\xi_n z)\right] + \frac{\xi_n}{a^2+\xi^2}\left[\sinh(az)\right]\left[\sin(\xi_n z)\right] \qquad \text{(F-12)}$$

2.671 #2

Therefore

$$\int_0^{\frac{h}{2}} u\,dz = \frac{a}{a^2+\xi_n^2}\int_0^{\frac{h}{2}}\left[\cosh(az)\right]\left[\cos(\xi_n z)\right]dz + \frac{\xi_n}{a^2+\xi_n^2}\int_0^{\frac{h}{2}}\left[\sinh(az)\right]\left[\sin(\xi_n z)\right]dz\,, \qquad \text{(F-13)}$$

But

$$\int_c^{\frac{h}{2}} \sinh(az)\ \sin\left(\xi_n z\right)dz = \left\{\frac{a}{a^2+\xi_n^2}\left[\cosh(az)\right]\left[\sin\left(\xi_n z\right)\right] - \frac{\xi_n}{a^2+\xi_n^2}\left[\sinh(az)\right]\left[\cos\left(\xi_n z\right)\right]\right\}_0^{\frac{h}{2}} \qquad \text{(F-14)}$$

2.671 #1

---

* The number to the right of an evaluation identifies the equation in reference 21.

From (F-10) through (F-14) one finds that

$$\int_0^{\frac{h}{2}} z\left[\sinh(az)\right]\left[\cos(\xi_n z)\right]dz = \frac{(-1)^n \xi_n}{a^2+\xi_n^2}\left\{\frac{h}{2}\left[\sinh\left(\frac{ah}{2}\right)\right]-\frac{2a}{a^2+\xi_n^2}\left[\cosh\left(\frac{ah}{2}\right)\right]\right\}. \tag{F-15}$$

Furthermore, one can show that the integral (c) is given by

$$\int_0^{\frac{h}{2}} \cos\left(\xi_n z\right)dz = \frac{(-1)^n}{\xi_n} \tag{F-16}$$

and that the integral (d) is given by

$$\int_0^{\frac{h}{2}} \left[\cos\left(\xi_n z\right)\right]^2 dz = \frac{h}{4} \tag{F-17}$$

(F-5) has been used in all of these evaluations.

It can be shown from (F-9), (F-10), (F-15), (F-16) and (F-17) that

$$C_n = \frac{4}{h}\frac{R_0^2(-1)^{n+1}}{\xi_n}\left[\frac{Q_0}{\pi h \upsilon R_0^2}\frac{\xi_n^2}{\left(a^2+\xi_n^2\right)^2}-\frac{a^2}{a^2+\xi_n^2}\right]e^{\frac{-h^2}{2Re_0'}\left(a^2+\xi_n^2\right)}. \tag{F-18}$$

To find G_0 and $G_{i\omega}$, one must first evaluate the integral in (61):

$$I \equiv \int_0^{\frac{h}{2}} \left[V_{\theta rel} V_i\right]_{r=R_1} dz . \tag{F-19}$$

One has

$$V_{\theta_{rel}}\Big|_{r=R_1} = \left\{\frac{g_1}{R_1}\frac{\cosh(az)}{\cosh\left(\frac{ah}{2}\right)}+R_1\left[\frac{\cosh(az)}{\cosh\left(\frac{ah}{2}\right)}-1\right] + \frac{1}{R_1}\sum_n C_n e^{\frac{h^2}{2Re_0'}\frac{R_1^2}{R_0^2}\left(a^2+\xi_n^2\right)}\left[\cos\left(\xi_n z\right)\right]\right\}\Omega_0 e^{i\omega t} \tag{F-20}$$

Just as in appendix D the linear term in R_1 can be ignored and the exponential term in the series set equal to 1. Thus,

$$V_{\theta_{rel}}\Big|_{r=R_1} = \frac{1}{R_1}\left\{ g_1 \frac{\cosh(az)}{\cosh\left(\frac{ah}{2}\right)} + \sum_n C_n \left[\cos\left(\xi_n z\right)\right]\right\} \Omega_0 e^{i\omega t} \qquad \text{(F-21)}$$

Therefore, from (28), (36), (37), and (F-21), (F-19) becomes

$$I = -\frac{Q_0}{2\pi h R_1^2}\left\{ \frac{1}{\cosh\left(\frac{ah}{2}\right)} \int_0^{\frac{h}{2}} g_1 \left[\cosh(az)\right] dz + \sum_n C_n \int_0^{\frac{h}{2}} \left[\cos(\xi_n z)\right] dz . \right. \qquad \text{(F-22)}$$

Now from (F-1)

$$\int_0^{\frac{h}{2}} g_1 \left[\cosh(az)\right] dz = \frac{Q_0}{2\pi h \nu a}\left\{ \frac{h}{2}\left[\tanh\left(\frac{ah}{2}\right)\right] \int_0^{\frac{h}{2}} \left[\cosh(az)\right] dz - \int_0^{\frac{h}{2}} z \left[\sinh(az)\right] dz \right. \qquad \text{(F-23)}$$

$$= \frac{Q_0 \cosh\left(\frac{ah}{2}\right)}{4\pi\nu a^2}\left\{ \left[\tanh\left(\frac{ah}{2}\right)\right]^2 + \frac{2}{ah}\left[\tanh\left(\frac{ah}{2}\right)\right] - 1 \right\}$$

Equation (F-23) can be checked by comparing its limit as a approaches zero with the result obtained by using (F-2) for g_1 in the integral on the left of (F-23). One finds that

$$\int_0^{\frac{h}{2}} {}_0 g_1 dz = \lim_{a \to 0} \int_0^{\frac{h}{2}} g_1 \left[\cosh(az)\right] dz = \frac{Q_0 h^2}{24\pi\nu} \qquad \text{(F-24)}$$

where the relationships $\tanh x \approx x - \frac{x^3}{3}$ and $\tanh^2 x \approx x^2$ are used.

If (F-16), (F-18) and (F-23) are substituted into (F-22), one finds that

$$\int_0^{\frac{h}{2}} \left[V_{\theta_{rel}} V_r\right]_{r=R_1} dz =$$

$$-\frac{Q_0}{2\pi h R_1^2}\frac{Q_0 h^2}{4\pi\nu}\left\{ \frac{1}{a^2h^2}\left[\tanh^2\left(\frac{ah}{2}\right) + \frac{2}{ah}\tan\left(\frac{ah}{2}\right) - 1\right] \right.$$

$$\left. -\sum_n \frac{16}{\xi_n^2 h^4 \left(a^2+\xi_n^2\right)}\left[\frac{\xi_n^2}{a^2+\xi_n^2} - \frac{\pi h a^2 \nu R_0^2}{Q_0}\right] e^{\frac{-h^2}{2Re_0'}\left(a^2+\xi_n^2\right)} \right\} \qquad \text{(F-25)}$$

Equation (63) can be evaluated from (F-25). If the limit of this expression as a approaches zero is found (with the help of (F-24)), (78) can be determined. Equation (79) can be obtained by using (F-15) in (60) and requiring that k_1 be chosen such that $\phi=1$ at $\omega=0$.

APPENDIX G. ERROR DUE TO NEGLECTING $\frac{\partial}{\partial r}\left(\frac{\partial u_2}{\partial r}+\frac{u_2}{r}\right)$ IF $k_1 = k_0$

For the case when $k_1 \equiv k_0 = 1$, (51) becomes

$$a^2 u_2 - \frac{A_0}{\nu}\frac{1}{r}\left(\frac{\partial u_2}{\partial r}+\frac{u_2}{r}\right) = \frac{\partial}{\partial r}\left(\frac{\partial u_2}{\partial r}+\frac{u_2}{r}\right)+\frac{\partial^2 u_2}{\partial z^2}\,. \tag{G-1}$$

If (54) and (56) are used, one finds that

$$\frac{d^2 f_n}{dr^2}+\left(1+\frac{A_0}{\nu}\right)\frac{1}{r}\frac{df_n}{dr}+\left[\beta_n+\left(\frac{A_0}{\nu}-1\right)\frac{1}{r^2}\right]f_n=0\,. \tag{G-2}$$

The coefficient of the first derivative can be simplified if one defines a new dependent variable $(f_3)_n$ such that

$$f_n = r^{-\frac{A_0}{2\nu}}(f_3)_n\,. \tag{G-3}$$

Then

$$\frac{d^2(f_3)_n}{dr^2}+\frac{1}{r}\frac{d(f_3)_n}{dr}-(f_3)_n\left\{\left(\frac{A_0}{2\nu}-1\right)^2\frac{1}{r^2}-\beta_n\right\}=0 \tag{G-4}$$

Finally, let

$$\eta \equiv r\sqrt{-\beta_n} = r\sqrt{a^2+\xi_n^2} \tag{G-5}$$

where (F-6) has been used to evaluate β_n. Then (G-4) becomes

$$\eta^2\frac{d^2(f_3)_n}{d\eta^2}+\eta\frac{d(f_3)_n}{d\eta}-\left[\eta^2+\left(\frac{A_0}{2\nu}-1\right)^2\right](f_3)_n=0 \tag{G-6}$$

The solution of this equation is given[23] by

$$(f_3)_n = C' I_{\left(\frac{A_0}{2\nu}-1\right)}(\eta) + C'' K_{\left(\frac{A_0}{2\nu}-1\right)}(\eta), \qquad \text{(G-7)}$$

where $I_{(Ao/2\nu)-1}$ is the modified Bessel function of the first kind of the order $(Ao/2\nu)-1$ and $K_{(Ao/2\nu)-1}$ is the modified Bessel function of the second kind. Since the latter function describes the propagation of information in the upstream direction (it decays as r increases), then $C'' = 0$. This latter solution will be used in section 2.4.3 to show how small the drain tube must be in order for the pickoff not to be aware of its presence.

If the series representation[23] of I is used, the (G-3), (G-5) and (G-7) can be used to show that for the case when $k_1 = k_0$,

$$(f_1')_n = \frac{1}{r}\left[\frac{1}{4}\left(a^2+\xi_n^2\right)\right]^{\frac{1}{2}\left(\frac{A_0}{2\nu}-1\right)} \sum_m \frac{\left[\frac{1}{4}\left(a^2+\xi_n^2\right)r^2\right]^m}{m!\,\Gamma\left(\frac{A_0}{2\nu}+m\right)} \qquad \text{(G-8)}$$

Here $(f_1')_n$ is the term that describes the propagation of ψ_n information in the downstream direction if the term $\partial/\partial r(\partial u_2/\partial r + u_2/r)$ is retained. If it is ignored, one finds from (58) and (F-6) that

$$(f_1)_n = \frac{1}{r}\, e^{(a^2+\xi_n^2)\frac{\nu r^2}{2A_0}}. \qquad \text{(G-9)}$$

Notice that the equation for ψ_n is unchanged if the term $\frac{\partial}{\partial r}\left(\frac{\partial u_2}{\partial r} + \frac{u_2}{r}\right)$ is included. Then for a given n, the shape of the mode for all r as well as the magnitude at R_0 does not depend on whether or not this term is included.

In either case, the contribution at some r can then be defined in terms of the ratio of the value $(f_1)_n$ at r to that at R_0.

From G-8, the ratio for n=0 is given by

$$\frac{(f_1')_0}{(f_1')_0\big|_{r=R_0}} = \frac{R_0}{r} \frac{\sum_{m=0}^{\infty} \frac{\left[\frac{1}{4}(a^2+\xi_0^2)r^2\right]^m}{m!\,\Gamma\left(\frac{A_0}{2\nu}+m\right)}}{\sum_{m=0}^{\infty} \frac{\left[\frac{1}{4}(a^2+\xi_0^2)R_0^2\right]^m}{m!\,\Gamma\left(\frac{A_0}{2\nu}+m\right)}} \qquad \text{(G-10)}$$

As r becomes small (of the order of R_1) this becomes

$$\frac{(f_1')_0\big|_{r\to 0}}{(f_1')_0\big|_{r=R_0}} = \frac{R_0}{r}\,\frac{1}{\sum_{m=0}^{\infty}\frac{\left[\frac{1}{4}(a^2+\xi_0^2)R_0^2\right]^m\Gamma\left(\frac{A_0}{2\nu}\right)}{m!\,\Gamma\left(\frac{A_0}{2\nu}+m\right)}} \tag{G-11}$$

From G-9, one has

$$\frac{(f_1)_0\big|_{r\to 0}}{(f_1)_0\big|_{r=R_0}} = \frac{R_0}{r}\,e^{-(a^2+\xi_0^2)\frac{\nu R_0^2}{2A_0}} \tag{G-12}$$

The ratio B from section 2.4.1 then becomes

$$\begin{aligned} B &= \frac{(f_1)_0\big|_{r=R_1}}{(f_1)_0\big|_{r=R_0}} \Bigg/ \frac{(f_1')_0\big|_{r=R_1}}{(f_1')_0\big|_{r=R_0}} \\ &= e^{-(i\omega'+\pi^2)\frac{\nu R_0^2}{2A_0h^2}} \sum_{m=0}^{\infty}\frac{\left[\frac{1}{4}(i\omega'+\pi^2)\frac{R_0^2}{h^2}\right]^m\Gamma\left(\frac{A_0}{2\nu}\right)}{m!\,\Gamma\left(\frac{A_0}{2\nu}+m\right)} \end{aligned} \tag{G-13}$$

APPENDIX H. SOLUTION IN THE DRAIN

If the flow field is incompressible and axisymmetric, if the vortex is weak, and if the streamlines lie on a cylindrical surface concentric with the drain walls, then (17), (18), (19), and (20) become

$$\frac{\partial p}{\partial r} = 0 \tag{H-1}$$

$$\rho\left(\frac{\partial V_\theta}{\partial t} + V_z\frac{\partial V_\theta}{\partial z}\right) = \mu\left(\frac{\partial^2 V_\theta}{\partial r^2} + \frac{1}{r}\frac{\partial V_\theta}{\partial r} - \frac{V_\theta}{r^2} + \frac{\partial^2 V_\theta}{\partial z^2}\right)\frac{\partial p}{\partial r} = 0, \tag{H-2}$$

$$\rho\left(V_z\frac{\partial V_z}{\partial z}\right) = -\frac{\partial p}{\partial z} + \mu\left(\frac{\partial^2 V_z}{\partial r^2} + \frac{1}{r}\frac{\partial V_z}{\partial r} + \frac{\partial^2 V_z}{\partial z^2}\right), \tag{H-3}$$

and

$$\frac{\partial V_z}{\partial z} = 0\,. \tag{H-4}$$

Equations (H-1), (H-3) and (H-4) can be combined to obtain

$$\frac{1}{r}\frac{d}{dr}\left(r\frac{dV_z}{dr}\right)=\frac{1}{\mu}\frac{dp}{dz} \tag{H-5}$$

If this equation is integrated twice and the boundary conditions are imposed, one obtains

$$V_z = A\left(1-\frac{r^2}{R_1^2}\right). \tag{H-6}$$

where A is determined by the total flow rate through the drain. Since there are two drains in this model, one finds that

$$V_z=\frac{Q_d}{\pi R_1^2}\left(1-\frac{r^2}{R_1^2}\right), \tag{H-7}$$

where Q_d is the volumetric flow rate specified by the total mass flow rate through the sensor and the static pressure in either drain.

Now let

$$V_\theta \equiv \left(V_1+V_2\right)\Omega_0 e^{i\omega t}, \tag{H-8}$$

where V_1 is the solution that satisfies the inhomogeneous boundary conditions at the drain wall and V_2 is the solution that is used to satisfy the inhomogeneous boundary conditions on the upstream and downstream boundaries of the drain region. Clearly, V_1 is a function of r only. Thus, from (H-2), (H-7) and (H-8) one finds that

$$r^2\frac{d^2V_1}{dr^2}+r\frac{dV_1}{dr}-\left(\frac{i\omega}{\nu}r^2+1\right)V_1=0 \tag{H-9}$$

with the boundary conditions

$$V_1(R_1)=R_1 \tag{H-10}$$

and

$$V_1(0)=0, \tag{H-11}$$

The solutions of (H-9) are the modified Bessel functions.[23] If the boundary conditions are applied, it is found that

$$V_1 = R_1 \frac{I_1\left(\frac{r}{R_1}\sqrt{\frac{i\omega'}{S_\ell^2}}\right)}{I_1\left(\sqrt{\frac{i\omega'}{S_\ell^2}}\right)}, \qquad \text{(H-12)}$$

where $S_\ell = h/R_1$.

Now consider V_2. It must satisfy the equation

$$\frac{i\omega}{\upsilon} V_2 + \frac{Q_d}{\pi R_1^2 \upsilon}\left(1 - \frac{r^2}{R_1^2}\right)\frac{\partial V_2}{\partial z} = \frac{\partial}{\partial r}\left(\frac{\partial V_2}{\partial r} + \frac{V_2}{r}\right) + \frac{\partial^2 V_2}{\partial z^2} \qquad \text{(H-13)}$$

Let

$$V_2 \equiv \sum_n (W_1)_n(r) e^{(\gamma_1)_n z} + \sum_n (W_2)_n(r) e^{(\gamma)_n z}, \qquad \text{(H-14)}$$

where Real $(\gamma_1)_n < 0$ and Real $(\gamma_2)_n > 0$.

The first series on the right side of this equation describes how information introduced at the upstream bounding surface decays as the fluid flows down the drain. The second series describes the propagation in the upstream direction from the downstream boundary, and will be ignored since it can be shown that the propagation in the upstream direction is of extremely short range.

In the actual model tested, the pickoff was located just outside the drain exit. For convenience the pickoff is treated here as if it were located inside the drain tube so that upstream propagation can be ignored. This latter model does not properly account for changes in output brought on by changes in Mach number near the actual pickoff, for it does not allow the streamline pattern to change with $\dot{m}$. However, the viscous losses predicted by such a model should be fairly accurate since the losses due to upstream propagation will be small if the pickoff is submerged in the exhaust jet at a point where the spread would not be great if the pickoff were not there.

In the actual model, the pickoff holes were less than a drain diameter downstream from the exit. Thus, the pickoff can be considered as being in the drain.

If (H-13) and (H-14) are used and the second series in (H-14) is ignored, then one has

$$\frac{i\omega}{\upsilon}(W_1)_n+\frac{Q_d}{\pi R_1^2\upsilon}\left(1-\frac{r^2}{R_1^2}\right)(\gamma_1)_n(W_1)_n = \frac{d}{dr}\left[\frac{d(W_1)_n}{dr}+\frac{(W_1)_n}{r}\right]+(\gamma_1)_n^2(W_1)_n \tag{H-15}$$

If we let

$$\eta=\frac{r}{R_1}\ , \tag{H-16}$$

then

$$\eta^2\frac{d^2(W_1)_n}{d\eta^2}+\eta\frac{d(W_1)_n}{d\eta}-(1+b^2\eta^2+c^2\eta^4)(W_1)_n=0\ , \tag{H-17}$$

where

$$b^2=\frac{i\omega'}{S_2^2}+2Re_1\lambda_n-\lambda_n^2\ ,$$

$$c^2=-2Re_1\lambda_n\ ,$$

and

$$\lambda_n=R_1(\gamma_1)_n$$

The order of the polynomial coefficient of the linear term can be reduced if a new dependent variable, $(W_3)_n$, is defined such that

$$(W_1)_n\equiv\frac{(W_3)_n}{\eta} \tag{H-18}$$

and a new independent variable, η_1, is defined such that

$$\eta_1\equiv\frac{\eta^2}{2}\ . \tag{H-19}$$

Then (H-17) becomes

$$\eta_1\frac{d^2(W_3)_n}{d\eta_1^2}-\left(\frac{b^2}{2}+c^2\eta_1\right)(W_3)_n=0 \tag{H-20}$$

The order can be reduced further if another dependent variable, $(W_4)_n$, is defined such that

$$(W_3)_n\equiv e^{c\eta_1}(W_4)_n\ . \tag{H-21}$$

Equation (H-20) becomes

$$\eta_1\frac{d^2(W_4)_n}{d\eta^2}+2c\eta_1\frac{d(W_4)_n}{d\eta_1}-\frac{b^2}{2}(W_4)_n=0\ . \tag{H-22}$$

Finally, let

$$\eta_2 \equiv -2c\eta_1 \tag{H-23}$$

Then (H-20) becomes

$$\eta_2 \frac{d^2(W_4)_n}{d\eta_2^2} - \eta_2 \frac{d(W_4)_n}{d\eta_2} + \frac{b^2}{4c}(W_4)_n \equiv 0 . \tag{H-24}$$

This is the confluent hypergeometric equation. The solution is given[22] by

$$\begin{aligned}(W_4)_n \equiv A' M\left[-\frac{b^2}{4c}, 0, \eta_2\right] \\ + B'\eta_2 M\left[\left(1-\frac{b^2}{4c}\right), 2, \eta_2\right] .\end{aligned} \tag{H-25}$$

If (H-16), (H-18), (H-19), (H-21) and (H-23) are used, (H-25) becomes

$$\begin{aligned}W_{in} \equiv A' \frac{R_1}{r} e^{\frac{cr^2}{2R_1^2}} M\left[-\frac{b^2}{4c}, 0, -\frac{cr^2}{R_1^2}\right] \\ - (cB')\frac{r}{R_1} e^{\frac{cr^2}{2R_1^2}} M\left[\left(1-\frac{b^2}{4c}\right), 2, -\frac{cr^2}{R^2}\right]\end{aligned} \tag{H-26}$$

Since V_θ must be bounded at r = 0, A = 0. It can then be shown that

$$W_{in} = B' \frac{r}{R_1} e^{-\frac{\delta_n}{2}\frac{r^2}{R_1^2}} M\left[\left(1+\frac{i\omega'}{4S_\ell^2\delta_n}+\frac{\delta_n^3}{16Re_1^2}-\frac{\delta_n}{4}\right), 2, \delta_n\left(\frac{r}{R_1}\right)^2\right] \tag{H-27}$$

where δ_n's are eigenvalues that satisfy the boundary condition

$$M\left[\left(1+\frac{i\omega'}{4S_\ell^2\delta_n}+\frac{\delta_n^3}{16Re_1^2}-\frac{\delta_n}{4}\right), 2, \delta_n\right] = 0 \tag{H-28}$$

Equation (85) can be found by using equation (H-8), (H-12), (H-14), and (H-27), and by noting that

$$(\gamma_1)_n = \frac{-\delta_n^2}{2Re_1}\frac{1}{R_1} \tag{H-29}$$

APPENDIX I. BEHAVIOR OF $G_{i\omega}$ FOR LARGE ω' AND SMALL Re_0'

If Re_0' is very small, (64), (65) and (66) can be used to show that from the parabolic solution

$$G_{i\omega} = \frac{630}{17}\left[\frac{-4}{3(\omega')^2}\left(1+i\frac{165}{\omega'}\right)-\frac{32}{(\omega')^2}\left(1-i\frac{55}{4\omega'}\right)\tanh\frac{\left(\frac{\sqrt{i\omega'}}{2}\right)}{\sqrt{i\omega'}}+\frac{4}{3(\omega')^2}\left(1+i\frac{3}{\omega'}\right)\tanh^2\left(\frac{\sqrt{i\omega'}}{2}\right)\right] \tag{I-1}$$

The expression for the frequency response obtained from the uniform solution when Re_0' is very small can be found from (78) and (79) to be

$$G_{i\omega}' = \frac{6}{i\omega'}\left[\tanh^2\left(\frac{1}{2}\sqrt{i\omega'}\right) + \frac{2}{\sqrt{i\omega'}}\tanh\left(\frac{1}{2}\sqrt{i\omega'}\right)-1\right] \tag{I-2}$$

An upper and lower bound for the behavior of the frequency response at large ω can be found by evaluating the limit of (I-1) and (I-2) as ω' approaches infinity.

This evaluation will be pursued for (1-1) first. It is necessary first to observe that

$$\tanh\left(\frac{1}{2}\sqrt{i\omega'}\right) = \frac{\tanh\left(\sqrt{\frac{\omega'}{8}}\right)+i\tan\left(\sqrt{\frac{\omega'}{8}}\right)}{1+i\tanh\left(\sqrt{\frac{\omega'}{8}}\right)\tan\left(\sqrt{\frac{\omega'}{8}}\right)} \tag{I-3}$$

Since

$$\lim_{\omega'\to\infty}\tanh\left(\sqrt{\frac{\omega'}{8}}\right)=1,$$

then from (I-3),

$$\lim_{\omega'\to\infty}\tanh\left(\frac{1}{2}\sqrt{i\omega'}\right)=1. \tag{I-4}$$

If the hyperbolic tangent terms in (I-1) are set equal to one then one has

$$G_{i\omega} = \frac{630}{17}\left[-\frac{1}{\sqrt{i}}\frac{32}{(\omega')^{5/2}} - i\frac{656}{(\omega')^{3}} + \sqrt{i}\frac{440}{(\omega')^{7/2}}\right] \qquad \text{(I-5)}$$

Then from (1-5), the limiting expression for the frequency response obtained from the parabolic solution is

$$\underset{\omega'\to\infty}{G_{i\omega}} = \frac{630\times32}{17}\frac{1}{(\omega')^{5/2}}e^{-\frac{5\pi}{4}i} \qquad \text{(I-6)}$$

If a similar procedure is followed, using (I-2), then one has

$$\underset{\omega'\to\infty}{G_{i\omega}} = \frac{12}{(\omega')^{3/2}}e^{-\frac{3\pi}{4}i} \qquad \text{(I-7)}$$

Since it has been established that these two solutions provide upper and lower bounds for the phase lag in this range of ω' and Re_0', then the phase lag in the stepwise solution approaches a value ϕ_{max} as ω' increases, where

$$135° < \phi max < 225°$$